INSTITUTO TECNOLOGICO Y DE ESTUDIOS SUPERIORES DE MONTERREY

MONTERREY CAMPUS
SCHOOL OF ENGINEERING AND INFORMATION TECHNOLOGIES
ENGINEERING GRADUATES PROGRAM

TEC de Monterrey.

DEL SISTEMA TECNOLÓGICO DE MONTERREY

METHODOLOGY BASED ON THE STATE TRANSITION CONCEPT FOR SIMPLE CONSTITUTIVE MODELING OF SMART MATERIALS

THESIS

PRESENTED AS PARTIAL REQUISITE TO OBTAIN THE ACADEMIC GRADE OF:

PhD IN ENGINEERING SCIENCES

BY:

MANUEL IGNACIO VARELA JIMENEZ

MONTERREY, N. L.   DECEMBER 2011

INSTITUTO TECNOLOGICO Y DE ESTUDIOS SUPERIORES DE MONTERREY

MONTERREY CAMPUS

SCHOOL OF ENGINEERING AND INFORMATION TECHNOLOGIES

ENGINEERING GRADUATES PROGRAM

TEC de Monterrey.
DEL SISTEMA TECNOLÓGICO DE MONTERREY

METHODOLOGY BASED ON THE STATE TRANSITION CONCEPT FOR SIMPLE CONSTITUTIVE MODELING OF SMART MATERIALS

THESIS

PRESENTED AS PARTIAL REQUISITE TO OBTAIN THE ACADEMIC GRADE OF:

PhD IN ENGINEERING SCIENCES

BY:

MANUEL IGNACIO VARELA JIMENEZ

MONTERREY, N. L.   DECEMBER 2011

METHODOLOGY BASED ON THE STATE TRANSITION CONCEPT FOR SIMPLE CONSTITUTIVE MODELING OF SMART MATERIALS

TEC de Monterrey

DEL SISTEMA TECNOLÓGICO DE MONTERREY

THESIS

PhD in Engineering Sciences

By

Manuel Ignacio Varela Jiménez

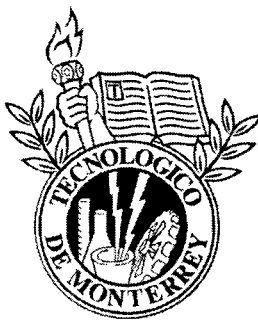**Instituto Tecnológico y de Estudios Superiores de Monterrey**

December 2011

INSTITUTO TECNOLOGICO Y DE ESTUDIOS SUPERIORES DE MONTERREY

MONTERREY CAMPUS

SCHOOL OF ENGINEERING AND INFORMATION TECHNOLOGIES

ENGINEERING GRADUATES PROGRAM

TEC de Monterrey

DEL SISTEMA TECNOLÓGICO DE MONTERREY

Methodology Based on the State Transition Concept for Simple Constitutive Modeling of Smart Materials

THESIS
PRESENTED AS PARTIAL REQUISITE TO OBTAIN THE ACADEMIC GRADE OF:

PhD IN ENGINEERING SCIENCES

BY:

MANUEL IGNACIO VARELA JIMENEZ

MONTERREY, NL   **December 2011**

Instituto Tecnológico y de Estudios Superiores de Monterrey
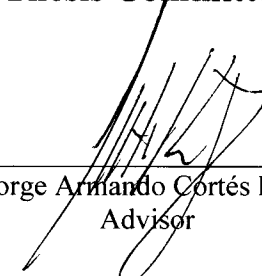
Monterrey Campus

School of Engineering and Information Technologies

Post-Graduate Program

The members of the thesis committee recommend that the present thesis presented by Manuel Ignacio Varela Jiménez be accepted as partial requisite to obtain the academic degree of:
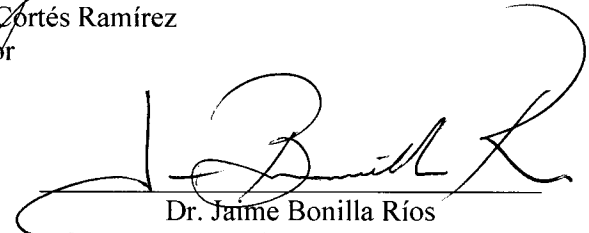
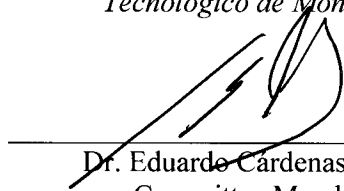## Doctor in Engineering Sciences

Thesis Committee

_____
Dr. Jorge Armando Cortés Ramírez
Advisor

_____
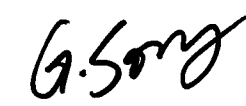Dr. Alex Elías Zúñiga
Committee Member
Tecnológico de Monterrey

_____
Dr. Jaime Bonilla Ríos
Committee Member
Tecnológico de Monterrey

_____
Dr. Eduardo Cárdenas Alemán
Committee Member
Tecnológico de Monterrey

_____
Dr. Gangbing Song
Committee Member
University of Houston

APPROVED

_____
Dr. Alex Elías Zúñiga
Director of PhD in Engineering Sciences

December 2011

Methodology Based on the State Transition Concept for Simple Constitutive Modeling of Smart Materials

By

Manuel Ignacio Varela Jiménez

T H E S I S

Presented to the Graduates Program of the School of Engineering and Information Technologies as partial requisite to obtain the academic grade of

PhD in Engineering Sciences
in the área of
Mechatronics and Advanced Materials

Instituto Tecnológico y de Estudios Superiores de Monterrey
Monterrey Campus

Monterrey, N.L. December 2011.

To my parents *Ignacio* and *Lourdes*… you are a constant source of love and motivation for me, I feel very lucky to be your son. I appreciate all your love and concern for educate me on the best form and instill values; for having fostered in me a winning mentality that has led me to not give up and to face problems; due to that today I finish successfully with this stage of my life.
Thanks for all your love, patience and dedication for me, my brother and sister!

To my brother *Ricardo Emilio*… you are my best example of how with commitment and effort is possible to achieve goals. I admire very much your intelligence and effort in all what you do.
I am very proud of you!

To my sister *Rosa Ofelia*… in these last years that we shared a home it has been impossible to do not catch of your joy and energy to motivate me to work. Thank you very much for keeping up with me, listening me and putting up with me through thick and thin.
I love you and I know that you have a very promising future!

To all my other *family* and *friends*… for supporting me and never stop believing in me. Because the memories of many moments with you have been the best inspiration for doing this work.

Acknowledgment

Methodology Based on the State Transition Concept for Simple Constitutive Modeling of Smart Materials

Manuel Ignacio Varela Jiménez

Instituto Tecnológico y de Estudios Superiores de Monterrey, 2011

Smart materials have the capability to sense and respond to environmental stimuli in a predictable and useful manner. Its existence has transformed the paradigm that materials can be used only for structural purposes into the concept that these can also be the basis for actuators or sensors, generating new possibilities for design of devices. However, development of these materials also creates necessity of proposition of new theories and concepts that allow understanding its behavior.

This dissertation focuses on development of a general constitutive model for describing response of several smart materials by considering that a microstructural change is stimulated in them, such a state transition that follows a sigmoidal behavior and can be modeled by a proposed expression that describes transition induced by an external factor. Such expression results flexible and able to adapt to take several kinds of external variable as the main parameter that induces transformation.

A methodology for purposing a state transition in smart materials and modeling its response to some stimulus through a common mathematical expression relating the effect of microstructural changes on some variable associated to the material is proposed and evaluated. This way, there were studied; 1) effect of twinned martensite - detwinned martensite – austenite strain/temperature induced phase transformation on stress of Nickel – Titanium shape memory alloy, 2) effect of glassy – active temperature induced state transition on stress of shape memory polymers, 3) effect of magnetic field induced arrangement of iron particles on shear yield stress of magnetorheological fluid and 4) effect of electric field induced arrangement of ions on the bending of a thin film of electroactive polymer.

A constitutive model is proposed for each material resulting in promising results due to good fitting with experimental data and comparison with some other models, although it has some limitations such as being unidimensional, considering only one way behavior of the materials or have been fitted for specific geometries or chemical composition and stills needs to be generalized. However, it can be considered as an initial approach for a general model for smart materials regardless of their atomic structure, chemical bonds or physical domain, that could be applied for design of materials and simulation of its behavior through numerical methods.

Contents

List of Figures

List of Tables

List of Symbols

SM	Smart Materials
SMA	Shape Memory Alloy
NiTi	Nickel - Titanium
EAP	Electroactive Polymer
SMP	Shape Memory Polymer
MRF	Magnetorheological Fluid
KJMA	Kolmogorov-Johnson-Mehl-Avrami equation
STE	State Transition Equation
SME	Shape Memory Effect
DSC	Differential Scanning Calorimetry
cfu/ml	Colony Forming Units/Milliliter
t	Time
K, n	KJMA constants
t_c	Characteristic time
X	External stimulus
X_c	Characteristic external stimulus
T	Temperature
T_c	Characteristic Temperature
T_r	Room Temperature
T_{as}	Temperature at which active state starts
T_{af}	Temperature at which active state finishes
ε	Plastic Strain
ε_c	Characteristic Strain
μm	Micrometer
σ	Stress
A	Austenite
TM	Twinned Martensite
DM	Detwinned Martensite
σ_t	Flow Stress of NiTi
σ_a	Flow Stress of Austenite
σ_{tm}	Flow Stress of Twinned Martensite
σ_{dm}	Flow Stress of Detwinned Martensite
V_f	Volume fraction
V_{fA}	Volume fraction of phase A
V_{fB}	Volume fraction of phase B
V_{fa}	Volume fraction of austenite
V_{fdm}	Volume fraction of detwinned martensite
V_{ftm}	Volume fraction of twinned martensite
T_g	Glass Transition Temperature
H	Magnetic Field Intensity
H_c	Characteristic Magnetic Field
V	Voltage
V_c	Characteristic Voltage
τy	Shear Yield stress

τ_y^{sat}	Saturation shear yield stress
τ_{yl}^{sat}	Saturation shear yield stress of liquid state
τ_{ys}^{sat}	Saturation shear yield stress of solid state
B_T	Fitting constant of temperature induced state transition of NiTi
B_ε	Fitting constant of strain induced state transition of NiTi
B_{SMP}	Fitting constant of state transition of SMP
B_{EAP}	Fitting constant of state transition of EAP
B_{MRF}	Fitting constant of state transition of MRF
ϕ	Volume fraction of particles in carrier fluid.
μ_0	*Permeability* of vacuum.
M_s	*Saturation* magnetic field of the material used as particles.
V_{fl}	Volume fraction of liquid phase
V_{fs}	Volume fraction of solid phase
$\lambda, A_\varepsilon, A_T$	NiTi constants
$J\,Q_\varepsilon, Q_T$	NiTi constants
$C_a, D_a,$	Austenite constants
F_a, G_a	Austenite constants
$C_{tm}, D_{tm},$	Twinned Martensite constants
F_{tm}, G_{tm}	Twinned Martensite constants
$C_{dm}, D_{dm},$	Detwinned Martensite constants
F_{dm}, G_{dm}	Detwinned Martensite constants
α, A	SMP constants
$\beta, \chi, \phi, \gamma$	EAP constants
α, β, χ	MRF constants

Part I. Theory

Chapter 1.

Introduction

1.1.   Background

There are materials that have been created or in which special abilities have been found, able to have controlled reactions under influence of some stimulus; they are known as 'smart materials' (SM) and its existence has transformed the paradigm that a material can be used only for structural or filling purposes into the concept that these can also be the basis for actuators or sensors, generating new possibilities for development of devices in several engineering areas.

Progress of SM creates the necessity of proposition of new theories and concepts for understanding its behavior, which cannot be described by the same laws or models for traditional materials. By proposing constitutive models for SM, simulation and validation of devices based on them can be carried out and appropriated design of these can be achieved.

This dissertation focuses on the development of a methodology and a common constitutive model for describing response of various SM by considering that in all them a microstructural change is induced, such a state transition.

1.1.1.   Smart Materials

SM have the capability to sense and to respond to environmental stimuli in a predictable and useful manner as well as being capable of active control of their response (Ouellette 1996), (UK Parlament, 2008). They have been much studied in recent years; other names for these are intelligent, adaptive, structronic or functional materials (Leo, 2007), (Arghavani, 2010). Although the term 'smart material' has been conventionally used, all materials are in general responsive but whether they are responsive in an adaptive way is questionable. A 'very smart' adaptive response is exhibited if materials are able to respond dynamically to a number of input stimuli and if this response is repeatable. This term also refers to materials that can (1) respond reversibly to the changes in the surrounding environment and (2)

contribute an optimal or useful response by either changing its physical properties, geometry, mechanical properties, or electromagnetic properties. The physical change is usually a significant one which can easily be observed and detected, in all cases, very smart materials are expected to provide a reversible and useful response to change in the adapted environment (Hu, 2007). Following this idea, SM can be considered part of smart technology, which possess an awareness of its situation and is capable of reacting to it; by condition it could mean the technology's environment, its condition or its motion (Worden, 2003).

Leo considers SM exhibit coupling between multiple physical domains. A domain is any physical quantity that can be described by a set of two state variables; for example the mechanical domain has as state variables the stress and strain within a material. Other examples are the electrical, thermal, magnetic, and chemical domains. Coupling occurs when a change in the state variable in one physical domain causes a change in the state variable of a separate physical domain. For example, changing the temperature of a material, which is a state variable in the thermal domain, can cause a change in the state of strain, which is a mechanical state variable (Leo, 2007).

For centuries, metals have played an important role as structural materials. The human ability to understand material behavior from microstructure and to engineer different material properties for a variety of applications has enabled the development of new alloys and composites (Kumar, 2010) and although most of the basic SM have been around since Marie and Pierre Curie experimented with piezoelectrics in 1880, the field has evolved (Ouellette, 1996) and over the past years, a number of materials have been given the term smart based on their interesting properties. Common examples of SM include that can convert electrical signals into mechanical deformation and can convert mechanical deformation into an electrical output. Others that convert thermal energy to mechanical strain, and even those that couple the motion of chemical species within the material to mechanical output or electrical signals (Leo, 2007). Other materials considered change color in response to changes in temperature or light conditions (UK Parlament, 2008). Their engineering properties differ greatly; some materials are capable of producing large forces but only small motions, whereas others are able to produce large deformations at the expense of smaller forces. Some materials can respond very quickly, whereas the response time of other materials is much slower (Leo, 2007).

The breadth and depth of applications that could potentially gain an advantage from SM systems is vast. Each application will have many of its own unique design criteria but the creation of all smart technologies necessitates a solution to the same dilemma: how to integrate the fundamental abilities of awareness and reaction into a coherent system with the minimum of complexity and cost. This requires a design philosophy that is inherently interdisciplinary and requires knowledge of a number of different

enabling technologies (Worden, 2003). Thus, applications of SM systems requires knowledge of the basic properties of various types of SM, methods for modeling the coupling mechanisms within these materials, and mathematical approaches to incorporating material models into models of engineering systems (Leo, 2007).

SM studied in this work are:

Shape Memory Alloy (SMA): shown in figure (Fig) 1-1; possess an interesting property by which the metal 'remembers' its original size or shape and reverts to it at a characteristic transformation temperature (Srinivasan, 2001).

Fig. 1-1. NiTi springs in their original shape (Grand-Illusions, 2011)

Shape Memory Polymer (SMP): has the ability of recovering its undeformed original shape in response to an environmental stimulus after undergoing a certain level of pre-deformation (Castro, 2009). Some specimens are depicted in Fig 1-2.
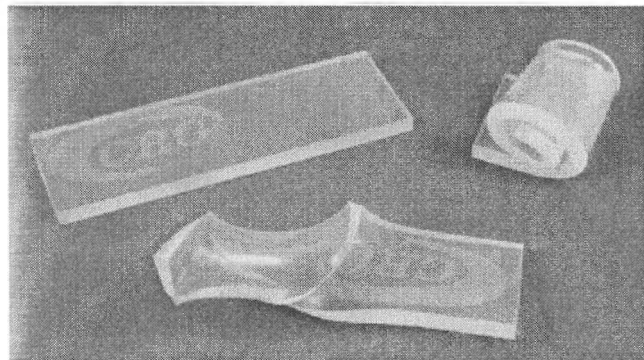
Fig. 1-2. SMP films in original (flat) and deformed (twisted) shape (CRG, 2011)

Electroactive Polymer (EAP): able to change their shape under electric stimulation (Ritter, 2007). Thin EAP films are shown in Fig 1-3.
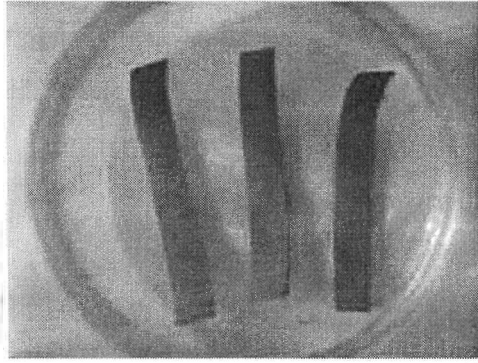
Fig. 1-3. EAP thin films

Magnetorheological Fluid (MRF): Suspensions that can reversibly change their state, from a liquid to a solid/gel like state, upon the application of an external magnetic field (Ciocanel, 2006). An image of such phenomenon is illustrated in Fig 1-4.
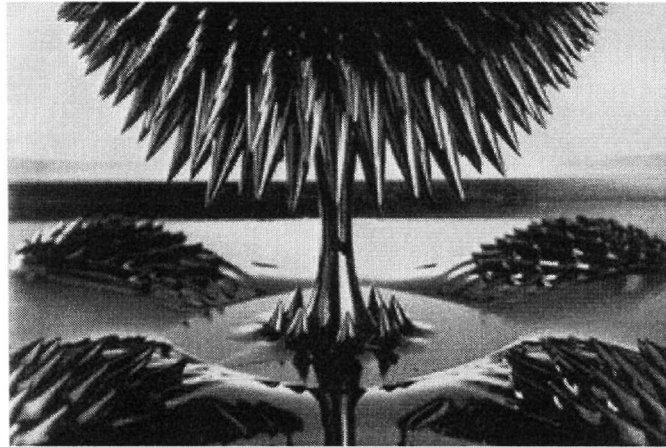
Fig. 1-4. MRF under influence of magnetic field (DesignVerb!, 2006)

Additional information about SM, their applications and impact can be found in Appendix 1.

1.1.2. Constitutive Model

A typical subject matter of materials science and engineering includes the description of phenomena and transformations occurring in materials (Dobrzanski, 2011). As part of this, a constitutive model is a way to mathematically describe the relationship between stress, strain and other state variables, allowing predicting material performance, selecting or developing the best material and to understand and avoid failure (Lujan, 2010).

Constitutive modeling is the mathematical description of how materials respond to various loadings and is the most intensely researched field within solid mechanics because of its complexity and the

importance of accurate constitutive models for practical engineering problems (Ottosen, 2005). For example, Hooke's law is the simplest of all constitutive models which relates stress and strain of a linear elastic material. However, different constitutive relations allow distinguishing between different materials. For example, polymer mechanics is very complex and various assumptions are made while developing a constitutive equation for them, then, it is generally infeasible to derive a universal constitutive model that would accurately represent their behavior under different loading conditions. Hence, the constitutive model that is developed for polymer is often limited to specific conditions of interest such as particular ranges of strain, stress, loading rate and temperature (Rajasekaran, 2011).

Formulation of constitutive models consists of (1) Perform experiments and observation, (2)Write relation between input and output, for example, stress and strain, (3) Do specific experiments to determine material coefficients and (4) Do predictive experiments to test theory (Lujan, 2010). It must be considered that constitutive models may be very different for the various materials used in engineering practice. However, to a large extent it is possible to employ the same principles and concepts in establishing constitutive relations for these different materials, despite the fact that the physics behind the macroscopical phenomena are entirely different. Indeed the characteristics of an engineering material are determined by its microstructure, all the way down to its atomic arrangement (Runesson, 2006).

Models of various forms have been developed nearly since the beginning of time and can be very simple, such as an 'if/then' relationship, or extremely complex mathematical expressions with numerous parameters, some of which may be easily measured and well understood and others that are not physically observable or readily inferred. All models have one thing in common: They attempt to provide improved understanding of the nature and the variables that influence and control the results of processes, whether a naturally occurring process or man-made. The study of processes leads to theories and subsequent models that can and are used to predict future applications of the studied process (Furrer, 2009). It must be considered that models represent the real object to some degree of completeness trying to be as simple as possible but not simpler (Gasser, 2005), these are just mathematical simplifications of a quite complex behavior, and there is no such thing as an 'exact' model (Runesson, 2006), for example Newton's motion equations are perfectly usable at 'normal' conditions, even if it is know that they are only special cases of the general relativity law. According to Gasser, the question for a model is 'does fulfills it the intended job?'. A good model predicts accurately the behavior of the real object/process; with respect to the intended use of the model, its complexity needs to be balanced with input variability (Gasser, 2005). Hence, the task of the engineer is to choose a model that is sufficiently accurate, yet not unnecessarily complex and computationally expensive (Runesson, 2006).

Manuel Ignacio Varela Jiménez

1.1.2.1. Types of Constitutive Models

According to Furrer, material behavior models can be grouped broadly into three classes: statistical, phenomenological, and mechanism based.

- **Statistical:** typically require large amounts of experimental data to derive a mathematical relationship between independent/controlled process parameters and predictions of process results. For example, linear regression analysis is often used to "fit" pairs or a series of data to determine relationships.

- **Phenomenological:** typically rely on equations that define the relationship between process variables and resulting microstructure, properties, and so on. These types of models can be used to describe phenomena such as recrystallization, grain growth, and creep of metallic materials. For example, Avrami (sigmoidal- type) equations have been used frequently to fit observations of the kinetics of static (and dynamic) recrystallization and other phase transformations during metals processing.

- **Mechanistic:** often called physics based due to their ability to include all of the relevant physical parameters that influence the outcome of a process to a high degree of fidelity. As such, mechanism-based models tend to be the most robust.

Additional information about constitutive models can be found in Appendix 2.

1.2. Research Justification

Nowadays it is expected to manufacture materials with properties ordered by products users, this changes the materials design methodology and the products materials design, as these have to be delivered on demand of products manufacturers with the appropriately formed structure, ensuring the required set of physical and chemical properties, and not as before when the manufacturers were forced to select material closest to their expectations from the delivered materials with the offered structure and properties, not meeting them fully, which is not permitted by this design methodology. Therefore, the actual trends force classification of engineering materials based on their functional characteristics and a change in the engineering materials role assessment is important, as they cannot be perceived any more as goods in themselves, with their applications sought for, and the market of the new engineering materials cannot remain the manufacturer's market any more (Furrer, 2009).

Design of devices based on SM requires of understanding its behavior and response to external conditions in order to evaluate their applicability and to avoid failure. This is obtained through constitutive

models that relate the stimulus applied and the reaction of the material to it.

Due to their special characteristics SM require of their own constitutive models and each one has been modeled and studied on a different way according to various principles and points of view. Thus, it is required to propose a common constitutive model that facilitates design of SM, analysis and simulation of devices based on them.

1.3. Hypothesis

SM can be described by a common constitutive model, despite of their origin, atomic structure, chemical bonds or physical domain.

1.4. Aims

1.4.1. General Objective

To generate a common theory for describing behavior of SM despite of their condition or natural or synthetic origin allowing proposition of constitutive models to understand and to analyze their response to an external stimulus.

1.4.2. Particular Objectives

- To propose a methodology for modeling SM and establishing constitutive models of their behavior and response to an external stimulus.

- *Shape Memory Alloy:* To model the effect of the twinned martensite - detwinned martensite – austenite strain/temperature induced phase transformation on the flow stress of Nickel – Titanium SMA.

- *Shape Memory Polymer:* To model the effect of the glassy – active temperature induced state transition on the flow stress of SMP.

- *Magnetorheological Fluid:* To model the effect of the liquid-solid magnetic field induced state transition on the shear yield stress of several MRF.

- *Electroactive Polymer:* To model the effect of the electric field induced concentration of ions on the bending of thin EAP thin films.

1.5. Methodology

Applied methodology to achieve aims of this dissertation consists of the next stages:

1. **Modeling of State Transition:** Based on phase transformation phenomena, state transition is described and two mathematical formulations to represent it are analyzed.

2. **Proposal of Strategy for Modeling SM by State Transition:** A mathematical expressions is taken as the basis for purposing a common methodology for modeling SM.

3. **Application of Modeling Strategy in SM:** Proposed strategy for modeling is applied for validation in four case studies: 1) NiTi SMA, 2)SMP, 3) EAP and 4) MRF.

4. **Conclusions:** Conclusions are done about the validation of the proposed constitutive models and the of the acceptance of the research hypothesis.

Stages 1 and 2 are covered in chapter 2 of this work. Chapters 3 to 6 present the case studies, while chapter 7 presents the conclusions.

Chapter 2.

Methodology for Constitutive Modeling of Smart Materials through the State Transition Concept

2.1. Background

To complement description of material behavior during processing, first principles approaches such as those based on atomistic and molecular dynamics calculations are developed to provide fundamental understanding of the mechanisms that control behavior of existing and emerging alloys. The refinement of models and modeling methods results in greater capability and accuracy of metallurgical predictions, such as phase equilibrium, microstructure, and subsequent mechanical properties. The linkage of component design, alloy design, and component manufacture through modeling and simulation methods will allow for continued advancement in the area of alloy research, advanced process and equipment development, and enhanced component capability. Modeling and simulation activities are increasing within the materials field as well as other science and engineering disciplines (Furrer, 2009).

2.1.1. Phase Transformation

A system may contain various kinds of materials. When it is under a set of external conditions such as a fixed temperature, the system approaches a unique state with well-defined characteristics. Once the system is in this unique state, it suffers no other change even after the lapse of indefinite time. After any temporary disturbance of the external conditions, the system returns to the initial state, which is the equilibrium or stable state under the given set of external conditions. The system usually contains regions which exhibit the same properties, such as specific volume, composition, and structure, these regions constitute a phase. Thus, a system at equilibrium may contain fixed volume fractions of a number of phases of well-defined characteristics. On alteration of the external constrains, the system would tend to change spontaneously to a mixture of phases whose structures, compositions, and morphologies are

different from those of the phases present initially in the system. Such changes are known as phase transformations which are invariably associated with changes in microstructure (Jena & Chaturvedi, 1992).

A phase has the following characteristics: (1) same structure or atomic arrangement throughout, (2) same composition and properties throughout and (3) there is a definite interface between the phase and any surrounding or adjoining phases (Askeland, 1994).

Microstructural characteristics of a system determine its properties. Therefore, transformation-induced microstructural changes also alter properties. By controlling the kinetics of transformations in a material, it should be possible to improve its performance considerably. Phase transformations are the basis of much of current materials technology. Significant advances in several engineering areas are based on understanding the thermodynamics and kinetics of transformations. Ability to work effectively with materials depends upon understanding of the basic principles of phase transformations and awareness of the methods of analysis (Jena & Chaturvedi, 1992).

A system starts to transform only when it is no longer stable. The stability of a system is determined by its thermodynamic characteristics. Transformation of an unstable system may involve considerable atomic rearrangement so that the required structural and compositional changes can occur. The atomic rearrangement may necessitate diffusion as well as reactions at the interfaces between the product and the parent phases. The exact nature of these processes is normally not known (Jena & Chaturvedi, 1992).

According to Zhigilei the process of phase transformation involves:

- **Nucleation of the new phase:** formation of stable small particles (nuclei) of the new phase. Nuclei are often formed at grain boundaries and other defects. It can be:
    - **Heterogeneous:** the new phase appears on the walls of the container, at impurity particles, etc.
    - **Homogeneous:** solid nuclei spontaneously appear within the undercooled phase.

- **Growth:** of the new phase at the expense of the original phase. Once a stable nucleus of the new phase exceeding the critical size r* is formed, it starts to grow. Atomically rough interfaces migrate by continuous growth, whereas atomically flat interfaces migrate by ledge formation and lateral growth (Zhigilei, 2010):

The process does not occur instantaneously and the time dependence of solid-state phase transformations at a fixed temperature is often described in terms of the time dependence of the fraction of transformation, as depicted in Fig 2-1.

Manuel Ignacio Varela Jiménez
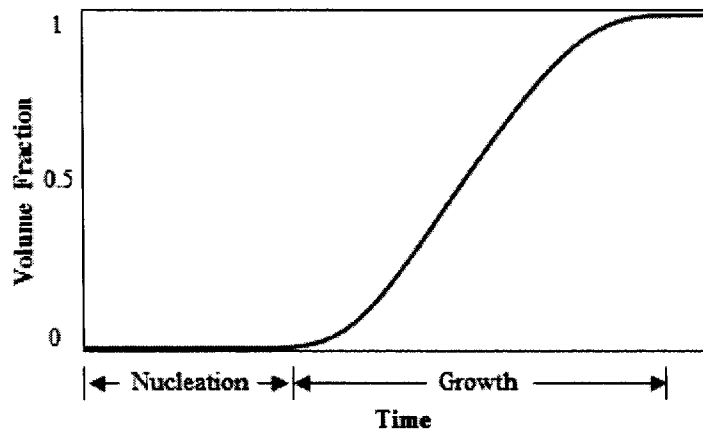
Fig. 2-1. Phase Transformation curve (Zhigilei, 2010)

2.1.2. Kolmogorov-Johnson-Mehl-Avrami Equation

The mechanism that drives numerous transition processes is the nucleation and growth of elementary objects of a new substance within the substance subject to transformations. The phenomena of this type are numerous and include crystal physics, metallurgy, polymer physics, ferroelectric domain switching, magnetization and metastability in statistical physics models, phase transitions in particle physics as well as biology or ecological landscapes. No matter how much these phenomena may differ, changes in the volume of the transformed fractions are described by the same statistical theory. The theoretical fundamentals of the mathematical formulae used nowadays were developed by Kolmogorov. Comprehensive case studies of the transformations are described in publications written by Johnson and Mehl and Avrami (Burbelko 2009).

Kolmogorov-Johnson-Mehl-Avrami (KJMA) equation describes how solids transform from one phase to another at constant temperature. It can specifically describe the kinetics of crystallization, but can also be applied generally to other phase changes of materials, like chemical reactions or the processes described in section 2.1.1. The equation was popularized when Melvin Avrami published a series of interesting papers in the *Journal of Chemical Physics* from 1939 through 1941 (Zang, 2010), so very often it is simply called Avrami equation. Since then, Avrami's theory has found several applications in different physicochemical contexts (Bosco, 1992).

Transformations are often observed to follow a characteristic S-shaped or sigmoidal profile as in Fig 2-1 where the transformation rates are low at the beginning and the end of the transformation but rapid in between. The initial slow rate can be attributed to the time required for forming a significant number of nuclei of the new phase. During the intermediate period the transformation is rapid as the nuclei grow into particles and consume the old phase while nuclei continue to form in the remaining parent phase. Once the

transformation begins to near completion there is little untransformed material for nuclei to form therein and the production of new particles becomes slow. Further, the particles already existing begin to touch one another, forming a boundary where growth stops (Zang, 2010).

The sigmoidal curve in Fig 2-1 is represented by KJMA equation (2-1) (Rollett, 2010)

$$Y = 1 - e^{-Kt^n} \qquad (2\text{-}1)$$

where K and n are constants while Y usually is the fraction of the transformed material. It is the volume fraction of the product phase which may be directly calculated from metallographic data. Measurements of resistivity, volume change and energy effects can also be used for a parametric representation of the extent of transformation (Jena & Chaturvedi, 1992). K and n are suitable parameters. K is temperature dependent. According to the original theory, n should be an integer from 1 to 4, the value of which should depend only on the type of the statistical model; however, it has become customary to regard it as an adjustable parameter that may be non-integral (IUPAC, 1997).

2.1.3. Cortes Equation for Phase Transformation

An example of phase transformations following a sigmoidal are austenitic stainless steels; on which an austenite-martensite phase transformation is induced by applying plastic strain during cold working according to the strain level and temperature. Cortes et al carried out compression tests monitoring the amount of martensite at several constant temperatures demonstrating that the rate of reaction is zero at the beginning and gradually increases to a maximum after a considerable amount of strain. This rate gradually decreases until almost no further transformation occurs upon further straining. The behavior is strongly influenced by the test temperature, as shown in Fig 2-2. As part of such work a model for the kinetics of strain-induced martensite phase transformation was developed (Cortes et al, 1992, 1993). Equation (2-2) expresses the volume fraction of strain-induced martensite

$$V_{fm} = \left[1 + \left(\frac{\varepsilon}{\varepsilon_c} \right)^{-B} \right]^{-1} \qquad (2\text{-}2)$$

where V_{fm} is the volume fraction of martensite, ε is the plastic strain, ε_c is the characteristic strain at which 50% of the phase transformation occurs and B is a constant experimentally determined.

Manuel Ignacio Varela Jiménez
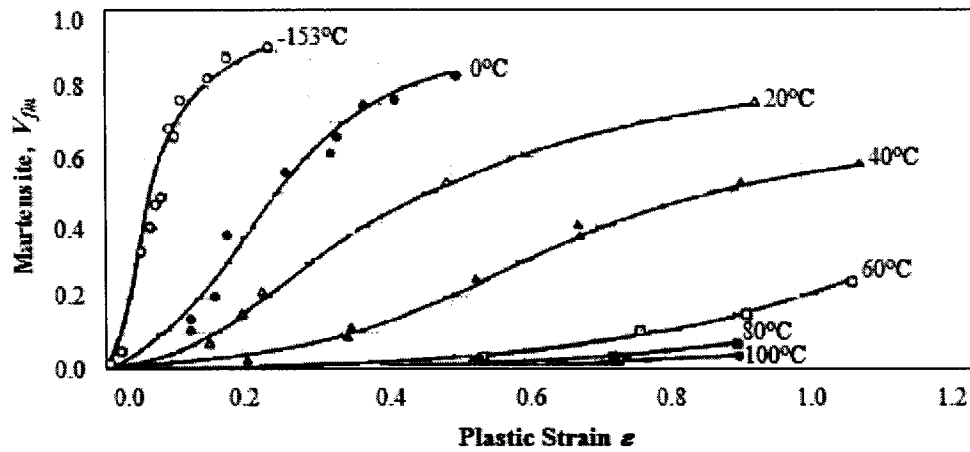
Fig. 2-2. Strain-induced martensitic transformation at several temperatures for 304 stainless steel (Cortes et al, 1992, 1993).
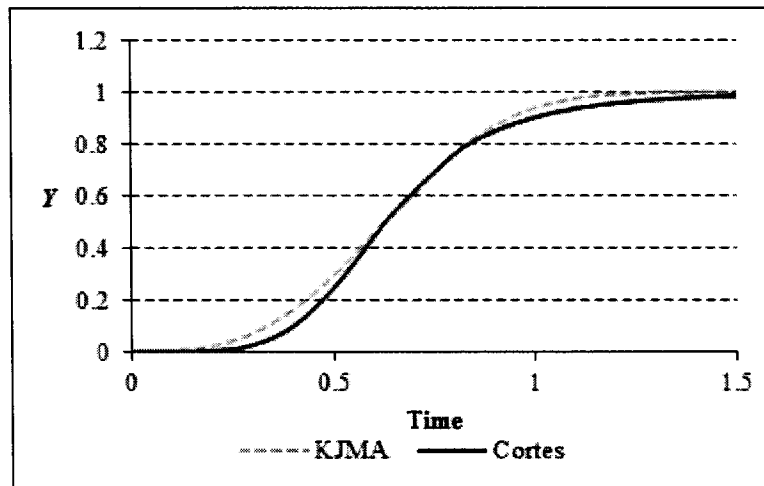
Fig 2-3. Fitting of KJMA and Cortes equations. K=2.8, n=3. t_c=0.63, B=4.83

2.1.4. Fitting of phase transformation equations

Due that equation (2-2) describes a sigmoidal phase transformation it can be applied for describing similar phenomena as KJMA equation if a correspondence between ε and t is done, resulting in expression (2-3) denoted as Cortes Equation

$$Y = \left[1 + \left(\frac{t}{t_c} \right)^{-B} \right]^{-1} \tag{2-3}$$

where t_c is the characteristic time at which 50% of the phase transformation occurs. This is demonstrated in Fig 2-3, where both equations are plotted. In this example case, the arbitrary assigned values of K and n are 2.8 and 3, respectively; it is observed that Y has a value of 0.5 when time is 0.63 and thus that is the

value of t_c. By least squares method, parameter B is determined in order to fit both plots, resulting in a value of 4.83 for B.

According to Fig 2-3, there is not a perfect fitting between both plots, however it is demonstrated that both equations describe sigmoidal behaviors. Comparing them, KJMA requires of two constants to be fitted while Cortes equation requires only parameter B to be determined through experimental work, which results in an advantage for modeling of materials.

2.2. State Transition Concept for Smart Materials

2.2.1. Constitutive Equation of State Transition

Phase transformations are natural phenomena that occur in some materials such as stainless steels or NiTi, however, kinetics of transformations from a state A to a state B are universal. Examples of these are; cell growth as described by Pitner et al illustrated in Fig 2-4 or turbidity change in liquid-crystalline polymer microparticles described by Liu et al, depicted in Fig 2-5. In both cases transition from an initial state A to a resultant state B follows a sigmoidal behavior as time is increased in the same way a phase grows up in steels by diffusion.
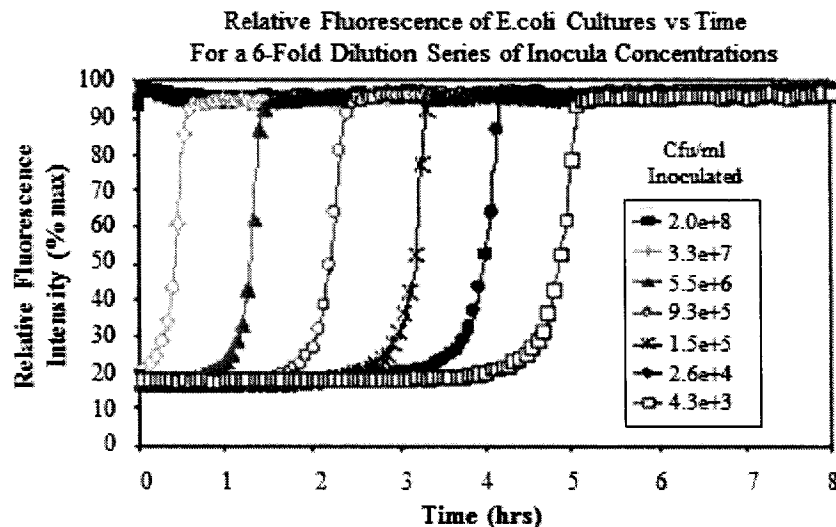
Fig. 2-4. Kinetics of cells growth (Pitner et al, 1999)

Following this concept, behavior of SM can be described as a state transition. According to the concepts of Jena & Chaturvedi; SM can be considered as a system in unique state under fixed external conditions, when an external stimulus is applied a disturbance of the conditions occurs and then the system is no longer in equilibrium, then it tends to transform in order to recover stability.

Manuel Ignacio Varela Jiménez
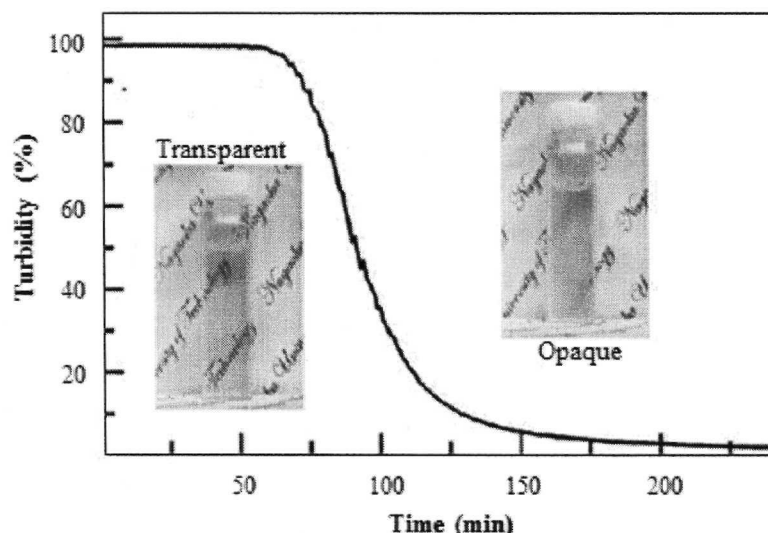
Fig. 2-5. Time course of the turbidity change of liquid-crystalline polymer microparticles (Liu et al, 2011)

By considering the state transition concept in SM it can be developed a methodology to study such materials by a common constitutive model, which facilitates its modeling and understanding of their behavior. Despite if these are metals, polymers or other kind of materials; in all SM exist a reaction to an external stimulus that generates transition between two states following a sigmoidal behavior, thus, the response of man-made SM such as EAP, MRF or SMP can be modeled by considering the volume fraction of each state of the material; initial state *A* has a volume fraction (V_{fA}) of 1, when the stimulus is applied the material transitions to state *B*, as it occurs V_{fA} decreases from 1 to 0 while V_{fB} increases from 0 to 1, as shown in Fig 2-6.

Taking into account that state transitions do not occur instantaneously and follow an S curve these can be modeled through a modified Cortes equation, adapted to the physical domain of the material that is being studied. However, a methodology to propose the transition and to fit the equation is still required.

In order to be applied in SM; Cortes equation is modified to describe V_{fB} as function of an applied stimulus *X* resulting in equation (2-4) which is referred as State Transition Equation (STE)

$$V_{fB} = \left[1 + \left(\frac{X}{X_c} \right)^{-B} \right]^{-1} \tag{2-4}$$

where the external stimulus *X* is a variable such as strain, temperature, voltage, magnetic field or any other engineering physical variable. X_c represents the value of X at which 50% of the state transition occurs and V_{fA} has a value of 0.5 and *B* is a fitting parameter which can be determined by least squares

method applied to the difference between experimental and predicted data of volume fraction. V_{fA} is given by equation (2-5)

$$V_{fA} = 1 - V_{fB}$$ (2-5)
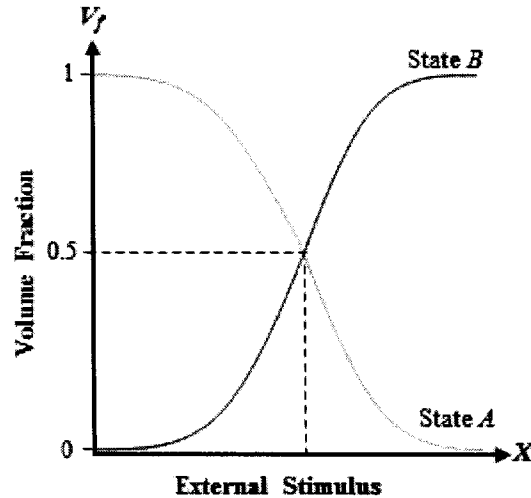
Fig. 2-6. State Transition of Smart Materials

2.2.2. Methodology for Modeling Smart Materials through the State Transition Concept

Use of equations (2-4) and (2-5) on SM requires of state transition proposition. For SM; as stated in section 2.2.1, steady state is assumed as state A, if an external stimulus X is applied the material reacts showing its 'smart' response transitioning to state B. For example in a MR fluid, when it is in liquid state it is state A, if an external stimulus; in that case a magnetic field, is applied the material increases its apparent viscosity becoming semisolid and transitioning to state B.

According to these phenomena the following methodology can be applied for fitting of STE:

Proposition of a state transition: An atomic arrangement A exists when SM is in steady state and atomic arrangement named B exists when an external stimulus is applied on the material, such arrangement is considered a state and rearrangement is assumed as a state transition.

Formulation of a model to describe state transition: A constitutive equation of state transition $A - B$ is proposed, in which the external stimulus X is the main variable of STE (2-4).

Experimental quantification of state transition: Response of the material to its external stimulus is quantified, based on this data volume fraction of each state is estimated. This is achieved through a controlled reaction of the SM response, for example measurement of the viscosity of a MR fluid as the magnetic field is increased.

Fitting of constitutive model: By using volume fraction – external stimulus data, STE (2-4) is fitted since V_f, X and X_c are experimentally known, then, by least square method B can be determined.

Validation of constitutive model: Constitutive model is applied and its approximation level is verified by comparison with experimental data.

2.3. Discussion

A methodology to model SM through the state transition concept based on phase transformation phenomena has been proposed, according to it, response of SM can be described by a common mathematical expression if a transition between two states can be proposed and quantified by a controlled reaction of the material.

Phase transformation is a natural phenomenon that occurs in metallic materials; however the behavior of the transition follows a sigmoidal behavior that also occurs in other kinds of materials or situations. This allows considering that contrary to what stated by Rajasekaran, it is possible to model SM by using a common constitutive model that represents its behavior based by a state transition concept based on phase state transition concept.

State transition of MRF, EAP or SMP; can be proposed by considering that when the material is in steady state A, if an external stimulus X is applied nucleation of state B occurs in the same way a phase transformation occurs; when X is at an determined level nucleation finishes and growth stage starts, then A transitions to B, if X keeps increasing also V_{fB} does it, but at some level, the increase rate of V_{fB} is near zero, at that time the phase transformation is finished.

If state transition in SM is proposed it should also be quantified. Volume fraction of each state can be measured by experimental work through controlled reaction of the material according to its physical domain. Examples of this are detailed in the following chapters of this dissertation.

State transitions occur gradually following a sigmoidal behavior that can be modeled through KJMA equation, however, Cortes equation can be modified in order to adapt to various physical domains and describe state transitions of SM resulting in the State Transition Equation (STE).

Based on Cortes' work, STE is flexible and able to adapt to any physical domain by taking any external variable as the main parameter which induces the state transition allowing modeling different kinds of SM, despite of its physical state, physical domain or composition.

KJMA equation could also be applied for modeling of SM, however it involves fitting of two unknown parameters that are not related to any physical domain, which results more complicated since STE involves only the fitting of a parameter which can be done through least squares method with experimental data.

STE can be adapted to any physical domain in a systematic way; its parameters can have a physical meaning and the parameter B is calculated by numerical methods. By experimental work and analysis each of the parameters of STE can be related to some variable of the material, enabling its application not only for analysis but also for material design.

Due that STE is flexible to any physical domain it can also be applied to other kind of system in which a transition between two states following a sigmoidal behavior occurs, such as the biological one presented by Patil.

Part II. Application

Chapter 3.

Unidimensional Constitutive Model of Stress of Nickel – Titanium Shape Memory Alloy

3.1. Background

Nickel – Titanium alloy (NiTi) is a smart material with properties such as shape memory effect (SME) and superelasticity (Chang & Wu, 2007). SME involves the recovery of residual inelastic deformation by raising the temperature of the material above a transition temperature, whereas in superelasticity, large amounts of deformation (up to 10%) can be recovered by removing the applied loads (Azadi et al, 2007). SME is demonstrated in Fig 3-1, in which a strained NiTi spring recovers its original length due to increase of temperature when heat is applied.
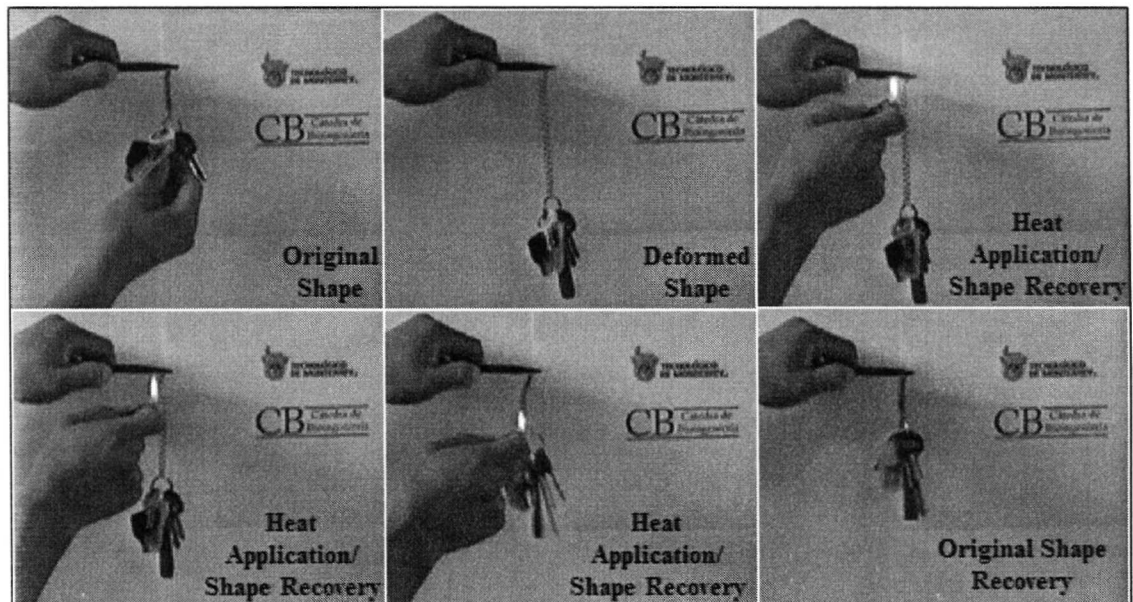
Fig. 3-1. NiTi shape recovery due to increase of temperature

The first reported works related to shape memory effect (SME) were taken in the 1930's when Ölander discovered the superelasticity behavior of the Au-Cd alloy. In 1938 Greninger and Mooradian observed the formation and disappearance of martensitic structure by decreasing and increasing the temperature of the Cu-Zn alloy. In 1960's, Buehler and his coworkers at the United States Naval Ordnance Laboratory discovered the SME in equiatomic NiTi which was named Nitinol: Nickel - Titanium Naval Ordnance Laboratory (Ryhänen, 1999).

3.1.1. Temperature Induced Phase Transformation

The microscopic mechanisms involved in SME are strongly correlated to the transformation from a highly ordered austenite at high temperature to a less ordered martensite structure at low temperature (Lahoz & Puértolas, 2004). It is a reversible, displacive, diffusionless, solid–solid phase transformation (McNaney et al, 2003). Austenite has a body centered cubic lattice while martensite is monoclinic. When NiTi with martensitic structure is heated, it begins to change into austenite. This phenomenon starts at a temperature denoted by A_s and is complete at a temperature denoted by A_f. When austenitic NiTi is cooled, it begins to return to its martensitic structure at a temperature denoted by M_s and the process is complete at a temperature denoted by M_f (Nemat-Nasser & Guo, 2006). Because austenite is usually higher in strength than martensite, a large amount of useful work accompanies the shape change (De Castro et al, 2007).
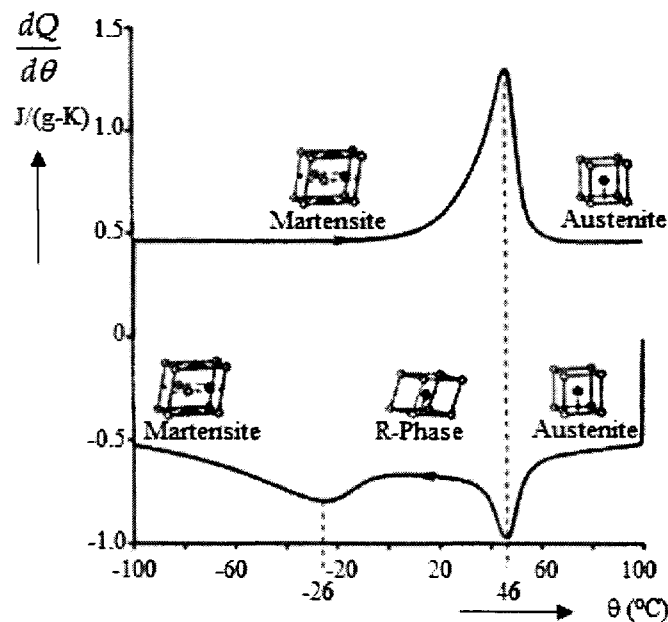
Fig. 3-2. DSC of NiTi wire (Shawn & Kyriakides, 1995)

The transformation of the material from one structure to another can be monitored through Differential Scanning Calorimetry (DSC). Fig 3-2 displays a thermogram in which the material was heated

from approximately -70°C to 100°C. At low temperatures the material is in martensite. The power peak at a temperature of approximately 50°C corresponds to an endothermic transition to austenite. The construction lines indicate idealized values for A_s and A_f. For temperatures within these values the two phases coexist. In the lower thermogram the material was cooled from approximately 100 to -70°C. It starts as austenite and finishes as martensite via an intermediate phase with a rhombohedral lattice known as the R phase (Shawn & Kyriakides, 1995).

It is considered that composition (Nemat-Nasser & Guo, 2006) and heat treatments have effect on the A_s, A_f, M_s and M_f called transformation temperatures; these are shown in Fig 3-5 and are the prerequisite for the material to exhibit the SME and are one of the key parameters for SME based actuation, they also define the proper application for a certain NiTi composition (Malukhin & Ehmann, 2006).

3.1.2. Strain Induced Phase Transformation

When NiTi is stressed at a temperature close to A_f, it can display superelastic behavior. This stems from the stress-induced martensite formation, since stress can produce the martensitic structure at a temperature higher than M_s, where macroscopic deformation is accommodated by the formation of martensite. When the applied stress is released, the martensitic phase transforms back into the austenitic phase and the specimen returns back to its original shape (Nemat-Nasser & Guo, 2006). The stress-induced austenite-martensite transformation is effected by the formation of martensitic structures which corresponds to system energy minimizers (McNaney et al, 2003) as result of the need of the crystal lattice structure to accommodate to the minimum energy state for a given temperature (Ryhänen, 1999). Strain induced martensite is shown in Fig 3-3.

Shaw explains in more detail martensite behavior, affirming that due to its low degree of symmetry, it exists either as a randomly twinned structure (low temperature, low stress state) or a stress-induced detwinned structure that can accommodate relatively large, reversible strains (Shaw, 2002). Temperature and strain induced temperatures are represented in Fig 3-4.

As shown in Fig 3-5; stress induced martensite transformation can start at temperatures above A_f after heating or M_s during cooling. However, in a determined temperature range ($T > A_s$), the tensile curves of NiTi exhibit superelastic 'flags', becoming more difficult to induce martensite by stress as the temperature increases. Along with the increase in the stress, the permanent set also increases with the temperature, this way; M_d is considered the temperature from which material is deformed like ordinary materials by slipping. Thus, stress-induced superelasticity behavior appears in a temperature range from near A_f and up to M_d (Pelton et al, 2000). The largest ability to recover occurs close to A_f (Ryhänen, 1999).
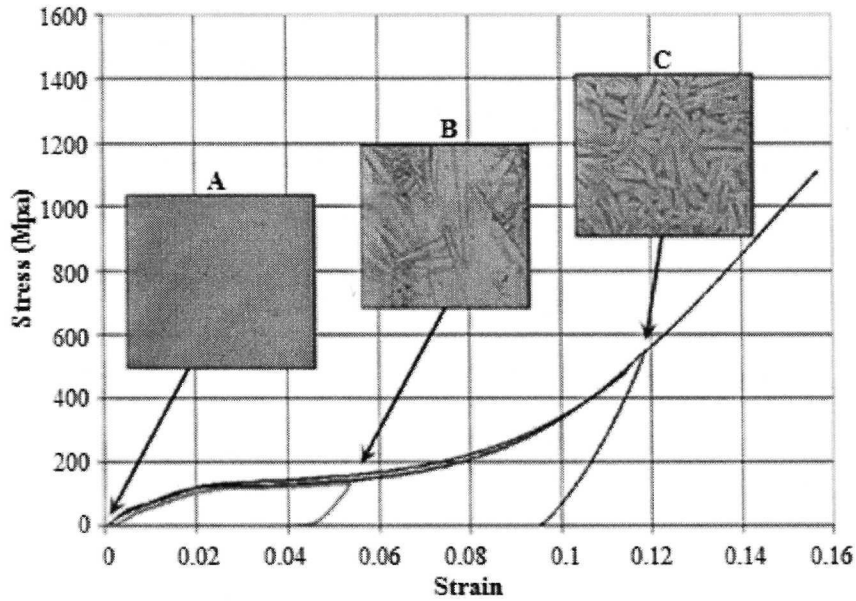
Fig. 3-3. Microstructural Evolution of NiTi along its Stress-Strain curve, where:
A)   Austenite, B) 50% Austenite 50% Martensite, C) 100% Martensite (de la Garza et al, 2007).
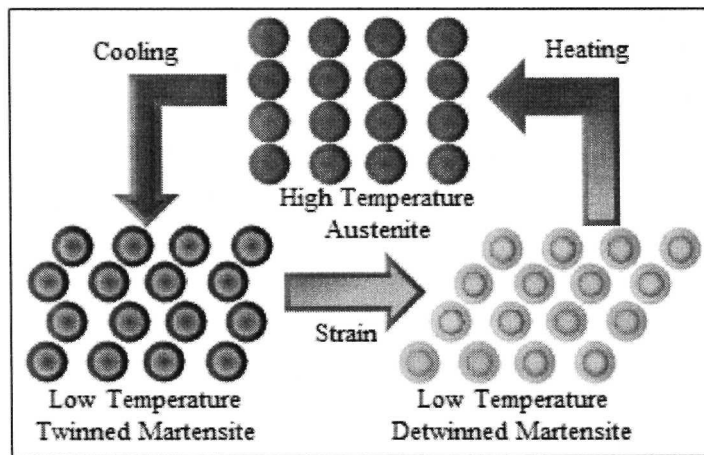
Fig. 3-4. Strain/Temperature Induced Phase Transformations in NiTi
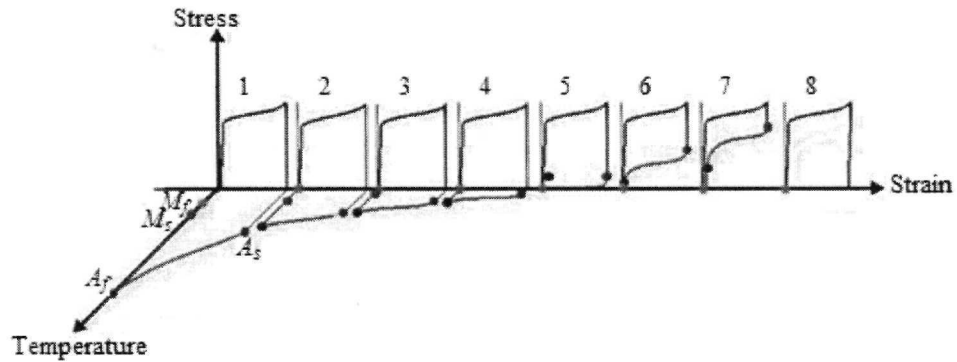
Fig 3-5. Relation between Temperature and Transformation
Temperature on Mechanical Behavior of Nickel – Titanium Alloy.
Curves 1-3) $T_x << A_f$, 4) $T_x < A_f$, 5) $T_x = A_f$, 6) $T_x > A_f$, 7) $T_x >> A_f$, 8) $T_x > M_d$

3.1.3. NiTi Applications and Research Justification

An application of NiTi is in medical area, stents are used for treatment of occluded blood vessels, applying characteristics of the material: biocompatibility, large recoverable deformation, good fatigue life, including superelasticity and SME around body temperature (Ng & Sun, 2006). This way, self-expanding stents can be manufactured with a diameter larger than that of the target vessel and a transformation temperature around 30°C, be crimped at room temperature and placed in a delivery system; then, at the target area in the vessel, the stent is released and expands at body temperature until it hits the artery wall and conforms to it (Burt & Hunter, 2006).

Up to day, several studies have been made about NiTi, but there is a lack in the development of numerical analysis of the phenomenology of the material (De la Garza et al, 2007), since its application requires a proper characterization; a constitutive model is needed in order to relate microstructure and thermo-mechanical behavior of NiTi.

3.2. Proposition of State Transition in NiTi

Fig 3-6 shows the thermomechanical response of a wire specimen first quenched in liquid nitrogen to minimize the appearance of the R-phase. It is first subjected to a load/unload cycle at low temperature, leaving an apparent permanent strain. The material starts in a twinned martensite (TM) state and becomes detwinned (DM) upon loading. The specimen is then subjected to a temperature increase while holding the load. The SME is seen as the strain is recovered and the material transforms to austenite (A). The temperature is then held at high value and the specimen is again subjected to a load/unload cycle. In this case the material shows superelasticity and transforms from austenite to detwinned martensite during loading and then back to austenite during unloading (Shaw, 2002).
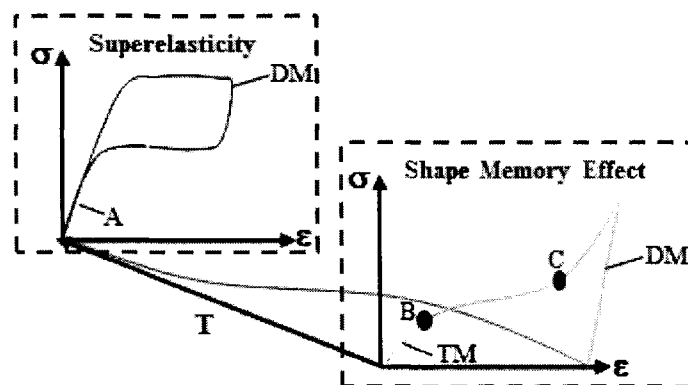
Fig. 3-6. Thermomechanical cycle of NiTi (Shaw, 2002)

According to Fig 3-6, volume fraction of each microstructure depends of the strain and temperature conditions and it also has influence on the mechanical behavior of the material. The possible phase

transformations or state transitions on NiTi are shown in Fig 3-7, strain induces detwinned martensite while temperature increase induces austenite.
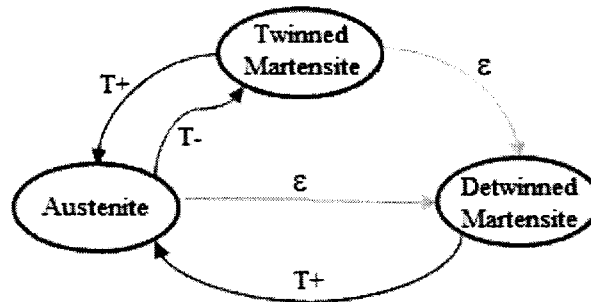
Fig. 3-7. Phase Transformations in NiTi and their induction stimulus

According to Fig 3-7, phase transformations or state transitions in NiTi are:

1. Twinned martensite to Detwinned martensite (Strain induced)

2. Detwinned martensite to Austenite (Temperature increase induced)

3. Austenite to Detwinned Martensite (Strain induced)

4. Twinned martensite to Austenite (Temperature increase induced)

5. Austenite to Twinned Martensite (Temperature decrease induced)

Following the concept presented in chapter 2, these phase transformations or state transitions occur following a sigmoidal behavior, in these cases induced by strain or temperature as shown in Figs 3-8 and 3-9. For this work, transitions that involve temperature decrease are not considered.
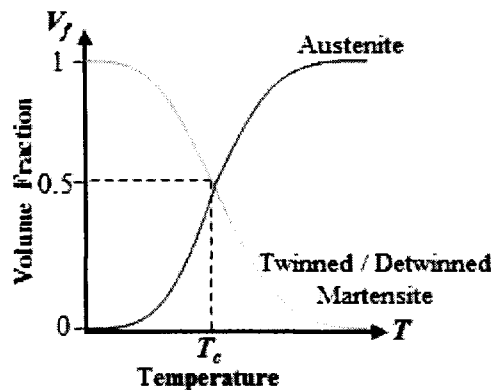
Fig. 3-8. Temperature Induced Phase Transformation on NiTi
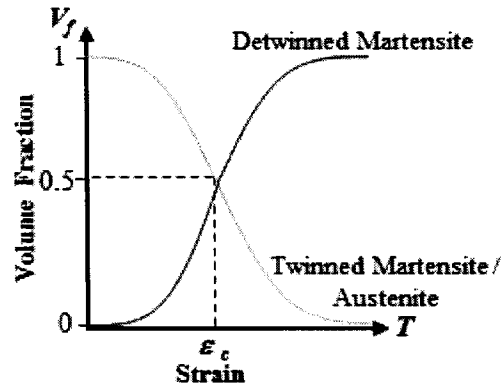
Fig. 3-9. Strain Induced Phase Transformation on NiTi

3.3. Formulation of model of state transition and flow stress of NiTi

Establishment of a constitutive equation for phase transformation in NiTi requires considering the thermomechanical cycle of Fig 3-6 and phase transformations/state transitions of Fig 3-7 that involve strain and temperature increase.

Following the concepts presented in chapter 2, STE can be adapted phase transformations of NiTi and consider them as state transitions. In addition, flow stress of the material can be described based on Cortes et al work, who developed a model for determining flow stress of aggregates, based on an energy criterion which defines the energy consumed to deform the phases in the system as being equivalent to energy consumed to deform the aggregate and it is able to predict the flow stress behavior of the material (Cortes et al, 1992, 1993).

In order to apply STE and Cortes model in SMAs; austenite, twinned and detwinned martensite are considered as the aggregates and the microstructural transition between them becomes the basis of the model; this way, the constitutive equation results in terms of the mechanical properties of each structure and its volume fraction.

3.3.1. Constitutive Model of Flow Stress

In the case of NiTi, the aggregate is composed of austenite and martensite, based on Cortes model V_f of each structure or aggregate are defined as:

$$V_{fa} = \frac{V_a}{V_t} \qquad\qquad V_{ftm} = \frac{V_{tm}}{V_t} \qquad\qquad V_{fdm} = \frac{V_{dm}}{V_t} \qquad (3\text{-}1)$$

where subscripts *a*, *tm* and *dm* indicate austenite, twinned and detwinned martensite, respectively. Cortes constitutive model of flow stress for multi phases aggregate (Cortes et al, 1992) applied in NiTi is

$$\sigma_t = V_{fa} \cdot \sigma_a + V_{ftm} \cdot \sigma_{tm} + V_{fdm} \cdot \sigma_{dm} \tag{3-2}$$

where σ_t is stress of NiTi and σ_a, σ_{tm} and σ_{dm} are stress of each structure.

3.3.2. Kinetics of Strain/Temperature Induced Twinned Martensite – Detwinned Martensite and Detwinned Martensite - Austenite Phase Transformation

Based on the thermomechanical behavior of Fig 3-6 and the phase transformations/state transitions shown in Fig 3-7, volume fraction of the microstructures varies by:

$$V_{fa} + V_{ftm} + V_{fdm} = 1 \tag{3-3}$$

$$V_{ftm} = 1 - V_{fa} - V_{fdm} \tag{3-4}$$

Fig 3-10 shows the influence of temperature and strain on the microstructural content of NiTi.
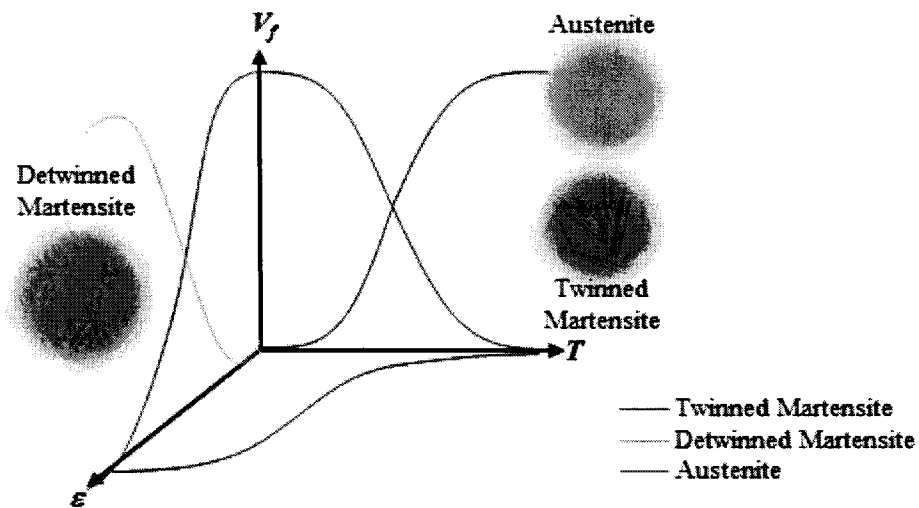
Fig. 3-10. Influence of temperature and strain on the microstructural content of NiTi

For strain induced detwinned martensite phase transformation:

$$V_{fdm} = \left[1 + \left(\frac{\varepsilon}{\varepsilon_c} \right)^{-B_\varepsilon} \right]^{-1} \tag{3-5}$$

For temperature induced austenite phase transformation:

Manuel Ignacio Varela Jiménez

$$V_{fa} = \left[1 + \left(\frac{T}{T_c} \right)^{-B_T} \right]^{-1}$$

(3-6)

where B is a fitting constant whose value depends of stimulus applied (strain ε or temperature T); while ε_c and T_c represent the values of strain and temperature, respectively at which 50% of the phase transformation is occurred. Experimental work is required for determining these values for each state transition.

3.4. Experimental quantification of state transition

3.4.1. Material

Flexinol® Muscle Wires® from *Muscle Wires*™ of 100, 200 and 300 µm of diameter were used as received for experiments; their activation temperature is 90°C. Wires were cut in samples of 25cm.

3.4.2. Methodology

Experiments consisting of electric resistance characterization, volume fraction estimation and tensile tests are carried out as described win Fig 3-11.
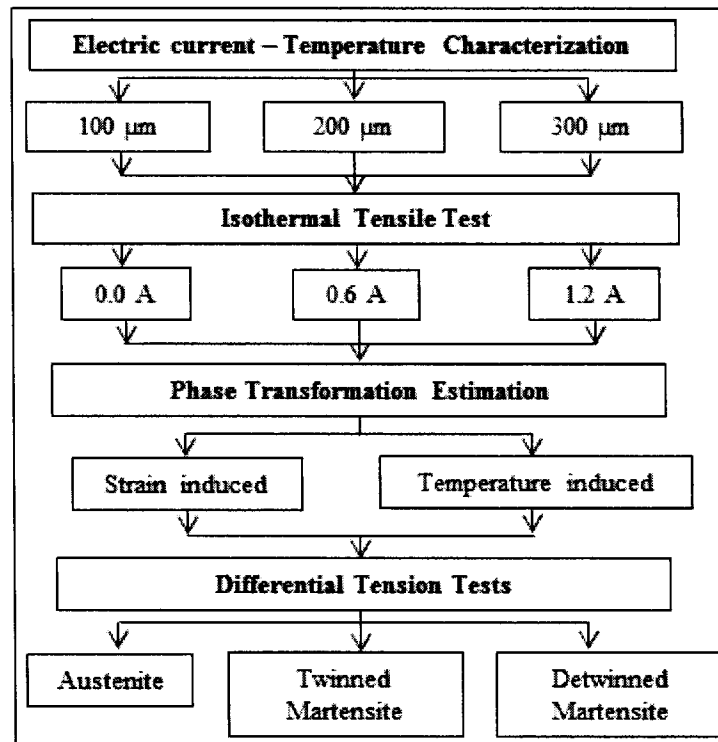
Fig. 3-11. Experimental work Methodology

3.4.2.1. Electric current – Temperature Characterization

Heating of NiTi wires by electrical current is characterized in order to control its temperature during mechanical experiments. A DC power supply (*B&K Precission*™ model 1761) generates electric current, when it is connected to NiTi wire it acts as resistor and voltage is generated. Tests are carried out by fixing the amount of electric current supplied to NiTi and measuring its temperature by using a thermocouple *Fluke*™.

3.4.2.2. Volume Fraction Estimation

A. Temperature Induced Phase Transformation

Detwinned martensite – austenite phase transformation is estimated by straining NiTi wires with an universal tension test machine (*MTS*™ model *Insight 2*), this way the length of wires is increased and detwinned martensite is induced. When these are heated, original length is recovered by increasing the volume fraction of austenite. From length measurement, strain is calculated for several temperatures and a strain – temperature relationship is plotted, having a behavior similar to the illustrated in Fig 3-6. Estimation of volume fraction is done by considering the strain axis of such plot, a V_f axis, with minimal and maximal values of 0 and 1, respectively; assuming that at maximal strain and minimal temperature the volume fraction of detwinned martensite (V_{fdm}) is 1; at the temperature where strain recovery start is observed it is assumed that martensite also starts to transform into austenite; at 50% of such process the inflexion point of strain – temperature curve exists and V_f of both microstructures is 0.5; at minimal strain and maximal temperature V_{fdm} is 0 and NiTi has recovered its original length.

B. Strain Induced Phase Transformation

According to Fig 3-6 detwinning of martensite occurs between points *B* and *C* which are found on experimental stress-strain plots of NiTi wires; at point *B* it is assumed that V_{ftm} is 1 and at point *C* it is assumed to be 0. This way, for each strain value between *B* and *C* a V_f value of twinned martensite between 0 and 1 is estimated, for example, at the middle strain value between *B* and *C* V_f is 0.5.

3.4.2.3. Differential Tensile Tests

Since NiTi contains a heterogeneous microstructure under given conditions, an incremental change test to determine hardening parameters in a given structure was carried out. Based in Cortes et al work, flow stress of austenite and martensite is determined under isothermal conditions, by pre-straining NiTi wires at a temperature at which only one microstructure exists, and then, the specimens were individually

Manuel Ignacio Varela Jiménez

deformed at a predefined electric current amount. The yielding point in reloading is registered as the flow stress at that electric current and strain conditions.

In order to define flow stress of the austenitic phase under isothermal conditions, differential tests are carried out. For each temperature condition, different wires are pre-strained at 120°C and at different strain levels: 2%, 4%, 6%. Under such conditions, V_{fdm} is insignificant. Then each specimen is deformed again, but now applying specific amounts of electric current during the test, and the point of yield on each strain level is measured. The curve obtained by fitting the yield points under recompression is defined as the flow stress of austenite under each temperature condition.

3.4.2.4. Tensile Tests

Tensile tests are carried out on NiTi wires under isothermal conditions at 22, 45, 68 or 120°C by supplying electric current to the material during the test. From such tests, strain induced phase transformation is estimated, as described in section 3.4.2.2.

3.4.3. Results

3.4.3.1.   Electric current – Temperature Characterization

Fig 3-12 shows behavior of temperature of NiTi wires when electric current is supplied. Equation (3-7) relates electric current i (in Amperes) and temperature T of NiTi as function of wire diameter d (in micrometers), where T_r is room temperature (in Celsius degrees), while J and λ are material constants.

$$T(i) = T_r \cdot e^{i(J \cdot e^{\lambda \cdot d})} \qquad\qquad (3\text{-}7)$$
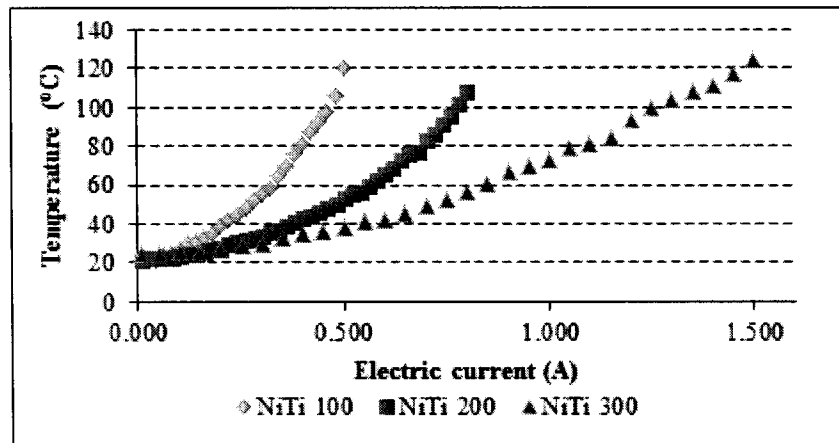
Fig. 3-12. Experimental Electric Current - Temperature behavior of NiTi wires of 100, 200 and 300 μm diameter

3.4.3.2.   Volume Fraction Estimation

A. Temperature Induced Phase Transformation

Approach to detwinned martensite – austenite phase transformation is shown in Fig 3-13, depicting behavior for different NiTi wire diameters.

Relationship between V_{fa} and electric current is given by equations (3-8) and (3-9), i_c is the characteristic current representing the condition under which 50% of the total volume changes to austenite on each isothermal curve as shown in Fig 3-12 while B_T is a material constant.

$$V_{fa} = \left[1 + \left(\frac{i}{i_c} \right)^{-B_T} \right]^{-1} \tag{3-8}$$

$$i_c = A_T \cdot e^{Q_T \cdot d} \tag{3-9}$$

A and Q are constants for NiTi. V_{fdm} can be calculated through equation (3-10)

$$V_{fdm} = 1 - V_{fa} \tag{3-10}$$
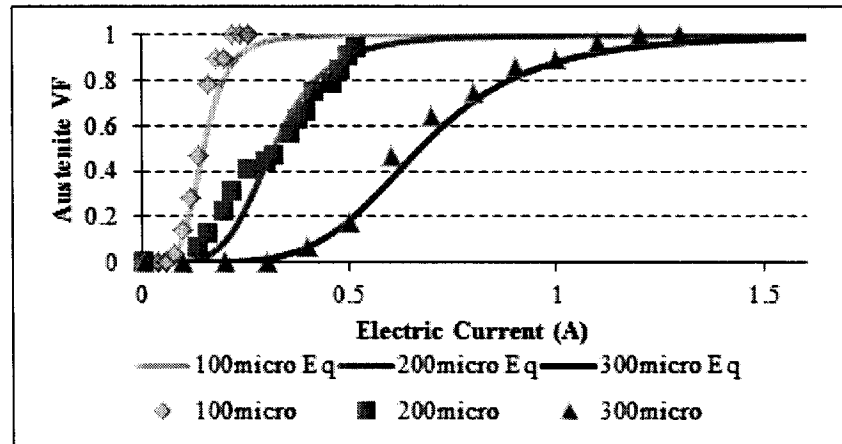
Fig. 3-13. Experimental (points) and Theoretical (line) Austenite Volume Fraction - Electric Current behavior of NiTi wires of 100, 200 and 300 μm diameter

B. Strain Induced Phase Transformation

Approach to twinned martensite – detwinned martensite phase transformation is shown in Fig 3-14 showing behavior at different temperatures.

Relationship between V_{fdm} and strain ε is given by equations (3-11) and (3-12), ε_c is the characteristic strain which represents the condition that 50% of the total volume changes to detwinned martensite on each isothermal curve as shown in Fig 3-12 while B_ε is a material constant

$$V_{fdm} = \left[1 + \left(\frac{\varepsilon}{\varepsilon_c}\right)^{-B_\varepsilon}\right]^{-1} \tag{3-11}$$

$$\varepsilon_c = A_\varepsilon \cdot e^{Q_\varepsilon \cdot i} \tag{3-12}$$

A_ε and Q_ε are constants for NiTi and i is the electric current supplied to the material. V_{ftm} can be calculated through equation (3-13)

$$V_{ftm} = 1 - V_{fdm} \tag{3-13}$$
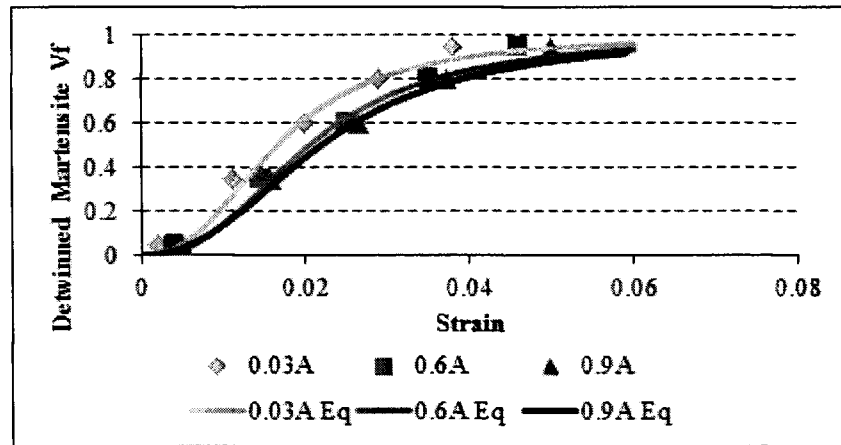
Fig. 3-14. Experimental (points) and Theoretical (line) Detwinned Martensite Volume Fraction - Strain behavior of NiTi wires of 100, 200 and 300 μm diameter

3.4.3.3.　Differential Tensile Tests

A. Twinned Martensite

Fig 3-15 shows flow stress of twinned martensite at different temperatures. Each curve represents the test at some specific temperature below A_f for a wire with initial twinned martensite structure.

From such curves, equations to predict stress of twinned martensite are obtained. These are as function of strain and electric current

$$\sigma_{tm} = K_{tm} \cdot \varepsilon^{N_{tm}} \tag{3-14}$$

　　　　　　　　　　　　　　　　　　　Manuel Ignacio Varela Jiménez

$$K_{tm} = C_{tm} \cdot e^{D_{tm} \cdot i} \tag{3-15}$$

$$N_{tm} = F_{tm} \cdot e^{G_{tm} \cdot i} \tag{3-16}$$
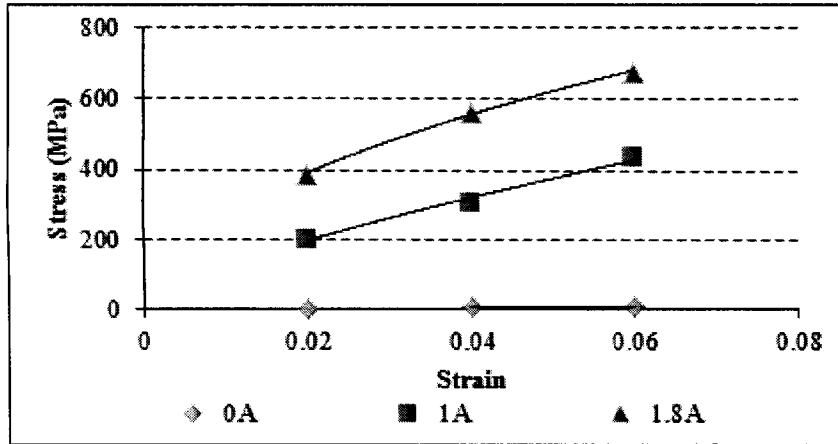
Fig. 3-15. Experimental Flow stress of Twinned Martensite under different electric current levels

B. Detwinned Martensite

Flow stress of detwinned martensite at different temperatures is shown in Fig 3-16. Each curve represents the test at some specific temperature below A_f for a wire with initial detwinned martensite structure.

Equations to predict stress of detwinned martensite function of strain and electric current are obtained from these tests

$$\sigma_{dm} = K_{dm} \cdot e^{N_{dm} \cdot \varepsilon} \tag{3-17}$$

$$K_{dm} = C_{dm} \cdot e^{D_{dm} \cdot i} \tag{3-18}$$

$$N_{dm} = F_{dm} \cdot e^{H_{dm} \cdot i} \tag{3-19}$$
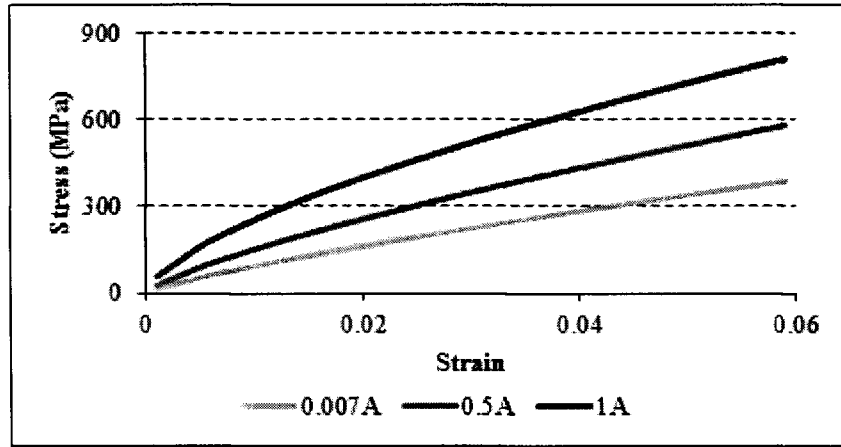
Fig. 3-16. Experimental Flow stress of Detwinned Martensite under different electric current levels

C. Austenite

Fig 3-17 shows flow stress of austenite at different temperatures. Each curve represents the test at some specific temperature above A_f.
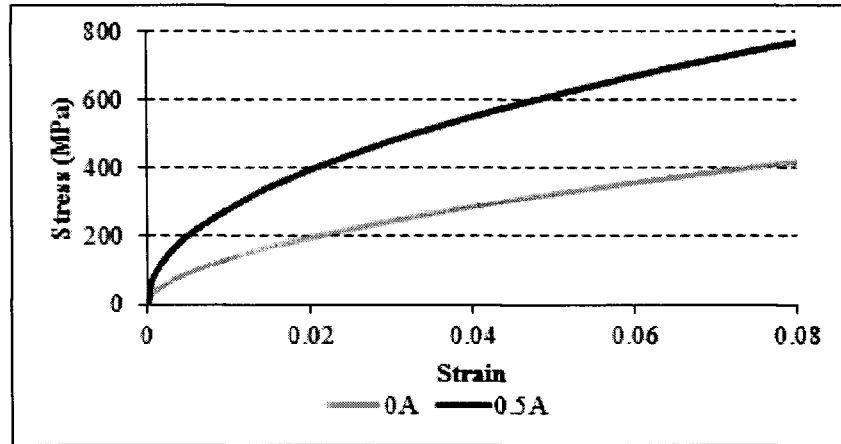
Fig. 3-17. Experimental Flow stress of Austenite under different electric current levels

From such curves, equations to predict stress of austenite are obtained. These are as function of strain and diameter.

$$\sigma_a = K_a \cdot \varepsilon^{N_a} \tag{3-20}$$

$$K_a = C_a \cdot e^{D_a \cdot i} \tag{3-21}$$

$$N_a = F_a \cdot e^{G_a \cdot i} \tag{3-22}$$

3.4.3.4. Tensile Tests

Fig 3-18 describes stress – strain behavior for NiTi wires at different temperatures by applying electric current as described in section 3.4.2.4. According to such figure, as temperature (electric current) is increased, NiTi becomes harder and higher stress levels are required to deform it; this demonstrates the presence of austenite, which is harder than martensite existent at low temperatures.
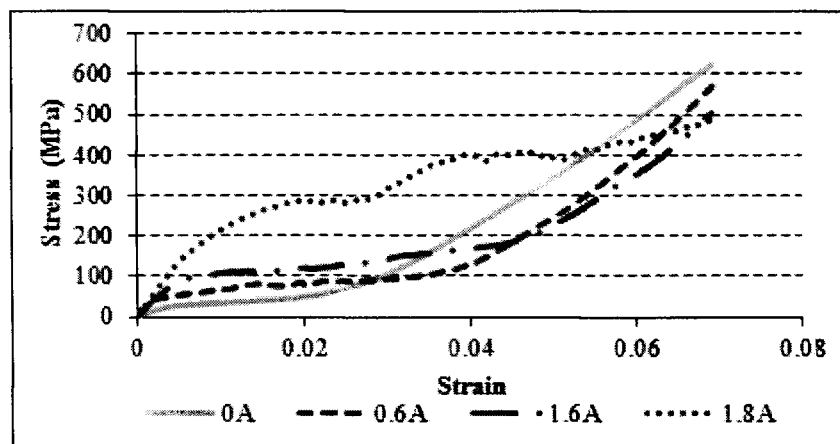
Fig. 3-18. Experimental Stress - Strain behavior of NiTi wires under different electric current levels.

3.5. Fitting of constitutive model

From volume fraction - temperature experimental data obtained for NiTi wires, parameters which fit PTE are determined. Once it is done, the expression is generalized in order to consider factors involved with the material. Then, equations to predict stress – strain behavior for martensite (twinned and detwinned) and austenite are obtained from differential tension tests results. Then, considering the expressions obtained, the constitutive model is proposed.

According to equation (3-2), total stress induced by strain or temperature on NiTi can be calculated. By substituting equations (3-8) to (3-22) on equation (3-2), the constitute model relates microstructure with thermo-mechanical behavior of NiTi as shown in equation (3-23)

$$\sigma_t = K_{tm}\varepsilon^{N_{tm}}\left\{1-\left[1+\left(\frac{\varepsilon}{A_\varepsilon e^{Q_\varepsilon i}}\right)^{-B_\varepsilon}\right]^{-1}-\left[1+\left(\frac{i}{A_T e^{Q_T d}}\right)^{-B_T}\right]^{-1}\right\}$$

$$(3-23)$$

$$+K_{dm}\varepsilon^{N_{dm}}\left[1+\left(\frac{\varepsilon}{A_\varepsilon e^{Q_\varepsilon i}}\right)^{-B_\varepsilon}\right]^{-1}+K_a\varepsilon^{N_a}\left[1+\left(\frac{i}{A_T e^{Q_T d}}\right)^{-B_T}\right]^{-1}$$

Manuel Ignacio Varela Jiménez

Table 3-1. Material constants determined from experimental work for NiTi

Parameter	Value
λ	-0.997
A_ε	0.0162
A_T	0.0707
B_ε	2.49
B_T	5.02
C_a	4921.3
C_{dm}	16.72
C_{tm}	2504.2
D_a	-2.596
D_{dm}	1.36
D_{tm}	0.482
F_a	0.7717
F_{dm}	53.048
F_{tm}	1.1531
G_a	0.2944
G_{dm}	-0.62
G_{tm}	-0.482
J	367.94
Q_ε	86.24
Q_T	65.43

3.6. Validation of constitutive model

Constitutive model is applied and verified by comparison with experimental stress – strain curve of a NiTi wire. Such comparison is depicted in figures 3-19 to 3-21. The trend of the theoretical plot is to fit with the experimental one, fitting has been done by experimental work and parameters determined specifically for the wires that have been used in tests.

Fitting is not perfect, which demonstrates that even if the experimental work applied give an approximation of the behavior of the material, these are not fully accurate and can be improved in future work, however allow to consider that assumptions and methods are valid for an initial approach.

Manuel Ignacio Varela Jiménez
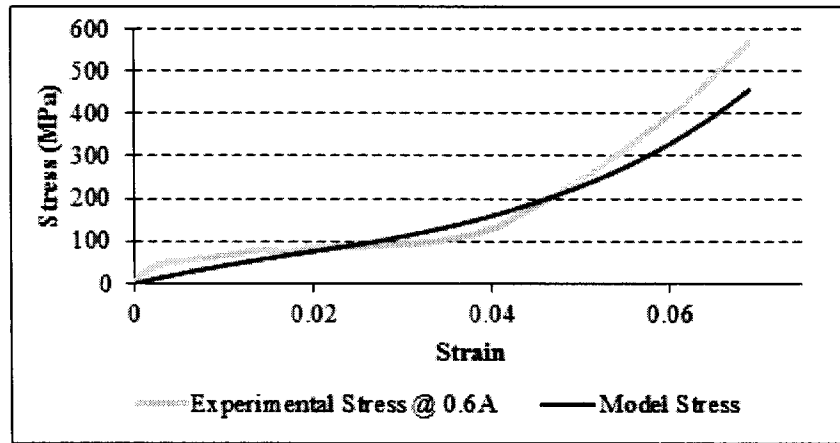
Fig. 3-19. Prediction of stress of NiTi by constitutive model (dark line), compared with experimental data, i=0.6A
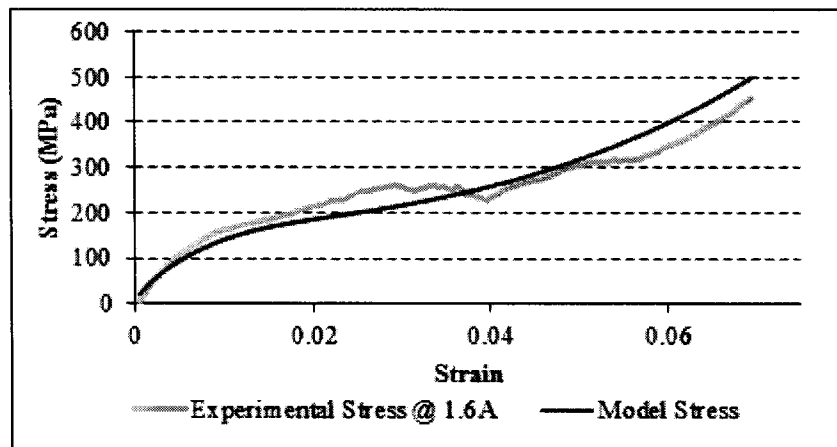
Fig. 3-20. Prediction of stress of NiTi by constitutive model (dark line), compared with experimental data, i=1.6A
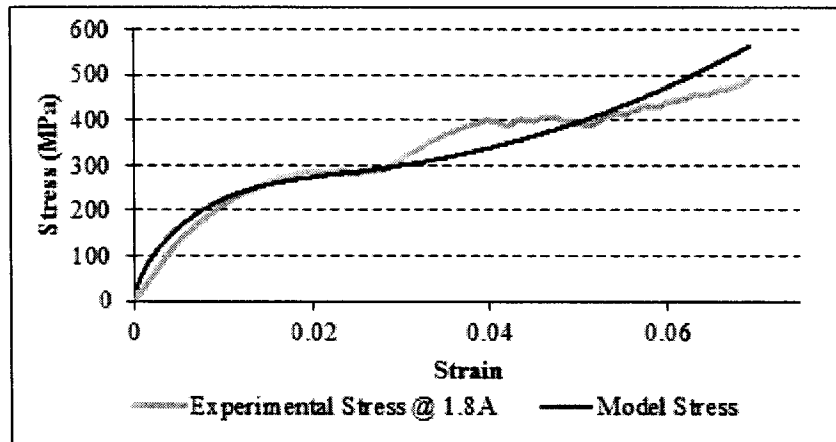
Fig. 3-21. Prediction of stress of NiTi by constitutive model (dark line), compared with experimental data, i=1.8A

Manuel Ignacio Varela Jiménez

3.6.1. Error Analysis

Accuracy of equations is evaluated by the standard deviation of the error, defined as the difference between the experimental and predicted data. It is shown in Table 3-2.

Table 3-2. Error analysis of Constitutive Model of Stress of NiTi

i (A)	Standard Deviation of Error	Average Standard Deviation of Error
0.6	37.1	
1.6	32.4	34.698
1.8	34.58	

3.6.2. Qualitative comparison with other constitutive models

3.6.2.1. Tanaka model

Tanaka model for SMA is based on thermo-mechanics. It is assumed that strain, temperature and the martensite volume fraction are the only state variables. An exponential expression describes the stress and temperature, rather than determining the free energy. The model includes as variables the temperature T, strain ε and martensite volume fraction ξ are the state variables. Constitutive equation is

$$\sigma - \sigma_0 = E(\xi)(\varepsilon - \varepsilon_0) + \Theta(T - T_0) + \Omega(\xi)(\xi - \xi_0) \tag{3-24}$$

where σ and ε are the stress and strain, respectively, E is the Young modulus, Θ is a thermo-elastic and Ω is a phase transformation constant. Subscript '0' refers to initial conditions of the material.

Martensitic phase transformation is represented, by an exponential formulation; a_A and b_A are constants related to the transformation temperatures M_f, M_s, A_s and A_f.

$$\xi = \exp(a_A(A_{s-T}) + b_A \cdot \sigma \tag{3-25}$$

3.6.2.2. Liang and Rogers model

Liang and Rogers improved Tanaka's work by considering a cosine dependence of the martensitic volume fraction. Austenite to martensite transformation is given by

$$\xi = \frac{1}{2}\left\{\cos\left[a_M(T - M_f) + b_a\sigma\right] + 1\right\} \tag{3-26}$$

Reverse transformation from martensite to austenite is given by

---

37   Manuel Ignacio Varela Jiménez

$$\xi = \frac{1}{2}\left\{\cos\left[a_M(T - M_f) + b_m\sigma\right] + \frac{1}{2}\right\} \tag{3-27}$$

where a_A, a_M, b_A and b_M are material properties derived from transformation temperatures M_f, M_s, A_s and A_f. The quantities of ε_M and ε_A are the initial martensite fractions for each transformations temperatures.

3.6.2.3. *Brinson model*

The model developed by Brinson is based on Tanaka's work with some modification by considering strain and temperature induced martensite.

$$\sigma - \sigma_0 = E(\xi)\varepsilon - E(\xi_0)\varepsilon_0 + \Omega(\xi)\xi_s - \Omega(\xi_0)\xi_{s0} + \Theta(T - T_0) \tag{3-28}$$

This model distinguishes between strain and temperature induced martensite by

$$\xi = \xi_S + \xi_T \tag{3-29}$$

The model includes expressions for determining ξ_s and ξ_T in martensite-austenite transformation or reverse. There are expressions according if T is above or below M_s and which also involve material constants derived from Tanaka's model.

3.6.2.3. *Boyd and Lagoudas*

Boyd and Lagoudas proposed a thermodynamic approach similar to Tanaka model.

$$G = -\frac{1}{2\rho}S\sigma^2 - \frac{1}{\rho}(\alpha(T - T_0) + \varepsilon^t) + c\left((T - T_0) - T\ln\left(\frac{T}{T_0}\right)\right) - S_0 T + u_0 + f(\varepsilon) \tag{3-30}$$

$$f(\varepsilon) = \begin{cases} \frac{1}{2}\rho b^M \varepsilon^2 + (\mu_1 + \mu_2)\varepsilon, \varepsilon > 0 \\ \frac{1}{2}\rho b^A \varepsilon^2 + (\mu_1 - \mu_2)\varepsilon, \varepsilon > 0 \end{cases} \tag{3-31}$$

Material constants $\rho b^M, \rho b^A, \mu_1$ and μ_2 define the transformation surfaces and the hardening during the forward and reverse transitions. The remaining material properties are effective compliance S, effective thermal expansion coefficient α, effective specific heat c, effective specific entropy at the reference state s_O and effective specific specimen internal energy at the reference state u_O.

A comparison between these and the model proposed in this work is shown in Table 3-2.

Manuel Ignacio Varela Jiménez

Table 3-2. Comparison between Constitutive Models for NiTi Stress

Author	Considered Microstructures	Constants function of	Fundamentals
Tanaka	Martensite, Austenite	TTR's	Thermodynamics
Liang and Rogers	Martensite, Austenite	TTR's	Tanaka model
Brinson	Austenite, Strain Martensite, Temperature Martensite	TTR's	Tanaka model
Boyd and Lagoudas	Austenite, Strain Martensite, Temperature Martensite	Hardening experiments, thermal behavior, entropy, energy	Isotropic hardening, adiabatic deformation,
Cortes-Varela	Austenite, strain martensite, temperature martensite	Diameter, electric current	Phase Transformation

3.7. Kinetics of Strain/Temperature Induced Twinned Martensite-Detwinned Martensite-Austenite Phase Transformation

As stated in section 3.3.2, the proposed model in this work does not describe the full thermomechanical cycle depicted in Fig 3-5 and phase transformations represented in Fig 3-6 due to that it does not consider mixed transformations from twinned/detwinned martensite to austenite or mixed twinned martensite/austenite to detwinned martensite. An improved model to consider mixed microstructures is proposed in this section.

According to equation (3-3), sum of V_{fa}, V_{ftm} and V_{fdm} is 1. Mixed transformations can be described by the following equations:

$$V_{fa} = (1 - V_{fa-dm}) \cdot V_{fa_0} + V_{ftm-a} \cdot V_{ftm_0} + V_{fdm-a} \cdot V_{fdm_0} \qquad (3-32)$$

$$V_{fdm} = (1 - V_{fdm-a}) \cdot V_{fdm_0} + V_{ftm-dm} \cdot V_{ftm_0} + V_{fa-dm} \cdot V_{fa_0} \qquad (3-33)$$

$$V_{ftm} = 1 - V_{fa} - V_{fdm} \qquad (3-34)$$

where subscripts 0 indicate the initial amount of each volume fraction. Strain induced detwinned martensite and temperature induced austenite phase transformations keep being described by equations (3-5) and (3-6) respectively and V_{ftm} is described by equation (3-4). Substituting (3-5) and (3-6) in (3-32) and (3-33)

$$V_{fa} = \left\{ 1 - \left[1 + \left(\frac{\varepsilon}{\varepsilon_{c_3}} \right)^{-B_3} \right]^{-1} \right\} \cdot V_{fa_0} + \left[1 + \left(\frac{T}{T_{c_4}} \right)^{-B_4} \right]^{-1} \cdot V_{ftm_0} + \left[1 + \left(\frac{T}{T_{c_2}} \right)^{-B_2} \right]^{-1} \cdot V_{fdm_0} \quad (3\text{-}35)$$

$$V_{fdm} = \left\{ 1 - \left[1 + \left(\frac{T}{T_{c2}} \right)^{-B_2} \right]^{-1} \right\} \cdot V_{ftm_0} + \left[1 + \left(\frac{\varepsilon}{\varepsilon_{c_1}} \right)^{-B_1} \right]^{-1} \cdot V_{ftm_0} + \left[1 + \left(\frac{\varepsilon}{\varepsilon_{c_3}} \right)^{-B_3} \right]^{-1} \cdot V_{fa_0} \quad (3\text{-}36)$$

where subscripts 1, 2, 3 and 4 represent the B, T_c or ε_c value corresponding to each one of the phase transformations represented in Fig 3-6. Experimental work is required for determining the values of B and ε_c for each phase transformation. This model can still be improved in order to describe the full thermomechanical cycle by considering also phase transformation 5 corresponding to austenite cooling.

3.8. Discussion

A 1D constitutive model for stress of NiTi based on a one way phase transformation/state transition from twinned/detwinned martensite to austenite as function of temperature and strain was proposed and validated getting promising results. Several limitations have been found but it can be considered as an initial approach of model of the stress of NiTi along its full heating – cooling thermomechanical cycle that could be applied in simulation of NiTi devices through finite element analysis.

The model is based on Cortes et al work for stainless steels; it was adapted to describe mechanical resistance of NiTi considering the three possible existent microstructures in NiTi. It relates the stress of each microstructure with their microstructural content that depends on the strain and temperature conditions, this way it represents effect of microstructural changes on the mechanical characteristics of the material. It has some limitations due that NiTi has a more complex behavior than stainless steel; the model does not describe all the possible scenarios for the material, for example, it does not describe mechanical behavior if temperature is decreased and it only works in one way, describing hardening of NiTi if temperature is increased but it does not describes softening of the material due to cooling.

This model works assuming that initial microstructure of NiTi is twinned martensite and if strain is applied, it describes by using state transition equation (STE) the transformation into detwinned martensite following a sigmoidal behavior as described in chapter 2. It also represents the effect of temperature on the mechanical resistance of the material in a way that as temperature is increased NiTi becomes harder due to higher content of austenite; this was demonstrated experimentally by tensile tests carried out at several temperature levels, coinciding with similar works found in literature.

Constitutive model is based on a single expression that considers the three possible existent microstructures and their strain/temperature induced phase transformation requiring easy inputs (temperature, strain, and geometry), this facilitates its understanding and its application. According to results, it tends to fit with experimental data, however standard deviation of the error indicates that more accurate fitting and experimental work is required. By now, mathematical expressions for this work have been fitted by simple experiments test such as tensile tests and controlled strain recovery tests; however, fitting can be improved if more sophisticated experiments such as DSC or Dynamic Mechanical Analysis (DMA) are used to estimate volume fraction in a more accurate way than doing estimations from strain-temperature data.

A shortcoming of this model is that it has been fitted for NiTi with a wire shape and a specific chemical composition which restricts it application in the case it be used for modeling NiTi wires manufactured by a different company o NiTi with a different geometry than wire. As future work, this model should be generalized in order to be adapted to chemical composition of NiTi and several shapes.

Compared with other constitutive models this one works only in one dimension and has been derived directly from the analysis of the natural behavior of the microstructure of the material and not by mathematical approaches such as Liang and Rogers or thermodynamics such as Tanaka. This model can be applied simply by considering 'easy' inputs such as diameter of the wire, electric current, strain and temperature conditions. In contrast Tanaka and other models require knowledge of transformation temperatures and elastic modulus. In the other hand, Brinson model is the most similar to the one proposed in this work, both consider two kinds of martensite; which, these are also considered by Boyd and Lagoudas but their model involves several constants and results more complicated for application.

A proposal for improvement of the model by considering variation of mixed twinned/detwinned martensite and austenite during heating of NiTi has been proposed by considering equations for predicting volume fraction of each microstructure as function of strain, temperature and initial amount of each microstructure. Additional experimental work is required in order to determine the values of the constants involved in mathematical expressions.

According to results obtained, these are promising and stress of NiTi can be modeled by STE, although in order to apply the model in simulation of NiTi devices by finite element analysis, additional work is required in order to improve fitting, extend the model to represent also the effect of cooling and being able to describe the material behavior under three dimensional conditions. Also it is required to obtain a general model in which constants depend of chemical composition and geometry, this way it could easily applied for modeling NiTi of any supplier or shape.

Chapter 4.

Unidimensional Constitutive Model of Stress of Shape Memory Polymer

4.1. Background

Shape Memory Polymers (SMP) are smart materials defined by their capacity to store and to recover an original shape as shown in Fig 4-1.
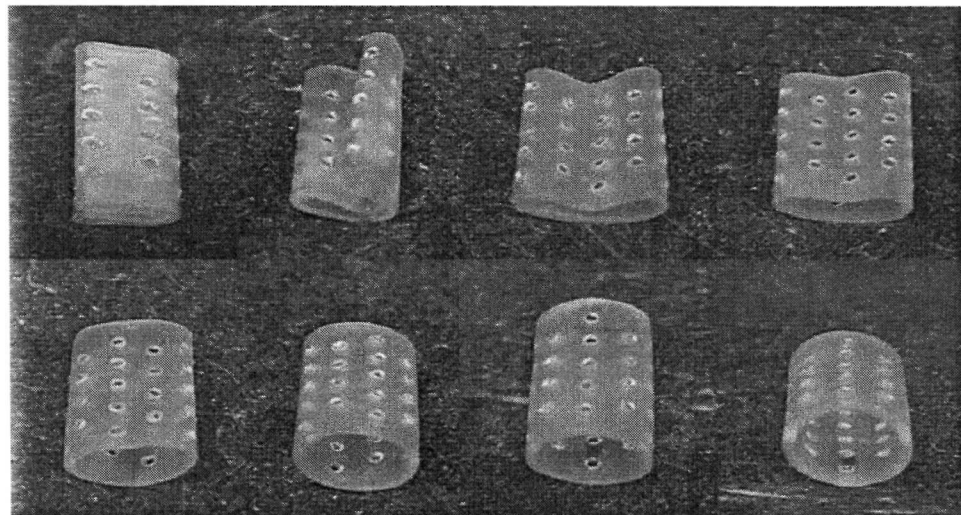
Fig. 4-1. Return of a cylinder SMP to its original shape as temperature is increased (UCM, 2008)

Shape memory behavior is typically induced by a change in temperature and has been observed also in metals and ceramics (Liu et al, 2006), however, in polymers it may be also induced by infrared light or magnetic nanoparticles embedded into the material (Safransky et al, 2008). SMP have several advantages over shape memory alloys (SMA) (Liu et al, 2004), including large recoverable strain, low energy consumption for shape programming, light weight, low cost, biodegradability, excellent manufacturability (Chen & Lagoudas, 2008); since low temperature curing and molding process for SMP fabrication allow

creating complex geometries at a reasonable cost, considering that SMP structures can be fabricated by casting, injection molding, extrusion or blow molding methods (Liu et al, 2004). In contrast, the main drawbacks of SMPs, when compared with SMAs, are the low actuation force and long strain recovery time (Chen & Lagoudas, 2008).

A particular temporary shape can be obtained by properly deforming the material before cooling (Chen & Lagoudas, 2008). This shape storage and large stain recovery occurs by application of a prescribed thermomechanical cycle (Liu et al, 2004), the one considered by Liu (Liu et al, 2006) and Chen and Lagoudas (Chen & Lagoudas, 2008) consists of the next stages, shown at Fig 4-2.
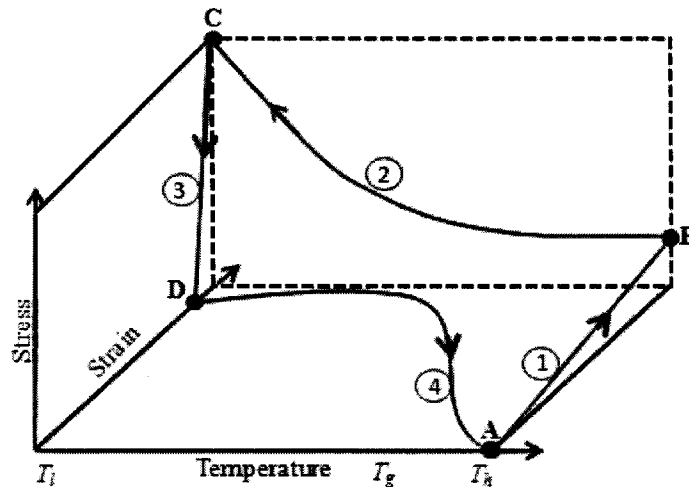
Fig. 4-2. Stress-strain-diagram of the typical shape memory cycle of SMP (Liu et al, 2006).

A) at high temperature when the material is in active state, stress is applied and strain occurs. B) SMP is cooled and strain is maintained. Due to thermal contraction the tensile stress needed to maintain the strain is increased as the temperature decreases. C) The stress is no longer applied and material remains in deformed shape at low temperature. D) Material is reheated without external applied stress and free recovery of the original shape occurs (Chen & Lagoudas, 2008).

4.1.1. SMP Fundamentals

A polymer exhibits shape memory if it can be stabilized in the deformed shape, which can be reached by using the network chains as a molecular switch; as consequence the flexibility of the segments should be a function of the temperature. One possibility for a switch function is a thermal transition (T_{trans}) of the network chains in a temperature range of interest. At temperatures above T_{trans} the chain segments are flexible, whereas the flexibility of the chains below the thermal transition is limited. Therefore, SMP show at least two separated phases; the state with the highest thermal transition T_{perm} acts as the physical crosslink and is responsible for the permanent shape. Above T_{perm} the polymer melts and can be processed.

Manuel Ignacio Varela Jiménez

A second phase serves as a molecular switch and enables the fixation of the temporary shape. The transition temperature for the fixation of the switching segments can be the glass transition temperature (T_g) (Lendlein & Kelch, 2002).

In the amorphous state, polymer chains have a random distribution, without the restriction given in semi crystalline polymers. All possible conformations of a polymer chain have the same inner energy and a strongly coiled conformation; which is the state of maximum entropy, represents the most probable state for an amorphous polymer. The terms 'glassy' state and 'rubbery' state are used referring to the material states in temperature ranges of $T<T_g$ and $T>T_g$, respectively (Liu et al, 2006). In the glassy state all movements of the polymer segments are frozen. The transition to the rubbery state occurs upon increasing the thermal activation; therefore the rotation around the segment bonds becomes unimpeded, enabling the chains to take up one of the possible, energetically equivalent conformations without disentangling significantly. The majority of the macromolecules will form compact random coils because this conformation is entropically favored and, as a result, much more probable than a stretched conformation. In the transition from the rubbery to the glassy state, the flexibility of the entire segment is limited. Strain induced crystallization of the switching segment can be initiated by cooling the material which has been stretched above T_{trans}; the crystallites formed prevent the segments from immediately reforming a coil structure and from spontaneously recovering the permanent shape that is defined by netpoints. The molecular mechanism of programming the temporary form and recovering the permanent shape is demonstrated in Fig 4-3 (Lendlein & Kelch, 2002).
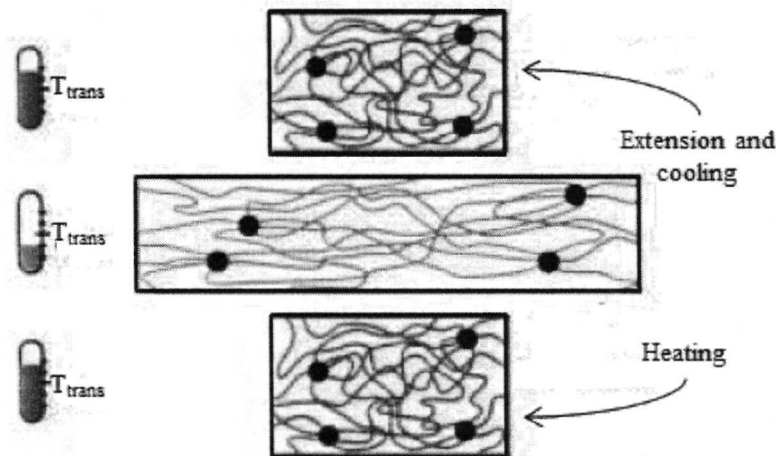
Fig. 4-3. Molecular mechanism of the thermally induced shape memory effect for a polymer network with $T_{trans}=T_g$. If $T>T_{trans}$ of the switching segments (represented by lines), these are flexible and the polymer can be deformed elastically. The temporary shape is fixed if $T<T_{trans}$ by cooling below T_{trans}. If the polymer is heated again, the permanent shape is recovered (Lendlein & Kelch, 2002).

After forming the material above the switching temperature, but below T_{perm}, the temporary shape can be fixed by cooling the polymer below the switching temperature. Heating up the material above T_{trans} again cleaves the crosslinks in the switching phase. As a result of its entropy elasticity the material is forced back to its permanent shape (Lendlein & Kelch, 2002).

T_g can be manipulated by changing copolymer composition or the degree of cross-linking, which is another benefit of SMPs, since their controllable activation temperature range is linked to T_g (Liu et al, 2004). The range of variation of T_g is of several hundred degrees by control of chemistry or structure (Gall et al, 2005). For some SMPs such as methacrylate networks, it has been established that T_g and rubbery modulus can be varied independently of each other by varying the amount and molecular weight of crosslinker and amount of mono-functional monomer (Safransky et al, 2008).

4.1.2. SMP Applications and Research Justification

SMPs have been of practical use since the 1960's, when radiation crosslinked polyethylene was used for heat shrink tubing (Safransky et al, 2008), wraps, foams and self-adjustable utensils (Liu et al, 2006). Given the actual extensive usage of polymeric materials, it is predicted that SMPs will be used in a very broad spectrum of applications, such as minimally invasive surgery, high-performance textiles, and self-repairing plastic components in domestic products (Chen & Lagoudas, 2008). In the case of medical devices, actually (Wache et al, 2003), develop cardiovascular stents based on SMPs, enhancing the use of the stent as drug delivery system and improving the post-surgery course through specific application of medicament. Other applications of SMPs in biomedical area include cardiac devices proposed as actuators for stroke victims and neuronal probes (Yacacki et al, 2008). Also, SMP have been applied for the development of BioMEMS which typically perform in vivo functions such as gripping or releasing of therapeutic medical devices within blood vessels (Gall et al, 2002).

Due to the fact that medical devices must undergo sterilization and validation before they can be used clinically, it is important that the method of sterilization does not adversely influence the chemical and mechanical properties, as well as biocompatibility and functionality of the material. (Yacacki et al, 2008). Hence, the design of SMP-based devices demands through characterization and constitutive modeling of the thermomechanical shape memory cycle that facilitate the prediction of recoverable stress and strain levels under varying degrees of constraints (Liu et al, 2006).

4.2. Proposition of State Transition in SMP

Following the concepts proposed by Liu et al, SMP can be considered as a mixture of 'glassy' and 'active' states, the glassy state is composed by a fraction of C–C bonds fully disabled with regard to the

conformational motion, while the active bond is composed by the rest of the C–C bonds that can undergo localized free conformational motions. As Liu et al, it can be assumed that at an arbitrary temperature the polymer is a mixture of two extreme states: the 'frozen' state' and the 'active' states, this lasts consists of the active bonds, so the free conformational motion can potentially occur. It is also assumed that the state transition follows a behavior as shown in Fig 4-4.
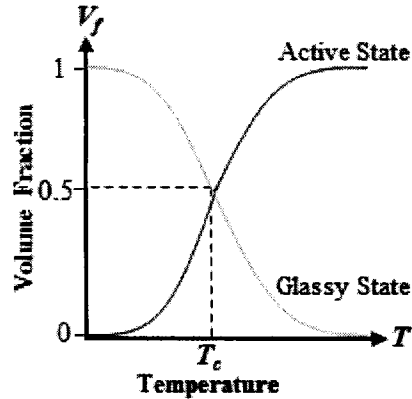
Fig. 4-4. State Transition in SMP as function of the temperature

4.3. Formulation of Model of state transition and stress of SMP

Chen and Lagoudas (Chen & Lagoudas, 2008) developed their model considering that the glassy state nucleates at some sites of the material as it cools to a certain temperature, growing continuously until the entire material is in the glassy state. As detailed in chapter 2, a similar phenomenon is considered by Cortes (Cortes et al, 1992), who developed a constitutive model for determining the flow stress of aggregates with phase transformation induced by strain, stress or temperature and demonstrated its use for stainless steels (Cortes et al, 1992). The model is based on an energy criterion which defines the energy consumed to deform the phases in the system as being equivalent to energy consumed to deform the aggregate and it is able to predict the flow stress behavior of the material. In order to apply STE in SMPs, by using the Liu (Liu et al, 2006) and Gall (Gall et al, 2003) experimental data; glassy and active states are considered as the aggregates and the microstructural transition between them becomes the basis of the constitutive model; this way, the constitutive expression will result in terms of the mechanical properties of each state and its volume fraction.

In the case of the present aggregate composed of glassy and active states, the volume fraction of each state is defined as

$$V_{fa} = \frac{V_a}{V_t} \qquad\qquad V_{fg} = \frac{V_g}{V_t} \qquad\qquad (4\text{-}1)$$

Manuel Ignacio Varela Jiménez

where subscript t indicates total while subscripts a and g indicate glassy and active, respectively. The compliance relationships allow considering nonlinear effects on the interaction of the microstructures with the mechanical properties. Cortes et al (Cortes et al, 1992) constitutive model of flow stress for the two-phases aggregate applied on SMPs is

$$\sigma_{SMP} = V_{fa} \cdot \sigma_a \cdot \phi_a + V_{fg} \cdot \sigma_g \cdot \phi_g \tag{4-2}$$

where σ_{SMP} is the stress of the SMP and σ_a and σ_f are the stress of each state. For SMPs, the value of ϕ_a and ϕ_f is assumed to be 1, however, determining the volume fraction is done applying STE presented in chapter 2 to represent kinetics of state transition, adapted for SMP results into

$$V_{fa} = \left[1 + \left(\frac{T}{T_c} \right)^{-B_{SMP}} \right]^{-1} \qquad V_{fg} = 1 - V_{fa} \tag{4-3}$$

where T is the temperature of the SMP, T_c is the characteristic temperature; given by the condition where the volume fraction of the glassy and active state is 50%; B_{SMP} is a constant of the material. This model assumes that SMP is initially in the glassy state; as temperature is increased the volume fraction of active state also increases by the transition of glassy into active state, as shown in Fig 4-3.

4.4. Experimental Quantification of State Transition

4.4.1. Methodology

As Chen and Lagoudas, experimental strain – temperature data for three SMPs with different T_g are obtained from literature and adapted into volume fraction of glassy states (V_{fg}) – temperature in order to determine the parameters which fit the STE, hence, the expression is generalized in order to consider factors involved with the material. After that, equations to predict stress – strain behavior for glassy and active states are proposed from experimental literature data. Finally considering all the expressions obtained, the constitutive model is applied and verified by comparison with experimental stress – strain curve for each SMP and its error is quantified.

4.4.2. Experimental Data

V_{fg} is estimated for three specimens of SMPs, whose specifications are shown at table 4-1; from the experimental strain – temperature data obtained by Liu (Liu et al, 2006) and Gall (Gall et al, 2005). Estimation is done by plotting on the strain axis of these curves, a V_{fg} scale, with minimal and maximal

values of 0 and 1, respectively; assuming a linear relationship between V_{fg} and strain ε and that at maximal strain and minimal temperature the volume fraction of glassy state is 1; at the temperature where the strain starts to decrease significantly the glassy state also starts to transform into active state; at 50% of the strain, the inflexion point of the strain – temperature curve exits and the volume fraction of the glassy and active state is 0.5 for each; at minimal strain and maximal temperature the V_{fg} is 0 and the SMP has recovered its original shape. By the use of the V_{fg} scale, a series of volume fraction of glassy state – temperature is obtained for each sample. The results are shown in Figs 4-6 to 4-7.

Table 4-1. Type and T_g of SMP specimens

Specimen	Type	$T_g(^oC)$	Reference
1	Epoxy system	70	Liu et al, 2006
2	Epoxy system	92	Liu et al, 2004
3	Poly tert-butyl acrylate	65	Gall et al, 2005
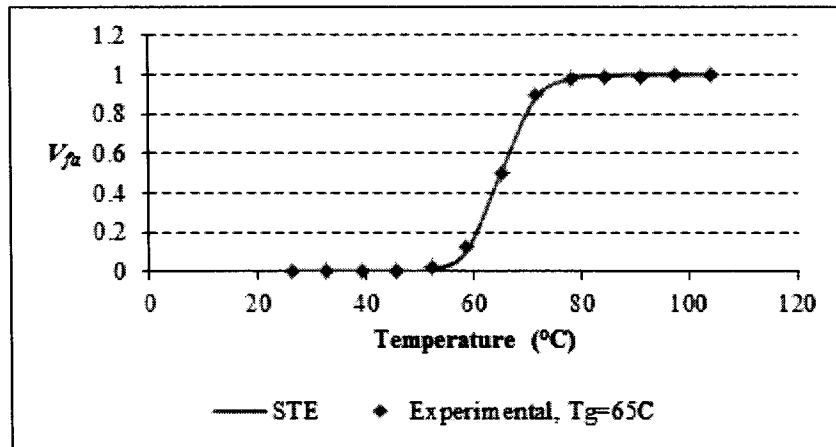
Fig. 4-5. Experimental (points) and Theoretical (points) Glassy State Volume Fraction Estimation for SMP with T_g=65°C
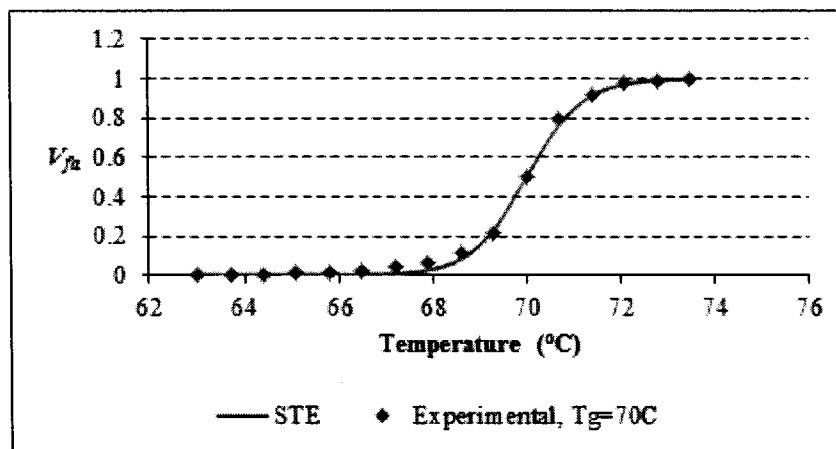
Fig. 4-6. Experimental (points) and Theoretical (points) Experimental Glassy State Volume Fraction Estimation for SMP with T_g=70°C
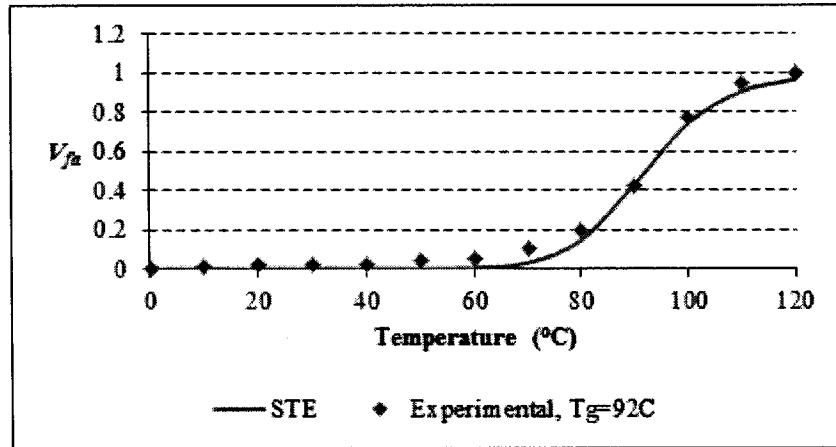
Fig. 4-7. Experimental (points) and Theoretical (points) Glassy State Volume Fraction Estimation for SMP with T_g=92°C.

By this estimation, it is observed that the temperature at which V_{fg} is 0.5 and by consequence, the active state is also 0.5; corresponds to the T_g of each specimen. It is also considered that no matter what the strain is, the SMP will be in glassy state at low temperature, since the state transition is induced by the temperature and not by the strain, however, it has allowed quantifying the state transition.

4.5. Fitting of Constitutive Model

From Fig. 4-4 to 4-6 it is found that T_c coincides with T_g, then any kind of SMP could be considered for applying of this model by only knowing its T_g and only requiring to determine the value of B_{SMP} in order to fit the expression to the experimental data, what in this case is done by applying the least squares method on equation (4-3) substituting a series of values for T and V_{fa} for each SMP with its specific T_g value. The resulting values of B_{SMP} are shown at table 2. Also from Fig 4-4 to 4-6, it is found B_{SMP} is related to the sensitivity to temperature of the material, described by a range R of temperature around which the state transformation is occurred

$$R = T_{af} - T_{as} \qquad (4\text{-}4)$$

where T_{af} is the temperature at which experimental volume fraction of active state is equal or greater than 0.9 and T_{as} is the temperature at which experimental volume fraction of active state is greater than 0.01; these temperatures are apparently related to the composition of the material. B and R are related by the expression

$$B_{SMP} = A \cdot R^{\alpha} \qquad (4\text{-}5)$$

Manuel Ignacio Varela Jiménez

for which parameters A and α are determined by numerical methods; these are shown at table 4-2. The resulting expression is shown in Fig. 4-7.

By substituting equations (4-4) and (4-5) into equation (4-3) and considering that the T_c coincides with T_g, the resulting expression for modeling the glassy – active state transition on SMPs results

$$V_{fa} = \left[1 + \left(\frac{T}{T_g} \right)^{A(T_{af} - T_{as})^{\alpha}} \right]^{-1} \tag{4-6}$$

as function of the temperature T, glass transition temperature T_g and transformation temperatures T_{as} and T_{af}. The theoretical results of equation (4-6) are compared with the experimental volume fraction data obtaining a good fitting between them. Then, the estimation of V_{fg} results valid.

From experimental isothermal stress-strain relations for the three SMP specimens obtained from literature (Liu et al, 2006), (Liu et al, 2004), (Gall et al, 2005), equations (4-7) and (4-8) for prediction of flow stress in SMP under small deformations ($\varepsilon<10\%$) in glassy and active state are obtained by numerical methods. A linear relation between the stress and strain is observed

$$\sigma_g = E_g \cdot \varepsilon \tag{4-7}$$

$$\sigma_a = E_a \cdot \varepsilon \tag{4-8}$$

where ε is the strain applied on the material, E_g is the elastic modulus of the glassy state; E_a is the elastic modulus of the active state. Elastic modulus for both states is obtained from experiments and by substituting the previous expressions developed in this work into equation (4-1) the stress of an SMP can be predicted.

$$\sigma_{SMP} = E_a \cdot \varepsilon \cdot \left[1 + \left(\frac{T}{T_g} \right)^{A(T_{af} - T_{as})^{-\alpha}} \right]^{-1} + E_g \cdot \varepsilon \cdot \left\{ 1 - \left[1 + \left(\frac{T}{T_g} \right)^{A(T_{af} - T_{as})^{\alpha}} \right]^{-1} \right\} \tag{4-9}$$

In this case, the equations for stress of each state resulted to be linear; however, given the flexibility of the model, in case that the stress had a different behavior the expression to describe it could be also obtained and substituted into equation (4-9).

Table 4-2. Values of A, α and B_{SMP} for each SMP specimen

Specimen	B_{SMP}	α	A
1	119.2	-0.895	-644
2	12.5	-0.895	-644
3	20.84	-0.895	-644
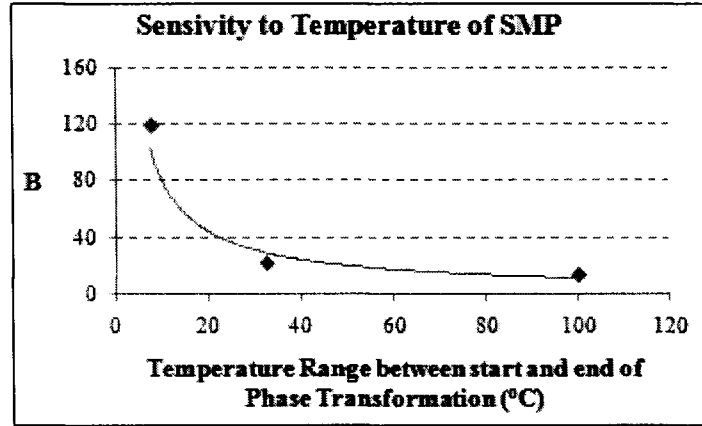
Fig. 4-8. Constant B_{SMP} as function of the range R of temperature between start and end of phase transformation.

4.6. Validation of Constitutive Model

Constitutive model predicts through equation (4-9) the stress of the SMP, as function of the microstructure, strain, temperature, glass transition temperature and transformation temperatures of the material. The results obtained from the equation are compared with the experimental data, as shown in Figs 4-11 to 4-13; demonstrating how SMP in frozen and active state exhibit a considerable difference in their mechanical properties and how as smaller is the value of constant B_{SMP} greater is the range of temperature around which the SMP can reconfigure its mechanical properties by changing its elastic modulus. In contrast, as constant B_{SMP} decreases, the elastic modulus requires a larger increase of temperature to be modified.
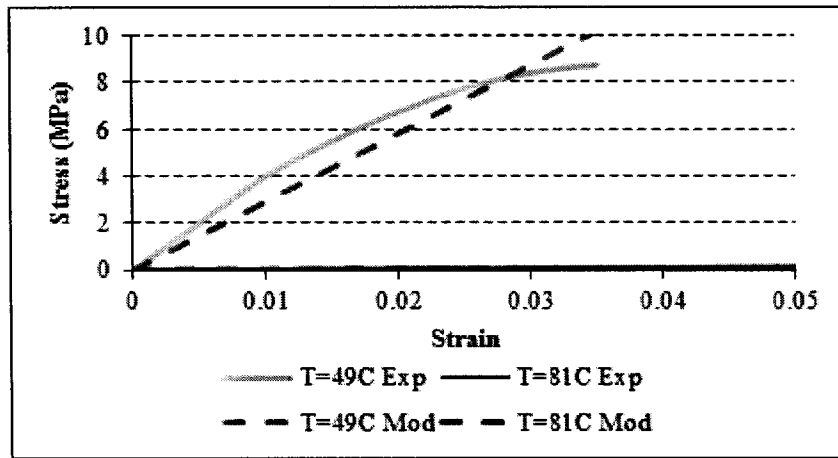
Fig. 4-9. Prediction of stress of SMP by constitutive model (Mod), compared with experimental data (Exp); T_g=65°C.
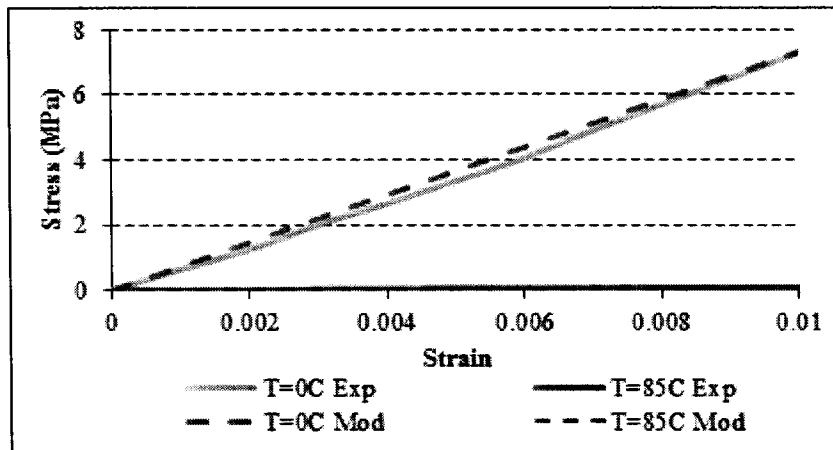
Fig. 4-10. Prediction of stress of SMP by constitutive model (Mod) , compared with experimental data (Exp); T_g=70°C.
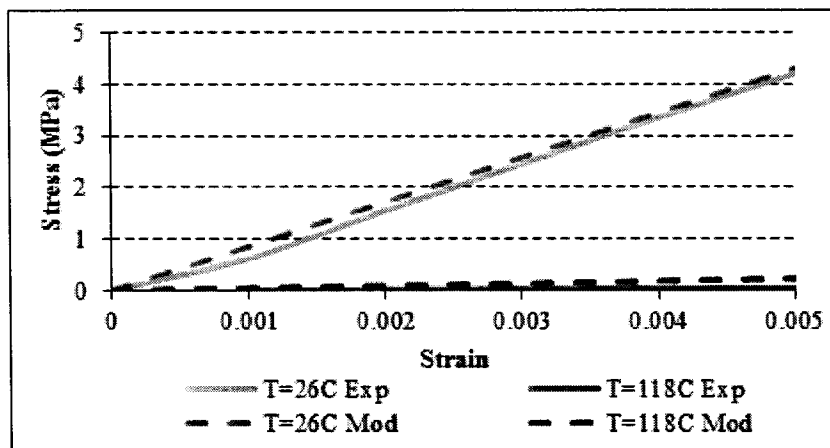
Fig. 4-11. Prediction of stress of SMP by constitutive model (Mod), compared with experimental data (Exp); T_g=92°C.

4.6.1. Error Analysis

Accuracy of equations is evaluated by the standard deviation of the error, defined as the difference between the experimental and predicted data. It is shown in Table 4-3.

Table 4-3. Error evaluation of Constitutive Model of Stress of SMP

SMP	Low Temperature	High Temperature	Average Standard Deviation of Error
Acrylate, T_g=65C	0.869	0.27	0.498
Epoxic Resin, T_g =70C	0.099	0.009	0.054
Epoxic Resin, T_g =92C	0.079	0.065	0.072

4.6.2. Other constitutive models

Liu et al proposed a 3D constitutive model to predict the thermomechanical behavior of SMP; focusing on the shape memory response of the polymer using a simplified phenomenological approach to model the temperature dependent shape memory behavior of a viscoelastic polymer. The temperature effect is separated from the time effect by fixing the cooling/heating rate. Thus, the time dependence is not included in the constitutive model (Liu et al, 2006).

At an arbitrary temperature, it is assumed that the polymer is a mixture of the frozen and active phases. By changing the ratio of these two phases, the glass transition during a thermomechanical cycle is embodied and the shape memory behavior can be captured. The change of the free volume fraction of the polymer with temperature is represented by the thermal expansion coefficient. The macroscopic strain tensor ε and temperature T are taken as state variables; the frozen fraction ϕ_f is defined as an internal state variable that is related to the extent of the glass transition and the state of the polymer. It is also assumed that a slow strain rate and constant heating/cooling rate are applied to the material (Liu et al, 2006).

At certain temperatures, entropic changes can be frozen and stored after unloading; therefore, if the material has been strained at a high temperature, $\phi_f(T)$ captures the fraction of strain storage as a function of temperature. For a 3D small strain model, when the material is subjected to a stress tensor σ, the stress-induced strain tensor is ε. In equation (4-10) the total stress σ is defined

$$\sigma = \phi_f \sigma_f + (1 - \phi_f)\sigma_a \tag{4-10}$$

Total strain ε is

$$\varepsilon = \phi_f \varepsilon_f + (1 - \phi_f)\varepsilon_a \tag{4-11}$$

Manuel Ignacio Varela Jiménez

where ε_f is the strain in the frozen phase and ε_a is the strain in the active phase. In the frozen phase, the entropic portion of the pre-deformation is assumed to be completely locked and stored during cooling. Due to the localized freezing process, the entropic frozen strain, ε^e_f can be anisotropic inside the growing frozen phase and should be considered as a function of the position vector x and an integral over the frozen fraction volume is used to sum the local contribution of ε^e_f. From the model, the deformation of the frozen phase arises from three parts: the average of the frozen entropic strain, the internal energetic strain ε^i_f and the thermal strain ε^T_f

$$\varepsilon_f = \frac{1}{V_{fg}} \int \varepsilon^e_f(x) dv + \varepsilon^i_f + \varepsilon^T_f \qquad (4\text{-}12)$$

where V_{fg} is the volume of the frozen phase. In the active phase, the deformation is composed of two parts: the external stress induced entropic strains ε^e_a and the thermal strain ε^T_a

$$\varepsilon_a = \varepsilon^e_a + \varepsilon^T_a \qquad (4\text{-}13)$$

Substituting equations (4-12) and (4-13) into (4-11)

$$\varepsilon = \left(\frac{1}{V_{fg}} \int \varepsilon^e_f(x) dv \right) + (\phi_f \varepsilon^i_f + (1 - \phi_f) \varepsilon^e_a) + (\phi_f \varepsilon^T_f + (1 - \phi_f) \varepsilon^T_a) \qquad (4\text{-}14)$$

ε^i_f and ε^e_a are elastic strains; the glassy state yield behavior is not considered and the non-linearity of rubbery elasticity is ignored for small strains, this way, it is assumed that the material behaves in a linear elastic manner in both the frozen and active phases. Thus, the internal variables, ε^i_f and ε^e_a, can be related to the stress tensor through the Generalized Hooke's law

$$\varepsilon^i_f = S_i : \sigma, \qquad \varepsilon^e_a = S_e : \sigma \qquad (4\text{-}15)$$

where S_i is the elastic compliance fourth order tensor corresponding to the internal energetic deformation, while S_e is the elastic compliance fourth order tensor corresponding to the entropic deformation. The total strain ε is decomposed into three parts, by defining the first term of equation (4-14) to be the 'stored strain' ε_s which reflects the strain storage as a function of temperature, the second additive term of equation (4-14) is the mechanical strain ε_m while the total thermal strain ε_T is defined by the third part of such equation and can be expressed in terms of thermal expansion coefficient α of the equivalent homogeneous material.

Manuel Ignacio Varela Jiménez

This way

$$\varepsilon = \varepsilon_s + \varepsilon_m + \varepsilon_T \tag{4-16}$$

Substituting into equation (4-10) and rearranging, the overall constitutive equation for the polymer in a thermomechanical cycle is defined as

$$\sigma = (\phi_f S_i + (1 - \phi_f)S_e)^{-1} : (\varepsilon - \varepsilon_s - \varepsilon_T) \tag{4-17}$$

In the constitutive equation (4-17), two internal variables ε_s and ϕ_f remain. The stress is dependent on a set of variables j: $\sigma = \sigma(j) = \sigma(\varepsilon, \varepsilon_s, T, \phi_f)$.

Liu et al explain that attention is focused on the stress–strain–temperature relations of the shape memory polymer thermomechanical responses and due that the concepts of internal energy and entropy are used to identify the deformation mechanisms a thermodynamic framework of their constitutive model is required, this way, they follow the development of a shape memory alloy constitutive model in formulating the free energy function of the proposed shape memory polymer model. From equation (4-16), the total strain ε can be decomposed additively into three parts; by considering the Helmholtz free energy $\psi(\varepsilon_m, \varepsilon_s, T, \phi_f) = U - T\eta$ where U is the internal energy, and η is the entropy. Because $\varepsilon_m = \varepsilon - \varepsilon_s - \varepsilon_T$, in fact, the free energy also depends on the set of variables j=$(\varepsilon, \varepsilon_s, T, \phi_f)$. The free energy function is used to describe the energy storage in a polymer due to thermomechanical loading. Corresponding to the deformation mechanisms of the shape memory polymer model that is proposed, the Helmholtz free energy is decomposed into two parts

$$\psi(\varepsilon, \varepsilon_s, T, \phi_f) = \psi_{mT}(\varepsilon_m, T, \phi_f) + \psi_s(\varepsilon_s, T) \tag{4-18}$$

The first part of equation (4-18) ψ_{mT}, consists of the mechanical energy, the thermal energy and the initial free energy of the material, the second part ψ_s corresponds to the entropic strain storage in the frozen phase due to an internal stress field. The second law of thermodynamics in the form of the Clausius–Duhem inequality is given as

$$\sigma = \dot{\varepsilon} - \rho(\dot{\psi} + \eta \dot{T}) - q \cdot \frac{\nabla T}{T} \geq 0 \tag{4-19}$$

where q is the heat flux vector and ρ is the mass density. Introducing the strain decomposition of equation (4-16) and the free energy function of equation (4-18) into the inequality, and considering that it must be

Manuel Ignacio Varela Jiménez

satisfied for any arbitrary thermomechanical process, the potential relations for the stress tensor and the entropy are obtained

$$\sigma = \rho \frac{\partial \psi_{mT}}{\partial \psi_{\varepsilon_m}}, \qquad \eta = -\frac{\partial \psi}{\partial T} + \frac{1}{\rho} \sigma : \frac{d\varepsilon_T}{dT} \qquad (4\text{-}20)$$

The general form of the constitutive equation for the stress in equation (4-20) is equivalent to equation (4-187. Furthermore, the change of entropy of a thermomechanical process can be determined if the free energy ψ as a function of temperature is known. The internal stress field σ_s that stores the entropic strain in the frozen phase can be defined as

$$\sigma_s = \rho \frac{\partial \psi_s}{\partial \varepsilon_s}, \qquad (4\text{-}21)$$

Then the Clausius–Duhem inequality simplifies into:

$$(\sigma - \sigma_s) : \dot{\varepsilon}_s - \rho \frac{\partial \psi_{mT}}{\partial \phi_f} \phi_f - q \cdot \frac{\nabla T}{T} \geq 0 \qquad (4\text{-}22)$$

Due that the rate dependence is not considered and it assumed that the storage strain ε_s depends only on temperature; $\dot{\varepsilon}_s = 0$. The shape memory response at a sufficiently slow constant cooling/heating rate is a near thermo-elastic process with a minimal hysteresis effect. From equation (4-22), the driving force for the evolution of the frozen fraction ϕ_f is $-\frac{\partial \psi_{mT}}{\partial \phi_f}$ which is the difference of the initial free energy between the active and the frozen phase. In equation (4-23), the thermal dissipation is given by $\delta_T = -q \cdot \frac{\nabla T}{T}$. By the Fourier law, it is defined that $q = -k \nabla T$ with $k{>}0$, so the heat conduction inequality is valid: $\delta_T = 0$. As a result, the Clausius–Duhem inequality is satisfied and the proposed constitutive model is thermomechanically admissible for an arbitrary thermomechanical process.

4.7. Discussion

An unidimensional constitutive model to describe stress of SMPs based on a glassy – active state transition as function of the microstructure, stress, strain, temperature, glass transition temperature and transformation temperatures of the material has been proposed and validated obtaining promising results, it can be considered as an initial approach for understanding thermomechanics of this material and be the basis of a model that could be applied for simulation of SMP devices thorough finite element analysis.

Constitutive model is based on kinetics of state transition and STE described in chapter 2, such phenomenon has effect on the mechanical properties of the material. Basing on Cortes et al work for stainless steel, STE is extended in order to describe mechanical behavior of SMP by relating the stress of each state with its volume fraction that depends on the temperature.

Due that model is based on previous work on stainless steels, it is proposed from a mechanical point of view, resulting simple because it does not consider thermodynamics of the material; it assumes that there is a small strain rate and that the heating rate is constant which simplifies it. Thus it should not be considered fully useful, additional work is required in order to validate its application under different conditions on which heating or strain rates be varied.

Experimental strain – temperature data for SMPs allowed estimating volume fraction of glassy state and then, fitting STE and extend it basing on Cortes et al develop a model for stress of SMPs. Experimental strain – temperature data from literature allowed to describe a state transition on the material by considering that V_{fg} reduces from 1 to 0 following the same curve than the strain in function of the temperature, this way, additional experiments were not required. The strain/glassy state volume fraction – temperature curve has an inflexion point at T_g where the strain is at 50% and the volume fraction of the glassy state is 0.5- For SMPs, characteristic temperature T_c at which both aggregates have the same volume fraction coincides with T_g at which the volume fraction of the glassy and active states is 0.5, which simplifies the model and demonstrates that it can be applied to SMP with different chemical composition than the ones analyzed for this work.

Constant B_{SMP} is related to the range of temperature around which state transition occurs with center at T_g. According to the results obtained, a 'small' value of B_{SMP} ($B_{SMP} < 10$) means the state transition occurs around a 'big' range R of temperature ($R \approx 50°C$), while a 'big' value of B_{SMP} ($B_{SMP} > 100°C$) means the state transition occurs around a 'small' range of temperature ($R \approx 6°C$). Apparently, constant B_{SMP} depends of the chemical composition of the SMP, however, it is required to determine the factors related to the composition from which constant B_{SMP} depends in order to improve the design of SMPs for specific applications, and also, according to Gall et al, SMPs may have a useful shape memory effect if they possess a distinct and significant glass transition; through this work it is found that constant B_{SMP} may be appropriate to evaluate the applicability of the SMPs.

The term 'transformation temperatures' refers to T_{as} and T_{af} which define the range of temperature around the state transition occurs. More research work is required to define the factors which define these temperatures and by consequence, the operation of the material.

Manuel Ignacio Varela Jiménez

In this case, the equation for stress prediction relates the stress on each state by a linear relation between strain and stress, however, given the flexibility of the model, with additional experimental data for nonlinear stress – strain relation the model could be fitted in order to consider other kinds of behavior on the material. Due to this condition, the model has a limited range of application and it can work adequately only for the range of strain at which the glassy state has a linear stress-strain relationship which is small compared with the large range of strain that a polymer can achieve, this results in a shortcoming of the model that restricts its use. Additional work is required in order to obtain an stress equation able to work under nonlinear condition extending the range of strain that can be described by the mathematical expression.

By simple observation, predicted stress results coincide with experimental data, therefore, the estimation of state transition done from literature data resulted valid, however in the case of the acrylate SMP, the average standard deviation of the error indicates that fitting can be improved by more accurate experimental evaluation of mechanical behavior of the material.

Results of the constitutive model result promising; allowing considering that it is possible to model the effect of temperature on the mechanical properties of the material by considering alteration on the microstructure such a state transition, although by now it cannot be affirmed by sure that it is possible to model behavior of polymers without considering the effects of thermodynamics and time on the material.

Chapter 5.

Constitutive Model of Displacement of Electroactive Polymers Films

5.1. Background

Electroactive polymers (PEA) are smart materials that have grasped the attention of researchers and engineers in recent years. Their potential to become mechanical actuators has led the efforts done so far to understand the deformations exhibited by these materials in the presence of an electric field. They consist of a group of polymeric materials and composites that respond to electrical stimulation, achieving displacements due to deformation produced by several factors triggered during stimulation; which depend on the type of material used. The forces produced with each displacement make them useful as mechanical actuators (Brown, 2004). Ionic Polymer-Metal Composites (IPMC) are electroactive polymers that consist in three-layer arrangements between an ion-exchange resin and a set of metal electrodes built on the polymer surface through chemical reactions. These materials are able to exhibit large deformations when placed in a time varying electric field (Oguro et al, 1992), (Shahinpoor, 1992) (Sadeghipour et al, 1992). Fig 5-1 shows an example of the deformation of an electrically stimulated IPMC.
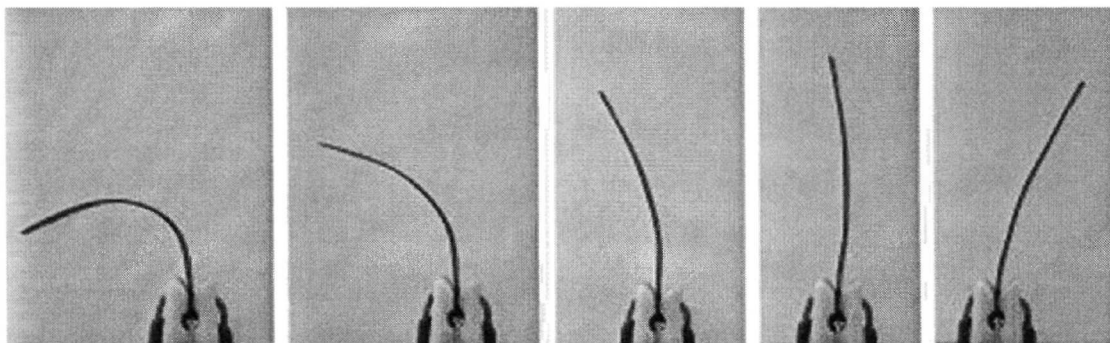
Fig. 5-1. Electroactive polymer deformation due to electric field application

5.1.1. EAP Fundamentals

An IPMC is able to deform, exhibiting a bending action, when subject to an electric potential difference. The electroactive mechanism by which the material shows its bending action is as follows: When both layers at the top and bottom surfaces of the base polymer membrane are connect to a circuit, and an electric potential difference is applied, the polarization created at both electrodes will promote the migration of the embedded cations inside the membrane into the cathode side (with negative charge). Since the cations are surrounded by water molecules, those are also carried by the cations into the cathode side. The accumulation of both cations and water molecules causes an imbalance which makes the current side to expand by the sudden increase in the concentration of these cations and molecules, while it contracts in the other side due to the decrease in the concentration. All these changes make the strip to build a curvature towards the anode side of the circuit, which is stated here as a bending. This reaction happens in a fraction of a second; enabling to have several deformations achieved at real time. Fig 5-2 shows a diagram which represents the IPMC before and after is electrically stimulated.
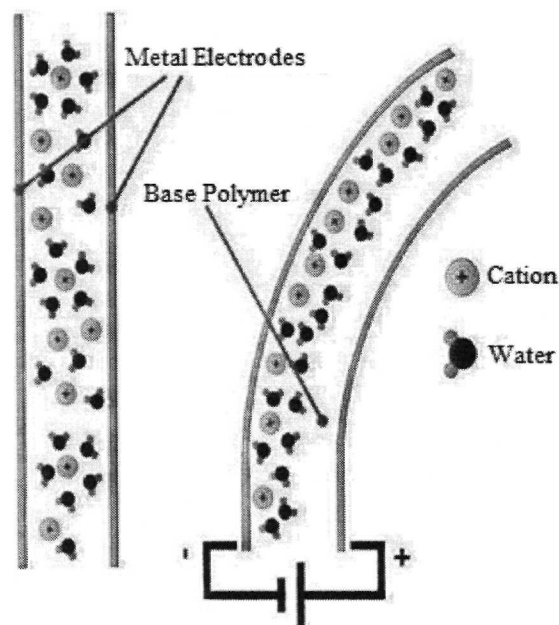
Fig. 5-2. Fundamentals of deformation presented at an EAP.

When the difference of potential is taken away, the ions and water molecules diffuse again within the cross section of the base polymer. This causes the strip to relax and to try return to its initial position. However, the sudden diffusion inside the polymer in response to the imbalance presented during the presence of the electrical stimulation creates a reciprocal bending towards the opposite side during relaxation. It has been observed that this reciprocal bending decreases by the increase of the frequency in the electrical input.

5.1.2. EAP Composition

Perfluorinated alkenes are broadly used as base polymers for their ion-exchange and mechanical properties. They are usually used in fuel cell applications. Nafion® is a perflourinated sulfonic acid ion exchange polymer manufactured by DuPont (DuPont, 2011). It is commonly available in the form of thin films and solutions. Another perflourinated product available is Flemion® by Asahi Glass (Asahi Glass, 2011), a perflourinated carboxyl polymer. It has been noticed that the effectiveness of these materials to produce an IPMC is the result of the ion exchange and mechanical properties of perflourinated polymers. The ion exchange side groups are important not only for the preparation procedure of the IPMC, but also are important to achieve the deformation phenomenon in the material. The mechanical properties in the other hand become crucial in order to have a suitable actuator. For example, when using another porous ionic polymer membrane such as P(AN-co-SSS), where the presence of sulfonic acid groups makes it suitable in the ion exchange part, it was not suitable in its mechanical properties because of its acrylonitrile back bone structure. Thus, the preparation procedure still uses Nafion ion-exchange material as the base polymer for the IPMC.

The conducting material to form the composite may consist in metals such as gold, platinum, palladium, silver, or cupper. Since the composite is usually formed by chemical deposition processes, the resulting product will vary its conductive properties based on the metal used.

5.1.3. Research Justification

Up to date research and development in the IPMC as actuators or sensors has given some fundamentals, preparation techniques, and modeling of the phenomena regarding the deformation of the material from a scientific point of view (Shahinpoor and Kwang, 2001, 2003, 2004), (Bar-Cohen, 2001). However, a bridge between the scientific research and the technological application is necessary for the engineering of these functional materials.

In the time scientists have been working with electroactive polymers, several of the phenomena associated to IPMC are still under active research. It is observed that in general, the phenomena associated to bending are still in a way to propose different approaches to model the particular features found in IPMC. At the same time, a tool for engineers to make designs for application of the materials is still in development. Then, formulation of a constitutive model represents the bridge where the scientific fundamentals of the material are linked to the design and simulation of reconfigurable tools and devices. In this work, a constitutive model for the bending phenomenon of an IPMC strip is established using the state transition concept presented in Chapter 2 of this work.

5.2. Proposition of State Transition in EAP

State transition in EAP is proposed by considering that diffusion of particles (ions and waters molecules) from state A to B promotes volumetric expansion in one side of the film and a volumetric contraction at the other side as shown in Fig 5-3.
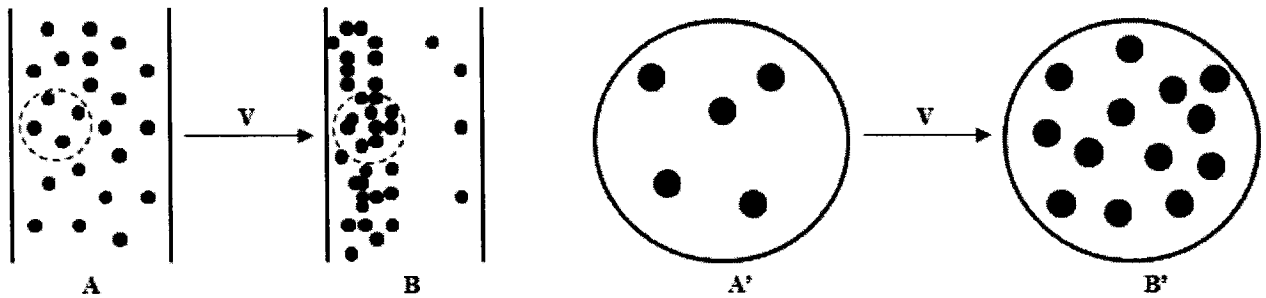
Fig. 5-3. State transition at one side of the cross section of the EAP film.

In a particular region at state A', lower concentration of counter ions is observed. After diffusion there is a larger volume of particles in the same region, this is considered state B'. Such change is considered a state transition induced by an external factor, in this case a potential difference. State transition follows a sigmoidal behavior as shown in Fig 5-4.
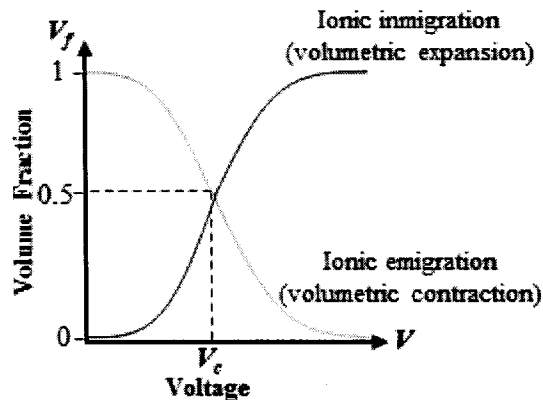
Fig. 5-4. Electric field induced state transition of EAP film.

As potential difference is applied state A transitions to state B, macroscopically this is observed as a bending of the film due to the migration of particles to one of the sides of the material.

5.3. Formulation of Constitutive Model of Displacement of EAP

Modeling of the displacement of EAP is done by considering it as a deforming beam. It begins with the characterization of the system to be analyzed in its external behavior. Shown in Fig 5-5, configuration of the IPMC is the same as a beam in a cantilever state, having one end fixed and the other end free for

movement. When a load is applied to the system, a reversible deformation is produced. Where P is the virtual load responsible for the movement and is the maximum displacement obtained from the deformation; taking in account the existence of a reciprocal deformation when the system enters relaxation after the load disappears.

$$\delta = \frac{\delta_a + \delta_b}{2} \qquad \delta_a > \delta_b$$
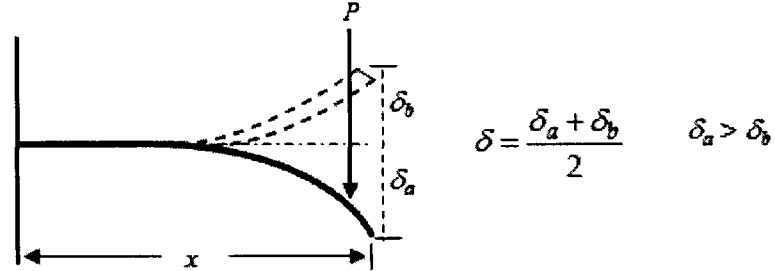
Fig. 5-5. Representation of EAP film bending by a cantilever beam deformed by a virtual load P.

Deformation of the system may be expressed mathematically as a function of the load and the material properties along the length of the beam. By Hooke's law, it is known that the deformation over a beam system as presented in Fig 5-5 is given by:

$$\varepsilon(\chi) = \frac{\sigma(x)}{E} = \frac{P \cdot x}{E \cdot Z} \tag{5-1}$$

where $\sigma(\chi)$ is the bending stress on a beam or strip at a distance x from the point of application of the load to its fixed end. E is the modulus of elasticity of the material which composed the beam. Z is the section modulus, which is constant while the geometric shape does not change.

In this case, there is not a load P responsible for the displacement δ. However, this load exists as a reaction. For this reason it will be called virtual load. On the other hand, it is known that the displacement δ is directly proportional to the virtual load P, then

$$P = a \cdot \delta \tag{5-2}$$

where a is a proportionality constant in mass/distance dimensions. Then equation (5-1) may be written as

$$\varepsilon(\chi) = \left(\frac{a \cdot X}{Z \cdot E}\right) \cdot \delta \tag{5-3}$$

or

$$\delta = \left(\frac{Z \cdot E}{a \cdot X}\right) \cdot \varepsilon \tag{5-4}$$

where K is equal to

$$K = \frac{Z \cdot E}{a \cdot X}$$

(5-5)

It is observed that a and E are parameters that depend on the material. Also X and Z depend on the geometry and the position of the material. In equation (5-3) K is called a factor for the virtual, geometric, and material conditions. At normal conditions, a and E are constant as the material does not change its properties. In this case, however, the material will change its composition properties at the diffusion zones, and thus a and E will also change. Nevertheless, to begin the modeling it is considered that these parameters will remain constant.

5.3.1. Determination of K factor

After establishing the principles for the external behavior for the bending beam system, the states and behavior explained in section 5.2 by Figs 5-3 and 5-4 are considered. This way V_{fi} is the volume fraction of the counter-ion present or missing in the material is expressed by the next equation

$$V_{fi} = \frac{V_i}{V_T}$$

(5-6)

having

$$1 \geq V_{fi} \geq 0$$

where V_i is the volume occupied by the counter-ion inside the polymer and V_T is the total volume in the material.

Since most of the attention is towards the surface that expands, where the most of the counter-ions migrate, and because of the reciprocity of the phenomenon, it is possible to just consider the surface that expands. This way, by constant frequency f conditions and the migration of a certain size of counter-ion specie, V_{fi} should be able to show the behavior shown in Fig 5-6.

In order to calculate the different curves of V_{fi} within different voltages and frequency conditions, STE may be applied according to the physical domain of EAP resulting in

$$V_{fi} = \left[1 + \left(\frac{V}{V_c} \right)^{-B_{EAP}} \right]^{-1}$$

(5-8)

where V is the potential difference in volts, V_c is a characteristic potential difference at specific frequency conditions, and B represents a factor for the constitution of the material system. Graphically, V_c represents the potential difference at 50% of the transition as depicted in Fig 5-8.

Equation (5-8) represents the volume fraction of the new state. This means that it represents the volume fraction of the immigrated ions by the effect of the potential difference applied to the IPMC and the type of counter ion being transported.
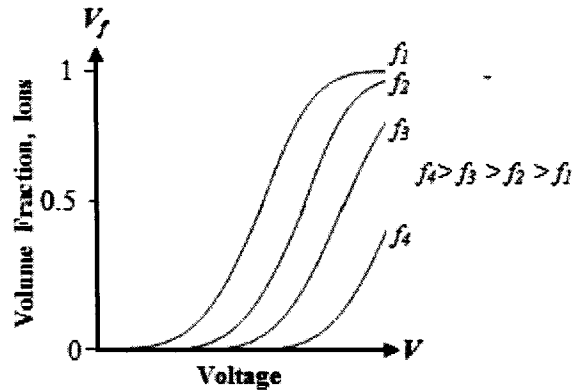
Fig. 5-6. Behavior of volume fraction V_{fi} at the expanding side of the cross section under several frequency conditions

Considering equations (5-4) and (5-5); emphasizing in the displacement of the strip in terms of the determination over the surface generated by the virtual load, and which it may be justified to be equal to the increase in the volume provided by the diffusion of the ionic state in the surface of the strip, the total displacement of the previous external beam system may be expressed as

$$\delta = K\varepsilon \tag{5-9}$$

for constant conditions of geometry and material properties it is expected to observe the behavior shown in Fig 5-9 When the material changes, its behavior may be observed as in Fig 5-7.
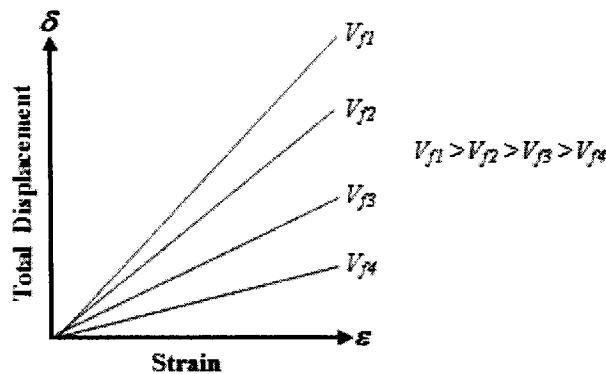
Fig. 5-7. Behavior of total displacement δ vs. strain ε under different voltage conditions

According to Fig 5-7, the change in the material, in terms of the of the volume fraction of the contained ion specie is observed as a particular composition of the achieved configuration. This way, each slope is a particular function of the type of material under constant geometric conditions. Thus

$$K = m \cdot V_{fi} \tag{5-10}$$

where m is a proportionality constant. Substituting equation (5-8) in (5-10) results into

$$K = m \cdot \left[1 + \left(\frac{V}{V_c} \right)^{-B_{EAP}} \right]^{-1} \tag{5-11}$$

which is the factor needed for equation (5-5). It may be noticed that the factor K in equation (5-11) is a function of the potential difference, the frequency, and the ionic characteristic. Also the proportionality constant m and the volume fraction of the ion play a role in the equations.

5.3.2. Determination of deformation as a function of the operational conditions

Substituting equation (5-11) into equation (5-4) it results

$$\delta = m \cdot \varepsilon \cdot \left[1 + \left(\frac{V}{V_c} \right)^{-B_{EAP}} \right]^{-1} \tag{5-12}$$

Considering deformation over a section of the surface as a variable with a very small magnitude and practically constant for the displacements obtained experimentally, it may be established that

$$\alpha = m \cdot \varepsilon = \text{constant}$$

then

$$\delta = \alpha \cdot \left[1 + \left(\frac{V}{V_c} \right)^{-B_{EAP}} \right]^{-1} \tag{5-13}$$

Equation (5-13) represents the constitutive model that let us predict the total displacement from the bending deformation action in the IPMC strip. In order to use this constitutive model, the three parameters, α, Vc, and B_{EAP} must be solved by experimental work.

Solving the constants of equation (5-13); by considering equations (5-3), (5-4) and (5-5) an expression of strain in terms of the geometry of the strip, the characteristics of the material, and the operational conditions may be obtained.

$$\varepsilon = \alpha \cdot \left(\frac{a \cdot X}{Z \cdot E} \right) \cdot \left[1 + \left(\frac{V}{V_c} \right)^{-B_{EAP}} \right]^{-1} \qquad (5\text{-}14)$$

By relating equations (5-4) and (5-14) it is possible to determine the modulus of elasticity for the material as a function of the operational and ionic characteristics present in the material.

$$E = \alpha \cdot \left(\frac{a \cdot X \cdot m}{Z} \right) \cdot \left[1 + \left(\frac{V}{V_c} \right)^{-B_{EAP}} \right]^{-1} \qquad (5\text{-}15)$$

Equation (5-15) confirms that the compound material, and particularly of variable composition even under control, possesses also variable mechanical properties; being this one of the most distinctive characteristics of a functional and reconfigurable material. Modulus of elasticity E traditionally is a material constant, however in equation (5-18) it is expressed as a function of the factors related to the external and internal changes in the system. In numerical simulation, it may serve the purpose of predicting the changes in the modulus of elasticity due to the change in the conditions given to the material.

5.4. Experimental Quantification of State Transition

5.4.1. Materials

Ionic Polymer-Metal Composites (IPMC) strips (1.0cm x 3.0cm) made of Nafion® 117 (DuPont) perflourinated membrane (0.018cm thick) as base polymer, with deposited metallic layers made of Platinum, were used with Lithium (Li^+), Potassium (K^+), Sodium (Na^+), Magnesium (Mg^{2+}), and Calcium (Ca^{2+}) counter-ions in individual experiments to obtain displacement measurements.

Detailed information about material synthesis and films preparation can be found in Guzman 2007.

5.4.2. Displacement evaluation

Design of the experimental setting is resumed as follows: for the electrical input, a function generator was used to provide stable electrical signal conditions by means of adjusting the voltage and frequency as required. In order to have a voltage over the IPMC, the strip was arranged in such a way that: 1) both

Manuel Ignacio Varela Jiménez

electrodes are connected to the circuit, 2) the IPMC is fixed in a cantilever configuration, and 3) it is easy to measure the displacement at each experimental run. Fig 5-8 shows a diagram of the proposed experimental setting for the displacement evaluation.
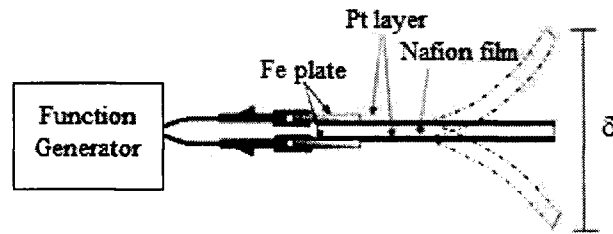
Fig. 5-8. Experimental setup for measuring the total displacement of an IPMC strip.

Plots of displacement as function of voltage at different frequency values for PEA containing ions of Potassium, Sodium, Calcium, Lithium and Magnesium are depicted in Figs 5-9 to 5-13.
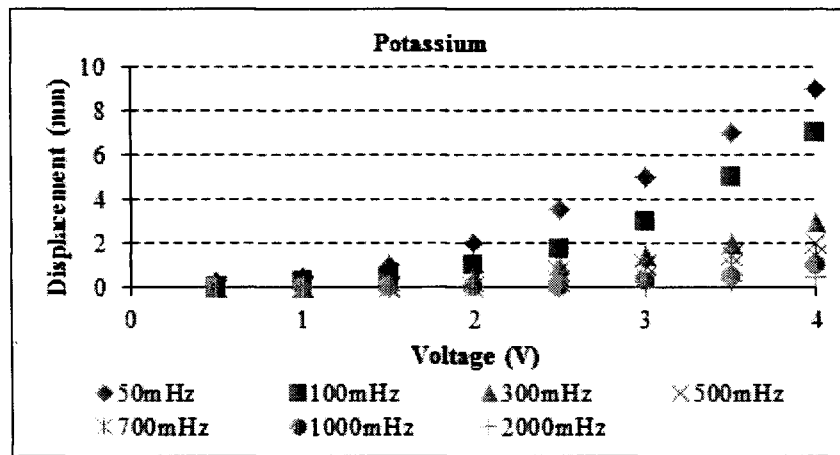
Fig. 5-9. Displacement at several frequencies of PEA film containing Potassium ions
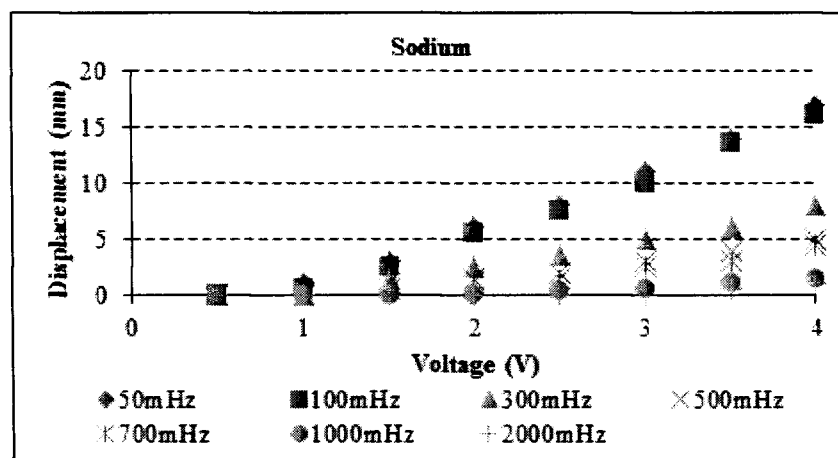
Fig. 5-10. Displacement at several frequencies of PEA film containing Sodium ions
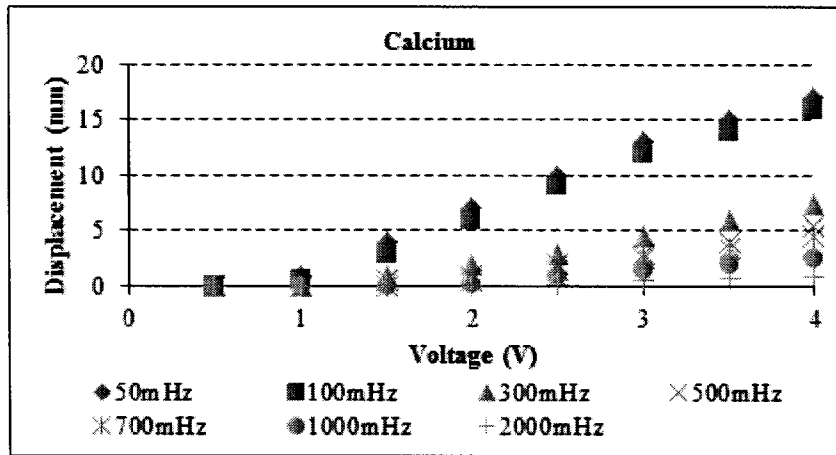
Fig. 5-11. Displacement at several frequencies of PEA film containing Calcium ions.
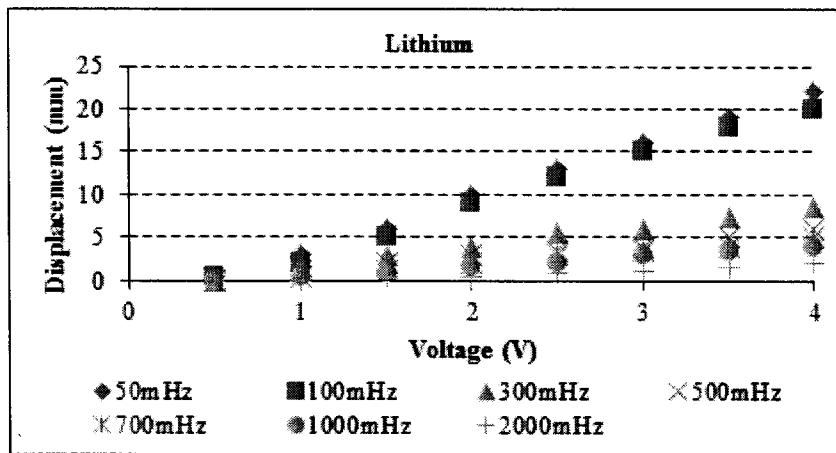
Fig. 5-12. Displacement at several frequencies of PEA film containing Lithium ions
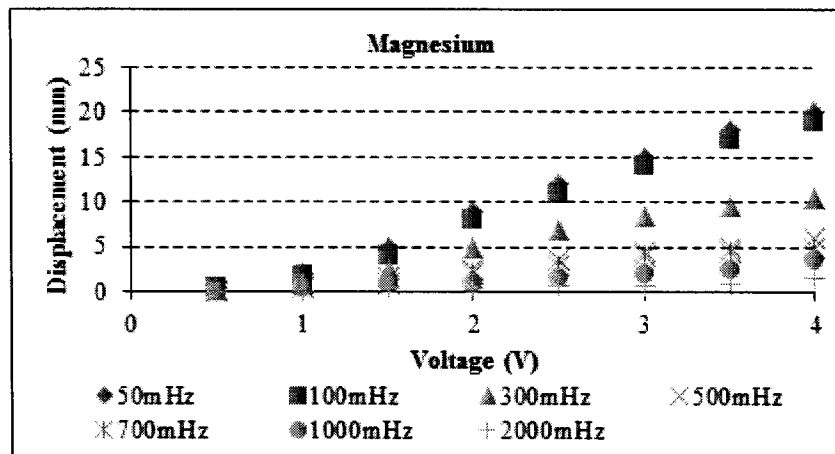
Fig. 5-13. Displacement at several frequencies of PEA film containing Magnesium ions

5.5. Fitting of Constitutive Model

Equation (5-13) is fitted to experimental displacement – voltage data of each one of the ions materials by defining the values of V_c, α and B_{EAP} using least squares method. For EAP, V_c is defined as the 50% of the maximum displacement, then, B_{EAP} and α are defined by numerical fitting and should be related to some physical variable.

From experimental displacement – voltage data it is observed that B_{EAP} has a constant value according to the counter ions used, their fitted values are shown in Table 5-1. On the same way it is observed that α and V_c depend on the frequency v having a behavior as described by equations (5-16) and (5-17).

$$\alpha = \beta \cdot f^{-\chi} \tag{5-16}$$

$$V_c = \phi \cdot f^{\gamma} \tag{5-17}$$

where f is in mHz units; β, χ, ϕ and γ are constants that depend on ion materials, their values are shown in Table 5-1.

Table 5-1. Material parameters β, χ, ϕ and γ for respective counter-ions used

Parameter	Counter Ions				
	Li^+	Na^+	K^+	Mg^{2+}	Ca^{2+}
β	609.12	620.33	302.2	388.31	621.16
χ	0.757	0.794	0.808	0.671	0.79
ϕ	1.984	2.573	2.966	2.046	2.429
γ	0.0001	0.0002	0.0001	0.0002	0.0001

5.6. Validation of Constitutive Model

Parameters shown in tables 5-1 are substituted in equations (5-16) and (5-17) and these are substituted in equation (5-13), the results are compared to experimental displacements shown in Figs 5-14 to 5-18 for three different frequency conditions. The dashed line represents the model results, while the markers represent the experimental data.
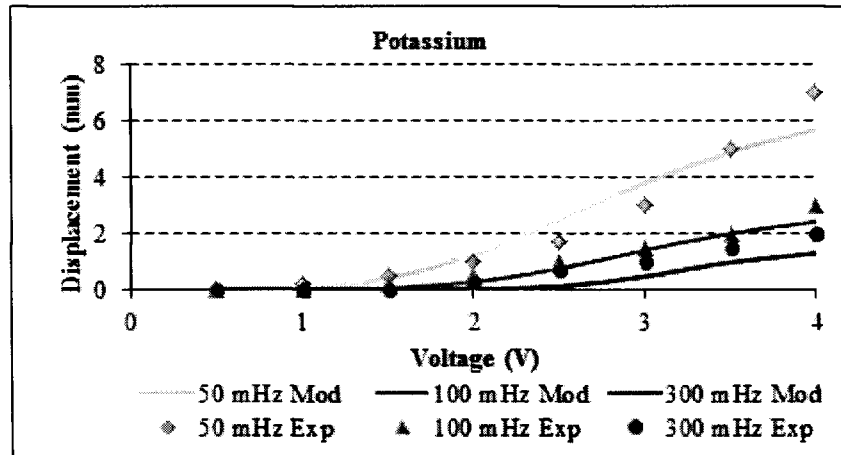
Fig. 5-14. Prediction of displacement by constitutive model (line) compared with experimental data (points) at different frequencies for Potassium ions EAP film
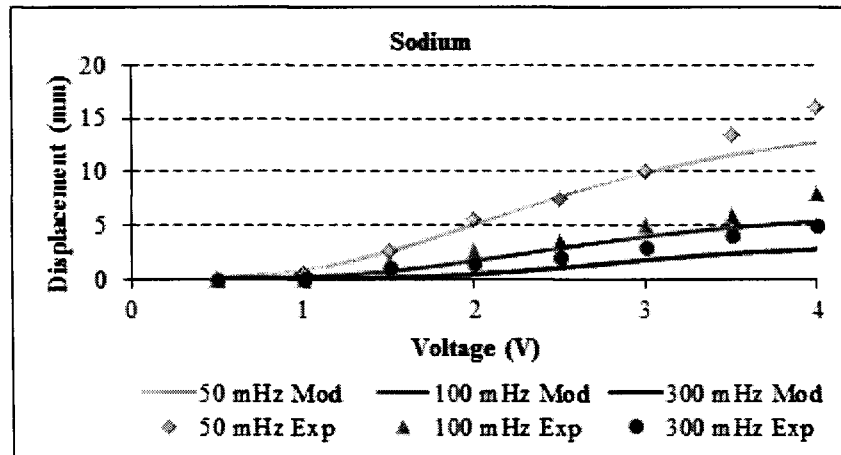
Fig. 5-15. Prediction of displacement by constitutive model (line) compared with experimental data (points) at different frequencies for Sodium ions EAP film.
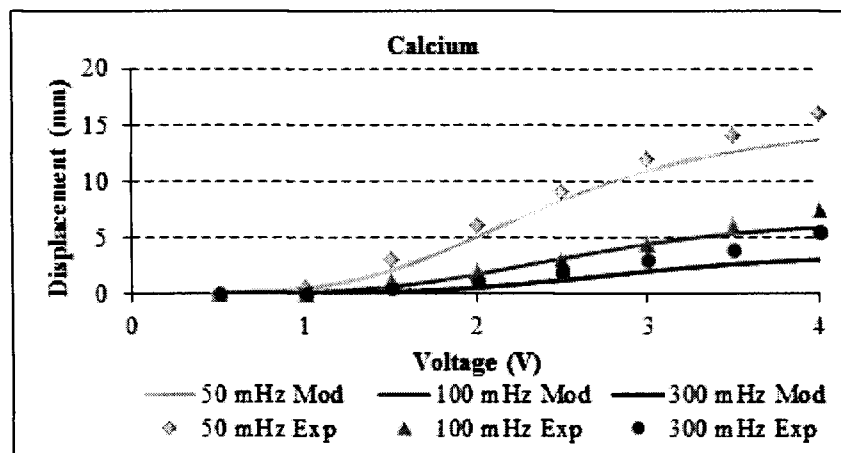
Fig. 5-16. Prediction of displacement by constitutive model (line) compared with experimental data (points) at different frequencies for Calcium ions EAP film

Manuel Ignacio Varela Jiménez
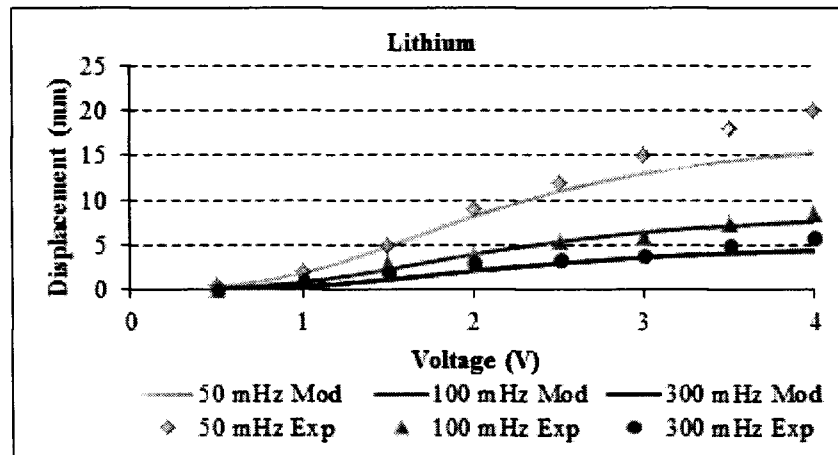
Fig. 5-17. Prediction of displacement by constitutive model (line) compared with experimental data (points) at different frequencies for Lithium ions EAP film
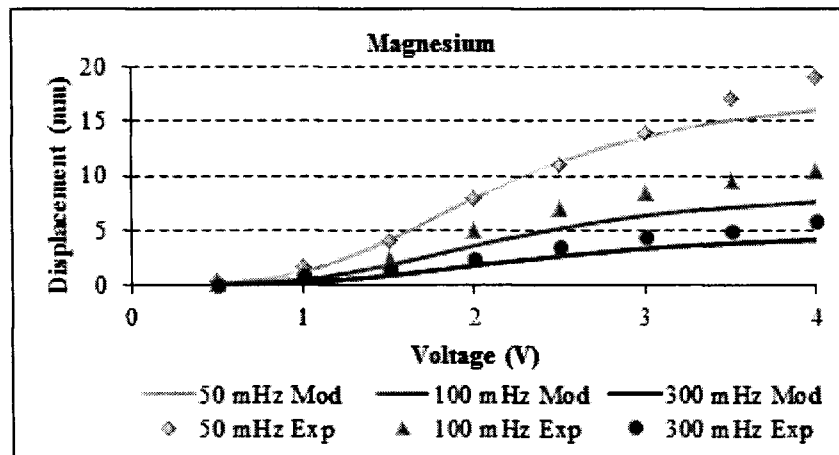
Fig. 5-18. Prediction of displacement by constitutive model (line) compared with experimental data (points) at different frequencies for Magnesium ions EAP film

6.6.1. Error Analysis

Accuracy of equations is evaluated by the standard deviation of the error, defined as the difference between the experimental and predicted data. It is shown in Table 5-2.

Table 5-2. Error evaluation of constitutive model of displacement of PEA films

Ions	Frequency (mHz)							Average Standard Deviation of Error
	50	100	300	500	700	1000	2000	
K	0.809	0.658	0.199	0.153	0.075	0.077	0.069	0.291
Na	2.52	1.27	0.864	0.473	0.543	0.327	0.112	0.873
Ca	2.959	0.736	0.575	0.508	0.537	0.116	0.208	0.806
Li	1.673	1.734	0.452	0.407	0.252	0.241	0.155	0.702
Mg	2.845	1.139	0.983	0.285	0.307	0.327	0.223	0.873

5.7. Discussion

A constitutive model for predicting displacement of an EAP film was proposed based on the transition from a steady state where ions are in random position to a state where these are concentrated at one of the sides of the material. Such model works in one way describing effect of electric field on the strain of the EAP film although this model has not been described to describe return of the material to its initial shape.

The constitutive equation is based in the bending deformation of a beam system subject to a virtual load; by the state transition equation (STE) it is correlated to a state transition at one of the sides of the EAP.

In this case, state transition was considered to correlate the internal change in the volume fraction of the contained counter-ions inside the polymer as a function of the applied voltage V, adjusted by a characteristic voltage Vc which depends on the frequency conditions, and a parameter B_{EAP} which depends of the ionic content of the material, a constant α for each ion content depends also on the frequency of the electric signal applied to the EAP.

From experimental displacement-voltage measurements, it is observed that films with counter ions with smaller ionic radius such as Lithium or Magnesium achieve larger displacements; this should be because due to the small size of the ions, these can find more free space to move and also a larger volume of them can be concentrated on the material.

The parameters needed for the model were defined using a mathematical fitting by lest squares method. The experimental data compared to the results from the model show an acceptable fitting for most of the systems; demonstrating the effectiveness of the model in this first approach using the state transition concept.

Due to the fitting between the theoretical and experimental data it can be considered that the assumptions and model setup result valid and that behavior of an EAP can be modeled through state transition concept.

Resulting expression predicts the displacement as function of the voltage and the frequency of the electric signal applied, also of the ions inside the film; thus, relating the external conditions of the material and its composition.

This model may be used as a tool for design and simulation of IPMC systems regarding the active positioning of the polymer strip based on the requirements of the engineers and designers, however it must be improved in order to be fully applied for simulation of EAP devices due that constants have been

determined for the ions specifically used for experiments. In addition, the model could be generalized and be adapted to determine the values of constants according to ionic radius, electronegativity or some other physical parameter; this would facilitate the use of the model without the need of carry out experiments for fitting parameters if different ions are used.

Chapter 6.

Constitutive Model of Shear Yield Stress of Magnetorheological Fluid

6.1. Background

Magnetorheological fluid (MRF) is a smart material whose rheological properties can be varied by an external magnetic field (Bompos and Nikolakopoulos, 2011), (Susan-Resiga et al, 2007). As illustrated in Fig 6-1 it can be rapidly varied from a liquid Newtonian-like fluid state to that of a stiff semisolid with the application of a magnetic field (Simon et al, 2001), (Ciocanel, 2006).
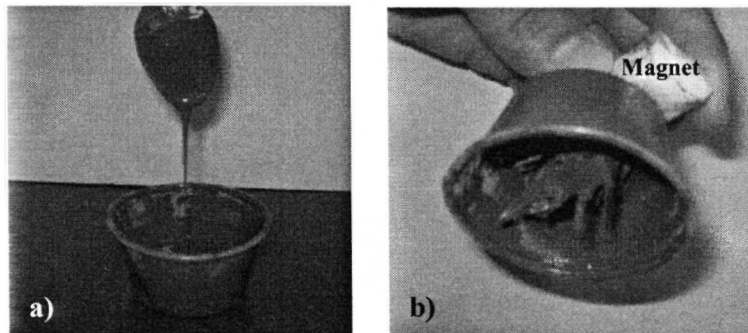
Fig. 6-1. MRF. a) Without magnetic field, (b) When magnetic field is applied by a magnet

6.1.1. MRF Fundamentals

MRF consists of a concentrated suspension of micron-sized magnetically permeable particles in a nonmagnetic low viscosity newtonian carrier fluid (Laun et al, 2008). The mechanism responsible of the behavior of the material is the induced magnetic interaction of particles within the matrix (Jolly et al, 1996) which in the presence of a magnetic field magnetize and form chain-like structures that align in the direction of the applied field (Simon et al, 2001) as shown in Fig 6-2. Consequently, the mechanical energy needed to yield chain-like structures increases as the applied magnetic field increases (Xin, 2003).

Manuel Ignacio Varela Jiménez

The configuration and rigidity of the chain structure will depend upon several factors including the strength and distribution of the applied field (Jolly et al, 1996), (Laun et al, 2008).

a)   **b)**   **c)**
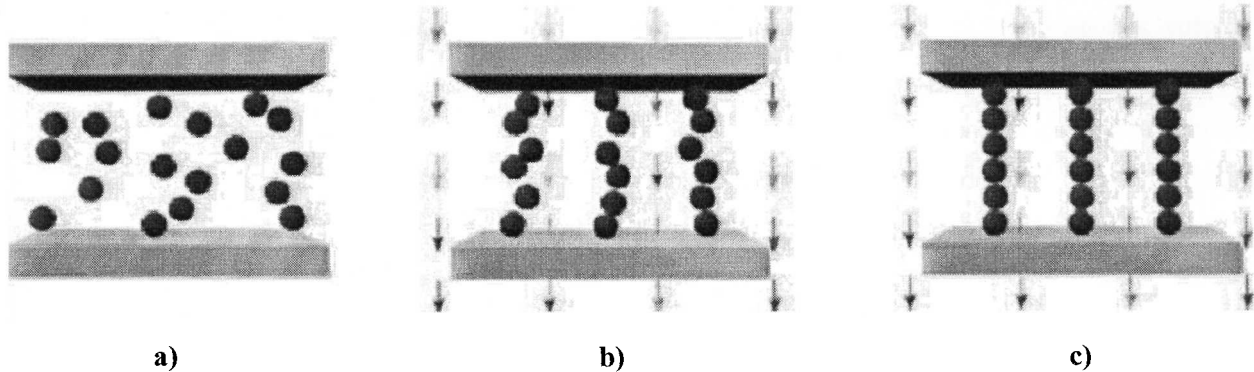
Fig. 6-2. Activation of MR fluid: a) no magnetic field applied; b) magnetic field applied; c) ferrous particle chains have formed (Goncalves, 2005).

Macroscopically, it is observed that when exposed to a magnetic field H MRF does not flow unless acted by at least some critical shear stress called shear yield stress τ_y (Ciocanel, 2006), this behavior is represented in Fig 6-3.
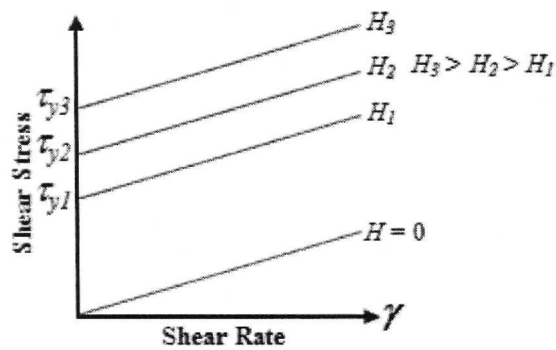
Fig. 6-3. Mechanical Behavior of MRF

The change in state is accompanied by an increase in viscosity (Ciocanel, 2006). However, the property of a controllable fluid that is observed to change upon an increase in applied field is not the viscosity of the fluid, but rather the shear yield stress defining the flow regime (Weiss and Duclos, 1994). Thus, a MRF could be defined as a material whose flow ability is reversibly controllable by an external magnetic field (Laun et al, 2008) since it shows a magnetically changeable shear yield stress (Nakano et al, 2005) which produces a change in its apparent viscosity (An and Won, 2003).

MRF should not be confused with ferrofluids or magnetic liquids. Due to the effect of Brownian motion on the colloids present in the ferrofluids, these magnetic liquids do not exhibit the ability to form particle chains (Weiss and Duclos, 1994).

6.1.2. MRF Composition

A typical MRF contents the following elements:

a) Magnetic particles: Carbonyl iron, nickel, cobalt or ceramic ferrites, 20 to 40 percent volume fraction of the MRF, with a diameter of 1–5 μm (Cesmeci et al, 2010). Since iron has the highest saturation magnetization ($\mu_0 M_s$ = 2.1T) it has common disperse phase for MRF. An increase in the particle volume fraction results in an increase in the maximum shear yield stress of the material and an increase of its off-state viscosity. When particles are larger than 10 μm the settling rate is increased and the fluid is less stable, in the other hand when these are small (<1 μm) they are more sensitive to temperature because of the Brownian motion and the agglomeration increases (Xin, 2003).

b) Carrier liquid: It should contribute to the overall stability and redispersibility of the MRF. The temperature dependence of the carrier fluid is the dominating factor in the temperature operating ranger of the material (Xin, 2003). Typical carrier fluids are water, mineral oil, hydrocarbon oil, silicone oil or glycol (Cesmeci et al, 2010), (Carlson, 2005).

c) Proprietary additives: these are necessary to prevent agglomeration and settling, promote particle suspension, enhance lubricity, modify viscosity and inhibit wear (Ciocanel, 2006). One way is by adding surfactants and another is use of a solid colloidal stabilizer. Some of the surfactants used are ferrous oleates, ferrous napthalates, oleic acid and phosphate esters. Some of the dispersants are nano structured silica or fibrous carbon (Xin, 2003).

An MRF was developed by Villarreal et al in Tecnológico de Monterrey, which was mainly a dispersion of iron powder 99.9% as the soft magnetic material in a carrier oil (Villarreal et al, 2005). Lord™ Corporation is a USA company that already commercializes MRF and other devices based on the material (Lord, 2011).

6.1.3. MRF Applications and Research Justification

MRFs were first developed in the late 1940s by Winslow and Rabinow (Ginder et al, 1996) and have attracted considerable interests because their mechanical properties can be electrically controlled, (Li et al, 2002), causing an increasing interest in their engineering applications. For example, MRF dampers are one of the most promising new semi-active devices for control of mechanical vibration due to the invariable damping feature, mechanical simplicity, robustness, low power consumption, and fast response. MRF dampers are not only advantageous in their ability to provide variable damping forces to the suspension; they are also inherent fail-safe devices from an electronic point of view (Cesmeci et al, 2010).

MRFs have been used commercially since the mid-1990s. The first application was a small controllable MRF brake in aerobic exercise equipment. In 1998, small, real-time controlled MRF damper systems were introduced commercially into heavy-duty truck and off-highways vehicle. A MRF damper is depicted in Fig 6-4. In 2002, the Cadillac Seville STS automobile was introduced with dampers based on MRF enabling simultaneous ride comfort control and body motion control. In 2004, MRF in small, liter-sized quantities cost about $600 USD per liter. When purchased in larger quantities MRF are priced in the range of $60 to $180 USD per liter depending on the details of the specific MRF formulation and the actual annual fluid production volume. MRF production levels in 2004 were in the order of hundreds of tons per year. The estimated number of MRF dampers, shocks, brakes and clutches in used worldwide is more than 10^5. This number is expected to rise into the millions over the next decade (Carlson, 2005).
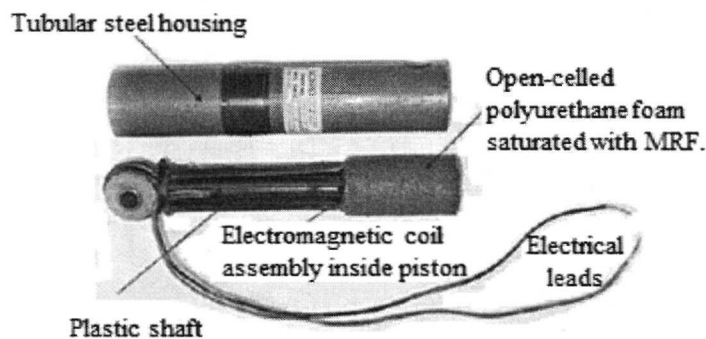
Fig. 6-4. Lord™ Corporation MR sponge damper (Goncalves, 2005).

Another application of MRF is a prosthetic leg that developed by Biedermann Motech which improves the mobility of leg amputees by mimicking a natural gait. Coupled with a combination of sensors and controllers, the device can adapt to varying movements, ranging from uphill and downhill motion to stairs, and even bicycling. MRF is also used for polishing of optical lenses. QED Technologies is currently producing a multiple axis CNC polishing machine that uses a slurry made of MRF and an abrasive (Goncalves, 2005).

Understanding the overall magnetic response of MRF and its dependence on microstructure is important to the design of improved MRF. Predicting the magnetic properties of these fluids, however, is a challenging task due not only to the size and density of the particles, but also to the nonlinear magnetization of the particles (Simon, 1999).

Several authors as Carlson or Ginder have tried to explain the behavior of this smart material in a form of a constitutive equation but due to its nonlinear behavior during magnetization there is not a model which relates the maximum shear yield stress, the material composition and magnetic field with the shear yield stress on the same expression. For instance, the purpose of this work is to develop a constitutive

equation that describes the behavior of the shear yield stress of the material as function of the magnetic field applied and its chemical composition.

6.2. Proposition of State Transition of MRF

MRF change its rheology and apparently becomes more viscous as a magnetic field is applied due to the alignment of the particles. Such process can be considered as a magnetically induced state transition. As shown in Fig 6-5, there is a liquid state when the particles are in random position, while the solid state when the particles are fully aligned.
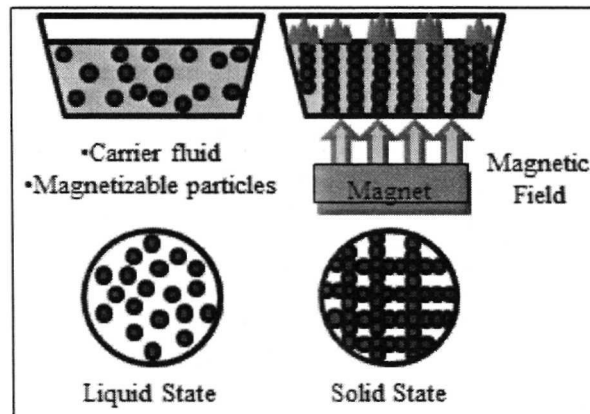
Fig. 6-5. States existent in MRF

State Transition behavior is shown in Fig 6-6. Without magnetic field the volume fraction of the liquid state is 1. As magnetic field increase, volume fraction of the solid state increases from 0 to 1.
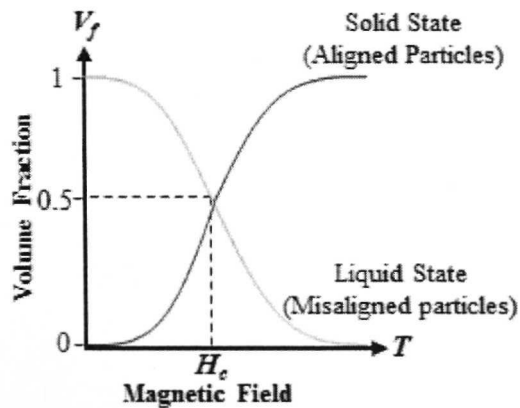
Fig. 6-6. Magnetically Induced State Transition in MRF

Macroscopically, the growth of the solid state can be identified by the increase of the shear yield stress of the MRF as function of the magnetic field, then, shear yield stress is the key parameter to describe the

state transition. According to literature it has the behavior shown in Fig 6-7 and depends of the amount ϕ and composition of particles on the carrier fluid. At some value of magnetic field H, shear yield stress τ_y becomes constant due to particles are aligned, this value is known as the saturation shear yield stress τ_y^{sat} (Ginder, 1994). At that point it is considered that liquid -solid state transition is finished.
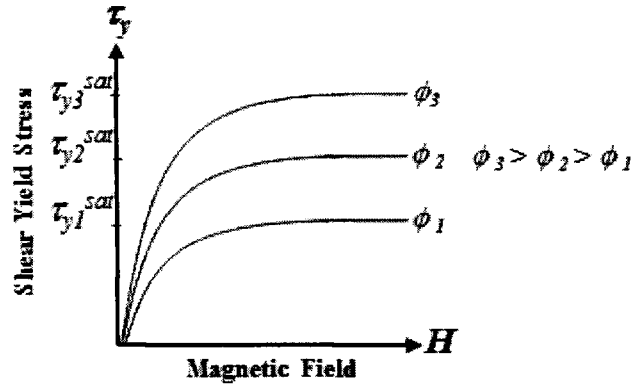
Fig. 6-7. Relation between yield stress τ_y and magnetic field H

6.3. Formulation of Model for State Transition and Yield Stress of MRF

Establishment of a constitutive equation for state transition in MRF requires considering the behavior of the shear yield stress of the material as function of the magnetic field H shown in Fig 6-7.

Following the concepts presented in chapter 2, STE be adapted to describe yield stress and state transition of MRF (Cortes et al, 1992, 1993). In this case; the liquid and the solid states are considered as the aggregates and the microstructural transition between them becomes the basis of the model; this way, the constitutive equation results in terms of the magnetic field, saturation stress of each state and its volume fraction.

6.3.1. Constitutive Model for Shear Yield Stress

In the case of MRF, the aggregate is composed of liquid and solid states, based on Cortes' model volume fraction V_f of each state or aggregate are defined as:

$$V_{fl} = \frac{V_l}{V_t} \qquad\qquad V_{fs} = \frac{V_s}{V_t} \qquad\qquad (6\text{-}1)$$

where subscripts l, s and t indicate liquid, solid and total, respectively. Cortes' constitutive model of flow stress for multi phases aggregate (Cortes et al, 1992) applied on MRF is

$$\tau_y = V_{fl} \cdot \tau_{yl}^{sat} + V_{fs} \cdot \tau_{ys}^{sat} \qquad (6\text{-}2)$$

where τ_y is the shear yield stress of MRF and τ_{yl}^{sat} and τ_{ys}^{sat} are the saturation yield stress of each state.

6.3.2. Kinetics of Magnetic Field Induced Liquid - Solid State Transition

Based on the state transition shown in Fig 6-5, volume fraction of the microstructures varies by:

$$V_{fl} + V_{fs} = 1 \qquad (6\text{-}3)$$

Magnetic field induced solid state can be described by STE

$$V_{fs} = \left[1 + \left(\frac{H}{H_c} \right)^{-B_{MRF}} \right]^{-1} \qquad (6\text{-}4)$$

Due to solid state grows from liquid state, volume fraction of this last, results as

$$V_{fl} = 1 - V_{fs} \qquad (6\text{-}5)$$

where B_{MRF} is a fitting constant; while H_c represents the values magnetic field at which 50% of the state transition is occurred, these values can be determined from experimental data.

6.4. Experimental Quantification of State Transition

6.4.1. Material

Experimental data of MRF commercially available by Lord company is used for quantification of state transition. The fluids analyzed are MRF-122EG, MRF-132DG and MRF-140CG. All of them are hydrocarbon based MRFs, the difference between them is the amount ϕ of particles which is 0.22, 0.32 and 0.4, respectively. Data sheets of each fluid are available in Appendix 3.

6.4.2. Methodology

6.4.2.1. Yield Stress - Magnetic field characterization

From data sheets of MRF-122EG, MRF-132DG and MRF-140CG, experimental yield stress – magnetic field data are obtained, these are plotted in Fig 6-8.

6.4.2.2. State Transition Estimation

From the plot of experimental yield stress –magnetic field, liquid - solid state transition is estimated by considering the yield strain axis of such plot, a V_f axis, with minimal and maximal values of 0 and 1, respectively; assuming that at maximal magnetic field V_{fs} is 1; at 50% of this process the inflexion point of yield stress – magnetic field curve exists and V_f of both states is 0.5, such point is the characteristic magnetic field H_c.

6.4.2.3. Estimation of saturation yield stress

By the use of equation (6-6) proposed by Ginder et al, the saturation yield stress is calculated for every fluid (Ginder et al, 1994)

$$\tau_y^{sat} = \frac{4}{5^{5/2}} \cdot \xi(3) \cdot \phi \cdot \mu_0 \cdot M_s^2 \qquad (6-6)$$

where $\xi(3)$ is a constant, μ_0 is the permeability of vacuum with value of $4\pi \cdot 10^{-7}$ and M_s is the saturation magnetic field of the material used as particles. Their values are shown in Table 6-2.

6.4.3. Results

6.4.3.1. Yield Stress - Magnetic field characterization

Fig 6-8 shows the plot of the yield stress – magnetic field relation for the MRF-122EG, MRF-132DG and MRF-140CG fluids obtained from Lord™ Corporation.
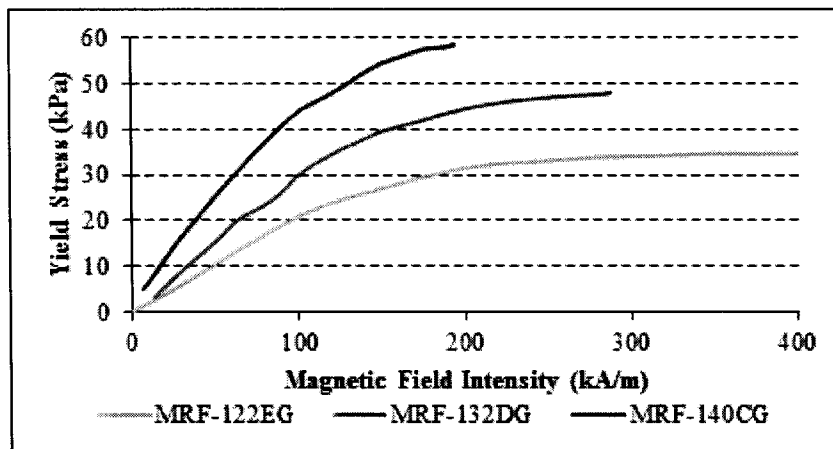
Fig. 6-8. Experimental Shear Yield stress – Magnetic field relation of MRF-122EG, MRF-132DG and MRF-140CG.

6.4.3.2. State Transition Estimation

Fig 6-9 shows the estimated liquid-solid state transition based on the variation of volume fraction of each state as function of the magnetic field for every MRF considered. It does not have a clear sigmoidal behavior as considered in Fig. 6-6.
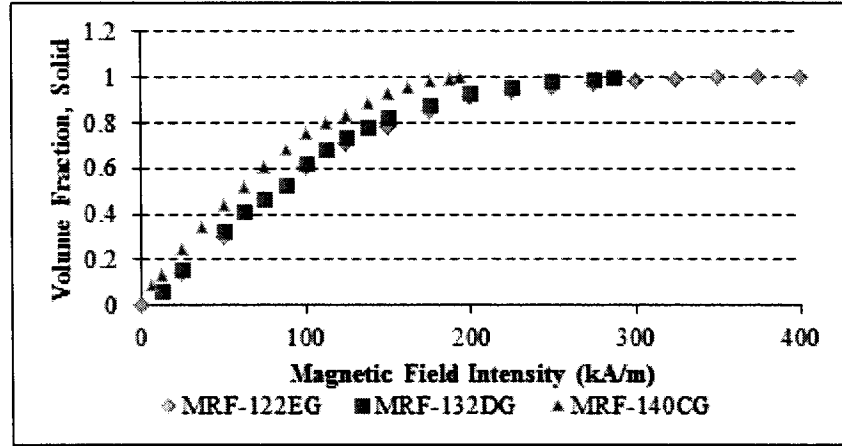
Fig. 6-9. Experimental Liquid – solid state transition estimation of MRF-122EG, MRF-132DG and MRF-140CG.

From Fig 6-9, H_c can be expressed as a function of volume fraction ϕ of particles as follows

$$H_c = \alpha\phi^{2'} + \cdot\beta\phi + \chi$$

(6-7)

6.4.3.3. Estimation of saturation yield stress

Resulting saturation shear yield stress for each MRF are in function of M_s, due that the material used as particles is unknown. These are shown in table 6-1.

Table 6-1. τ_y^{sat} of MRF-122EG, MRF-132DG and MRF-140CG fluids.

MRF	τ_y^{sat}
MRF-122EG	$.01892M_s$
MRF-132DG	$.02752M_s$
MRF-140CG	$.0344M_s$
Carrier fluid	$.086(1-\phi)M_s$

6.5. Fitting of Constitutive Model

6.5.1. Kinetics of State Transition

From experimental volume fraction – magnetic field data, PTE (6-4) is fitted. In order to determine

the role of constant B, V_{fs} values are plotted versus H/H_c values. By using the least squares method it is shown that B can be defined by a specific value which is independent of the magnetic field conditions as is observed in Fig 6-10. Therefore, substituting equation (6-7) into equation (6-4)

$$V_{fs} = \left[1 + \left(\frac{H}{\alpha\phi^2 + \beta\phi + \chi} \right)^{-B} \right]^{-1}$$

(6-8)

α, B, β and χ constants are determined from experimental data. Their values are summarized in Table 6-2, for the analyzed commercial MRFs.
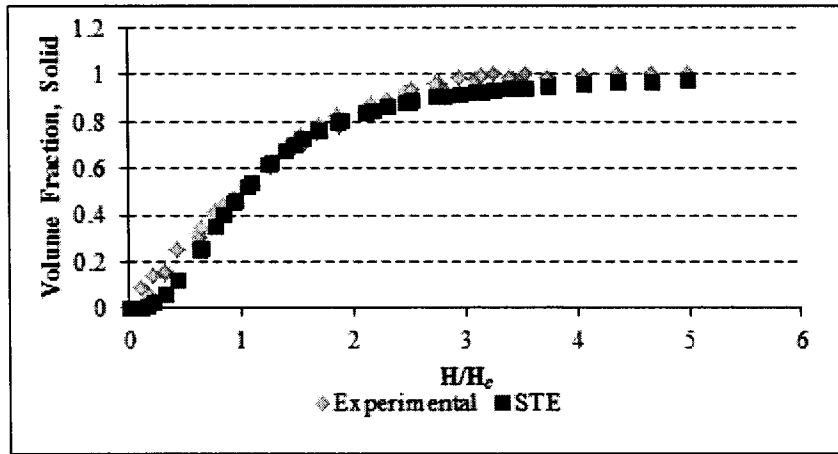
Fig. 6-10. Experimental Volume fraction of solid state against H/H_c

6.5.2. Saturation Yield Stress

From Fig 6-8, experimental $\tau_y{}^{sat}$ values are determined and used for fitting of the expressions of Table 6-1 by using least squares method, thus the value of M_s of the particles is estimated and shown in Table 6-2. In the case of M_s corresponding to the carrier fluid, it is assumed to be 0 since such material does not respond to magnetic fields, this way

$$\tau_{yl}^{sat} = 0$$

(6-9)

6.6. Validation of Constitutive Model

Substituting equations(6-6), (6-8) and (6-9) into equation (6-2) constitutive model for shear yield stress of MRF is obtained by an expression which results in terms of the volume fraction of particles, magnetic field and the material that composes the particles

$$\tau_y = \left[1 + \left(\frac{H}{\alpha\phi^2 + \beta\phi + \chi} \right)^{-B_{MRF}} \right]^{-1} \bullet \left[\frac{4}{5^{5/2}} \cdot \xi(3) \cdot \phi \cdot \mu_0 \cdot M_s^2 \right] \tag{6-10}$$

Units used in this expression are; H and M_s in A/m, μ_0 in N/m, this way τ_y results in Pascals (Pa), volume fraction and other constants are dimensionless.

Constitutive model represented by equation (6-10) is applied and verified by comparison with experimental shear yield stress – magnetic field data provided by Lord™ corporation. Comparison plots are shown in Fig 6-11.
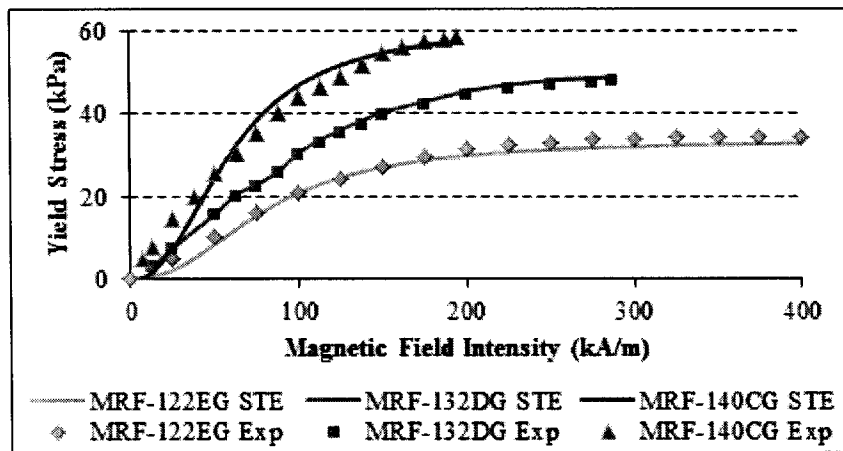
Fig. 6-11 Comparison of experimental (points) and theoretical shear yield stress by constitutive model (line)

Table 6-2. Material constants determined from experimental data for MRF-122EG, MRF-132DG and MRF-140CG fluids.

Parameter	Value
α	-1547.2
β	844
χ	-30.544
B	2.267
M_s	1192
$\xi(3)$	1.202
μ_0	$4\pi \cdot 10^{-7}$

6.6.1. Comparison with other constitutive models

In order to evaluate the accuracy of the proposed constitutive model it is compared with other similar works available in literature. Some of the most cited are the equations proposed by 'Dr. Dave' and Ginder.

Manuel Ignacio Varela Jiménez

6.6.1.1. *'Dr. Dave' Equation*

In his work *MR fluid and devices in the real world*, Carlson cites an empirical equation proposed by 'Dr. Dave' to provide a practical and convenient description of virtually any MR fluid., which is

$$\tau_y = C \cdot 271700 \cdot \phi^{1.5239} \cdot Tanh(6.33 \cdot 10^{-6} \cdot H)$$

(6-11)

where ϕ is the volume fraction of iron particles, τ_y is in Pa, H is the magnetic field intensity in A/m, and the constant C equals 1.0, 1.16 or 0.95 depending on whether the carrier fluid is hydrocarbon oil, water or silicone oil. This equation generates a curve that describes the nonlinear behavior of the yield stress as function of the magnetic field applied to the MRF. Due that analyzed MR fluids in this work have a hydrocarbon oil C is 1. Comparison with constitutive model based on STE is shown in Figs 6-11 to 6-13.

6.6.1.2. *Ginder equations*

Ginder proposes a series of equations for predicting shear yield stress and saturation shear yield stress of MR fluids, such equations are obtained as an approach from Finite Element Analysis of interaction between magnetic particles in a carrier fluid. Resulting equations are

$$\tau_y = \sqrt{6} \cdot \phi \cdot \mu_0 \cdot M_s^{1/2} \cdot H^{3/2}.$$

(6-12)

Equation for saturation shear yield stress is equation (6-6), already applied in this work. For application, equation (6-12) describes the increase of shear yield stress, its limit is obtained by equation (6-6). Comparison with constitutive model based on PTE is shown in Figs 6-12 to 6-14.
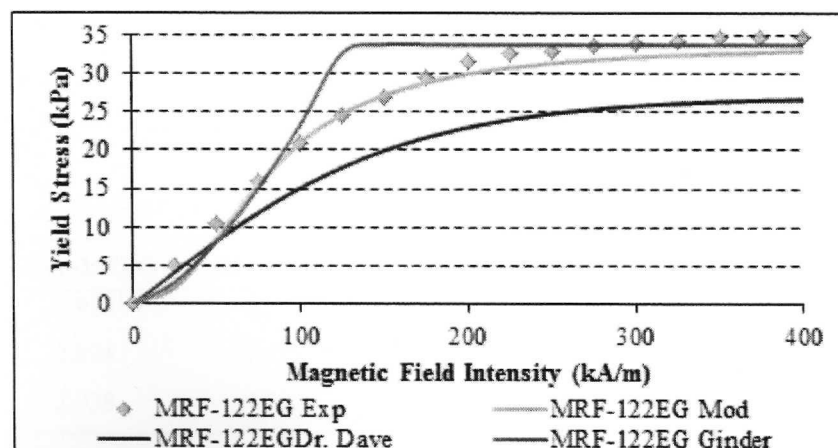
Fig. 6-12. Comparison of experimental (points) and theoretical yield stress for, MRF-122EG by STE, Ginder and 'Dr. Dave' equations.
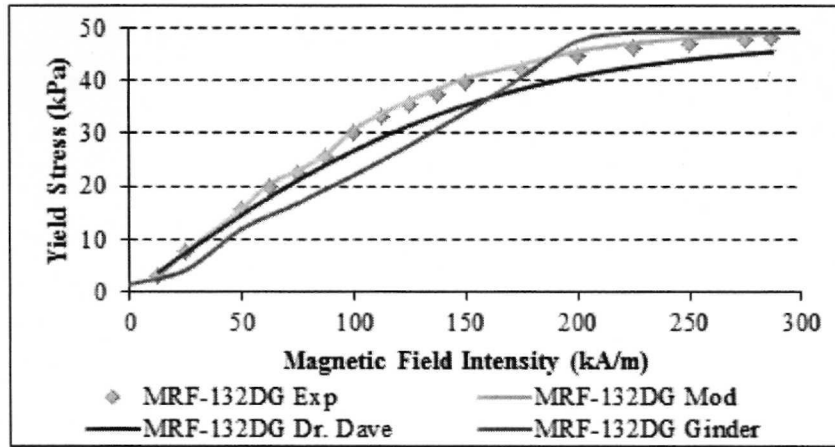
Fig. 6-13. Comparison of experimental (points) and theoretical shear yield stress for MRF-132DG by STE, Ginder and 'Dr. Dave' equations.
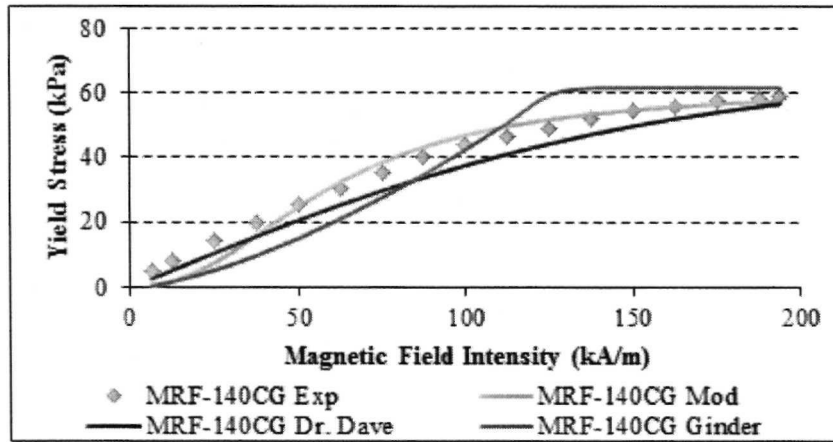
Fig. 6-14. Comparison of experimental (points) and theoretical shear yield stress for MRF-140CG by STE, Ginder and 'Dr. Dave' equations.

6.6.2. Error Analysis

Accuracy of equations is evaluated by the standard deviation of the error, defined as the difference between the experimental and predicted data. It is shown in Table 6-3.

Table 6-3. Standard deviation of error of shear yield stress prediction

Model	MRF-122EG	MRF-132DG	MRF-140CG	Average Standard Deviation of Error
STE	0.928	0.339	3.347	1.538
Dr. Dave	2.824	1.475	1.369	1.889
Ginder	2.938	4.992	7.274	5.068

6.7. Discussion

A constitutive model for yield stress of MRF has been proposed consisting of an expression that relates composition of the material and the stimulus applied, in this case a magnetic field obtaining promising results. The equation associates the volume fraction of particles, magnetic field and the material that composes the particles. Such model works in one way describing the effect of increase of magnetic field on the yield shear stress of the material.

A liquid-solid state transition in MRF was proposed having a sigmoidal behavior as described in chapter 2, considering that nucleation is started by the magnetic field is applied and as it is increased the volume fraction of the solid state also becomes higher.

Experimental yield stress-magnetic field data for commercial MRF allowed to estimate the state transition, demonstrating that magnetic field has a immediate effect on the material by observing that even if the magnetic field is low it produces an increase on the yield stress. Then, it can be considered that solid state growth stage starts almost immediately with a very short nucleation stage, in contrast with the phase transformation of austenite in NiTi or active state of SMP on which nucleation occurs and a specific amount of heat must be applied to activate the growth of the transition.

From experimental liquid-solid state transition estimation is observed that MRF with larger amount of particles saturates at a lower magnetic field that those with less particles. It is considered that this occurs due that a larger amount of particles makes the material more sensitive to the magnetic field. An estimation of this can be done by assuming that as lower results the characteristic magnetic field of MRF the material is more sensitive to magnetism.

STE is used for describing state transition, even if it is not clearly sigmoidal, the equation results flexible and can get a good fitting with experimental data.

The model proposed in this work could be substituted in Bingham equation and applied to describe shear stress of MRF as function of shear rate.

The model allows designing MRF by selecting the degree of sensitivity to magnetic field and the saturation yield stress. From the behavior observed, it can be considered that a good MRF should have a high saturation yield stress and low magnetic sensitivity, this way there is more range of applicability of the material in reconfigurable devices such as dampers or prosthetic legs.

Compared with models proposed by Ginder and Dr. Dave (Carlson, 2005), this can describe the nonlinear magnetization of the material and how its yield stress becomes saturated as magnetic field is

increased with a lower degree of error. According to the comparison carried out, this model is more accurate than Dr. Dave equation, however it requires more constants and additional material data such as magnetic saturation of particles which, which may rest simplicity. These models work in one way describing only effect of increase of magnetic field on shear yield stress but not consider transition from solid to liquid state.

Due to this constitutive model achieved a good fitting with experimental data it is demonstrated that effect of magnetic field on rheology of MRF can be described based on a mathematical expression applied in other kind of materials such as NiTi, EAP or SMP. The model could be improved by extending it in order to describe transition from solid to liquid state becoming into a two way constitutive model.

Part III. Results and Conclusions

Chapter 7.

Conclusions and Future Work

7.1. Conclusions

A methodology for modeling smart materials based on a state transition concept was proposed. It was applied and validated preliminary to describe stress-strain behavior of Nickel-Titanium SMA wires, stress-strain behavior of shape memory polymers of different glass transition temperature, displacement of electroactive polymers with different ionic content and magnetic field – shear yield stress behavior of magnetorheological fluid.

According to results obtained, an approach for initial modeling of smart materials behavior can be carried out considering a common state transition concept, using a similar methodology and mathematical expressions adapted to the physical domain of each material; although it is a common model this causes that not all the parameters involved in materials behavior can be considered, which gives to the model limitations and shortcomings in which work is still required.

For each material, transition between two states induced by an external stimulus is considered, similar to a phase transformation that occurs in metals like NiTi. Following this concept, materials in which a controlled transition between two states is observed could be modeled by the methodology presented in this work, such transition must be proposed and quantified through experimental work based on controlled application of the external stimulus.

Due to agreement between model prediction and experimental data for each material evaluated it can be considered that the methods and assumptions considered in this work are valid. Promising results are obtained, demonstrating partially that modeling of different kind of smart materials can be done by using a common concept and methodology, despite of their composition of physical state. Due that the model is proposed from a mechanical point of view and does not consider all the possible parameters that can affect

material behavior, for example, in the case of polymer it does not considers thermodynamics of effects of time in the strain of the material. Then, additional experimental work is required in order to determine if the model is completely valid.

In the case each material evaluated in this work, a constitutive equation in terms of the external stimulus applied and material components has resulted. It relates the response of the material with its environment and its composition, which can be useful for design materials with specific conditions as it required nowadays.

Each constitutive model applies a state transition equation derived from Cortes et al work, such expression results flexible and simple, which facilitates its fitting to different physical domains.

A constitutive model for flow stress of NiTi relating microstructure with thermo-mechanical behavior of NiTi has been proposed and validated.

A constitutive model to describe stress on SMPs based on a glassy – active phase transformation as function of the strain, temperature, glass transition temperature and transformation temperatures of the material has been developed and validated.

A constitutive model for the bending deformation of an electrically induced IPMC was proposed. The constitutive equation was based externally in the bending deformation of a beam system subject to a virtual load, and was internally correlated to a phase transformation at one of the sides of the cross section of the IPMC. Such model has been validated.

A constitutive model for yield stress of MRF is proposed consisting of an expression that relates composition of the material and the stimulus applied, in this case a magnetic field. The equation associates the volume fraction of particles, magnetic field and the material that composes the particles.

Resulting methodology for modeling by a state transition concept is an initial approach for developing a constitutive model that work in three dimensional conditions, considering also return of materials to their initial state, this way it could be used for simulation by finite element analysis of devices that apply smart materials.

Due that model derives from previous work in stainless steels it adapts to NiTi considering stress, strain and could be extended to consider chemical composition; however, even the model could be adapted for modeling of polymers it does not describes them considering thermodynamics as traditionally occurs. Thus, results obtained by now are promising but still need to be validated in order to confirm if

this model can be really used to describe several kinds of materials. Such validation may be improved by extending the use of model to other smart materials such as piezoelectric ceramics.

7.2. Future Work

Constitutive models proposed in this work can be improved in order to achieve a better understanding of the material composition on the reaction to an external stimulus and also for extend its use to simulation through numerical methods. Thus:

- Models proposed for NiTi and SMP should be extended to three dimensional conditions in order to be applied in simulation of devices through Finite Element Analysis.

- NiTi model can also be improved by considering wires of different manufacturers and geometries in order to identify a relation between the chemical composition and geometry and the value of the material constants. This way the model could be applied in NiTi of whatever manufacturer or shape.

- The model for SMP can be improved by synthesis of an own polymer in which its composition be varied in an organized form, allowing to determine a mathematical expression that describes the effect of the chemical composition on the glass transition temperature. This model should also be compared quantitatively with others that consider thermodynamics effects on the material, in order to validate if polymers can be described by this model with accuracy.

- The model for EAP could be improved by synthesis of films with varied quantified concentration of ions, in order to relate the effect of ions concentration on the material constants.

- The model for MRF can be improved by preparing an own material in which the amount of particles be varied and quantify through experiments an own mathematical expression that relates the amount of particles with the saturation yield stress.

- In order to give a full use and validation to the methodology proposed in this work, it should also be considered for modeling of other materials in which a state transition can be assumed to occur such as piezoelectric ceramics, liquid-crystalline polymer microparticles or Nanoflex™ steel. It could also be adapted to other kinds of systems such as cells growth.

Bibliography

1. An J, Kwon D. Modeling of a Magnetorheological actuator including magnetic hysteresis. Journal of Intelligent Material Systems and Structures. Vol 14 No 9 (2003), pp 541-500.

2. Aravas N, Spyrou L. A. Muscle and Tendon Tissues: Constitutive Modeling and Computational Issues. Journal of Applied Mechanics. Vol. 78. July 2011.

3. Auricchio F. A review on phenomenological shape memory alloy constitutive modeling approaches. Computational Mechanics & Advanced Materials Group Universita di Pavia. 2009.

4. Asahi Glass, Co. LTD. Retrieved from <http://www.agc.co.jp/english/rd/topics_04.html>

5. Arghavani J, Auricchio F, Naghdabadi R, Reali A. On the constitutive modeling and numerical implantation of shape memory alloys under multiaxial loadings – part I: Constitutive Model development at small and finite strains. Smart structural systems technologies. 2010.

6. Askeland, D.R. The Science and Engineering of materials. 3rd edition, PWS Publishing Company, Boston. 1994.

7. Azadi, B., Rajapakse, R., & Maijer D. Multi-dimensional constitutive modeling of SMA during unstable pseudoelastic behavior. *International journal of solids and structures*,Vol. 44, No, 20, (2007), pp. 6473-6490, ISSN 0020-7683

8. Bar-Cohen, Y. Structural Dynamics, and Materials Conference (SDM) Gossamer Spacecraft Forum(GSF), Seattle WA, USA, 2001.

9. Bompos D A, Nikolakopoulos P G. CFD simulation of magnetorheological fluid journal bearings. Simulation Modeling Practice and Theory. Vol 19 (2011), pp 1035–1060.

10. Bosco E. Some new insights into the old Avrami's equation. Journal of Chemical Physics. Vol 97 No 2. 1992.

11. Brown, C. Getting a grip on artificial muscles. Electronic Engineering Times. Vol 1341 (2004).

12. Burbelko A A. Transformation kinetics for instantaneous nucleation in the finite volume – application of statistical theory of shielding. Archives of Metallurgy and Materials. Volume 54-2. 2009

13. Burt H.M and Hunter W.L 2006 Drug-eluting stents: A multidisciplinary success story *Advanced Drug Delivery Reviews* 58 350-357.

14. Carlson J. MR fluids and devices in the real World. International Journal of Modern Physics B. Vol 19 No 7, 8&9 (2005), pp 1463-1470.

15. Castro F. Thermomechanical Behavior of Shape Memory Polymers. University of Colorado. 2009.

16. Cesmeci S, Engin T. Modeling and testing of a field-controllable magnetorheological fluid damper. International Journal of Mechanical Sciences. Vol 52 (2010), pp 1036–1046.

17. Ciocanel C. A particle based constitutive model for MR (magnetorheological) fluids. Doctoral Thesis (2006). University of Toledo.

18. Chang, S., & Wu S. Internal friction of R-phase and B19' martensite in equiatomic TiNi shape memory alloy under isothermal conditions. *Journal of Alloys and Compounds*, Vol. 437, (2007), pp. 120-126, ISSN 0925-8388

19. Chen Y, Lagoudas D. A constitutive theory for shape memory polymers. Part I Large deformations. J Mech Phys Solids 2008; 56: 1752-1765.

20. Chen Y, Lagoudas D. A constitutive theory for shape memory polymers. Part II A linearized model for small deformations. J Mech Phys Solids 2008; 56: 1766-1778.

21. Ciocanel C. A Particle Based Constitutive Model for Magnetorheological Fluids. University of Toledo. 2006.

22. Cortes, J.; Tsuta, T.; Mitani, Y.; Osakada, K. Flow stress and phase transformation analyses in the austenitic stainless steel under cold working. Part 1. Phase transformation characteristics and constitutive formulation by energetic criterion. Int. J. of Jap. Soc. Mech. Eng. 1992, 35 (2), 201–209.

23. Cortes J, Tsuta, T. Flow stress and phase transformation analyses in the austenitic stainless steel under cold working. Part 2. Incremental Theory under multi-axial stress state by finite element method. Int. J. of Jap. Soc. Mech. Eng. 1993, 36 (1), 63.

24. Crandall J. Constitutive Modeling. Center for Applied Biomechanics University of Virginia. 2011.

25. CRG. Retrieved from <http://www.crgrp.com/technology/materialsportfolio/veriflex.shtml>

26. Da Costa Machado G, Alves M K, Al-Qureshi H A, Rossi R. Constitutive modeling of the large strain behavior of crushable foams using the element-free Galerkin method. Mechanics of Solids in Brazil 2007

27. De Castro J A, Melcher K J, Noebe R D, Gaydosh D J. "Development of a numerical model for high-temperature shape memory alloys". Smart Materials and Structures. Vol 16. pp 2080-2090. (2007).

28. De la Garza R, Cortes J, Gallegos S, Florez L and Martinez M, "Constitutive Equation Based on Phase Transformations for Shape-Memory Actuators of Reconfigurable Systems", *Materials and Manufacturing Processes* 22 318-322. (2007).

29. DesignVerb! <http://www.designverb.com/2006/02/>

30. Dobrzański L A. Introduction on the importance of the materials structure and properties forming processes for contemporary industrial production. Open Access Library. Volume 1. 2011.

31. DuPont™. Retrieved from <http://www.dupont.com/fuelcells/pdf/dfc101.pdf>

32. Furrer D.U., Semiatin S. L. Introduction to Fundamentals of Modeling for Metals Processing. 2009.

33. Gall K, Dunn M L, Liu Y, Finche D, Lake M, Munshi N A. Shape memory polymer nanocomposites. Acta Mater 2002; 50: 5115-5126.

34. Gall K, Yakacki C M, Liu Y, Shandas R, Willett N, Anseth K S. Thermomechanics of the shape memory effect in polymers for biomedical applications. J Biomed Mater Res 2005; 73A: 339–348

35. Gasser T C, Nilsson F. Aspects on solid mechanics modeling. Royal Institute of Technology.

36. Ginder J, Davis L, Elie L. Rheology of a Magnetorheological Fluids: Models and Measurements. International Journal of Modern Physics B, Vol 10 No 23&24 (1996), pp 3293-3303.

37. Ginder J, Davis L. Shear stresses in magnetorheological fluids: Role of magnetic saturation. Applied Physics Letters. Vol 65 No 26 (1994), pp 3410-3412.

38. Goncalves F. Characterizing the Behavior of Magnetorheological Fluids at High Velocities and High Shear Rates. Doctoral Thesis (2006) Virginia Polytechnic Institute and State University.

39. Grand-Illusions. Retrieved from <http://www.grand-illusions.com/acatalog/Nitinol_Springs.html>

40. Guzman J. Modeling and Principles of Ionic Polymer-Metal Composite Electroactive Polymers as Actuators for Position Reconfigurable Devices. Master Thesis. Tecnológico de Monterrey (2007).

41. Guzman J. F, Cortes J A, Fuentes A, Kobayashi T, Hoshina Y. Modeling the displacement in three-layer electroactive polymers using different counter-ions by a phase transformation approach. Journal of Applied Polymer Science. Volume 112-6. 2009.

42. Han H N, Lee J K, Kim H J, Jin Y-S. A model for deformation, temperature and phase transformation behavior of steels on run-out table in hot strip mill. Journal of Materials Processing Technology 128 pp 216–225. 2002

43. Hu J. Shape Memory Polymers and Textiles. WP. 2007.

44. IUPAC. Avrami equation. IUPAC Compendium of Chemical Terminology. 2nd Edition. 1997.

45. Jena AK, Chaturvedi MC. Phase Transformations in Materials. Prentice Hall. 1992.

46. Jolly M R, Bender J W, Carlson D. A model of the behavior of magnetorheological material. Smart Materials and Structures. Vol 5 (1996), pp 607–614.

47. Kumar A. Comprehensive modeling of shape memory alloys for actuation of large-scale structures. Doctoral Thesis. University of Akron. 2010.

48. Kwang, J. K.; Shahinpoor, M. Ionic polymer–metal composites: II. Manufacturing techniques. Smart Materials and Structures, Vol 12 No 1 (2003) pp 65-79.

49. Lahoz, R., & Puértolas, J. Training and two-way shape memory in NiTi alloys: influence on thermal parameters. *Journal of Alloys and Compounds*, Vol. 381, (2004), pp. 130–136, ISSN 0925-8388

50. Laun H m, Gabriel C, Schmidt G. Primary and secondary normal stress differences of a magnetorheological fluid (MRF) up to magnetic flux densities of 1 T. Journal of Non-Newtonian Fluid Mechanics. Vol 148 (2008), pp 47–56.

51. Leo D J. Engineering Analysis of Smart Material Systems. Wiley. 2007.

52. Li W H, Du H, Yeo S H. Experimental investigation of creep and recovery behaviors of magnetorheological fluids. Materials Science and Engineering A333 (2002), pp 368–376.

53. Liu H, Kobayashi T, Yu H. Easy Fabrication and Morphology Control of Supramolecular Liquid-Crystalline Polymer Microparticles. Macromolecular Rapid Communications. Vol 32, Issue 4. February 2011. pp 378–383.

54. Liu Y, Gall K, Dunn M L, Greenberg A R, Diani, J. Thermomechanics of shape memory polymers: Uniaxial experiments and constitutive modeling. Int J Plasticity 2006; 22: 279-313.

55. Liu Y, Gall K, Dunn M L, McCluskey P. Thermomechanics of shape memory polymer nanocomposites. Mech Mater 2004; 36: 929-942.

56. Lord corporation. Retrieved from <www.mrfluid.com>. November 2011.

57. Lujan T. Constitutive Modeling. Legacy Research and Technology Center. 2010.

58. Malukhin K and Ehmann K 2006 Material Characterization of NiTi Based Memory Alloys Fabricated by the Laser Direct Metal Deposition Process *Journal of Manufacturing Science and Engineering* 128 691-696.

59. McNaney J.M, Imbeni V, Jung Y, Papadopoulos P and Ritchie R.O 2003 An experimental study of the superelastic effect in a shape-memory Nitinol alloy under biaxial loading *Mechanics of Materials* 35 969–986.

60. Nakano M, Satou A, Sugamata Y, Nishiyama H. Dynamic shear flow behavior of magneto-rheological fluid between two rotating parallel disks under relatively weak magnetic field. JSME International Journal B, Vol 48 No 3 (2005), pp 494-500.

61. Nemat-Nasser S and Guo W 2006 Superelastic and cyclic response of NiTi SMA at various strain rates and temperatures *Mechanics of Materials* 38 463–474.

62. Oguro, K.; Kawami, Y.; Takenaka, H. Bending of an ion-conducting polymer film-electrode composite by an electric stimulus at low voltage. Trans. Journal of Micromachine Society, Vol 5 (1992) pp 27-30.

63. Ottosen N, Ristinmaa M. The Mechanics of Constitutive Modeling. Elsevier, 2005.

64. Ouellette J. How Smart are Smart Materials?. The Industrial Physicist. 10. American Institute of Physics. 1996.

65. Patil P D, Feng J J, Hatzikiriakos S G. Constitutive modeling and flow simulation of polytetrafluoroethylene (PTFE) paste extrusion. Journal of Non-Newtonian Fluid Mechanics. 139 pp 44–53. 2006.

66. Pelton A.R, DiCello J and Miyazaki S 2000 Optimization of processing and properties of medical grade Nitinol wire *Minimally Invasive Therapy and Allied Technologies* 9(1) 107–118.

67. Pitner J B, Timmins M, Kashdan M, Nagar M, Stitt D T. High-Throughput Assay System for the Discovery Of Anti-Bacterial Drugs. Presented at AAPS - New Orleans, LA November, 1999

68. Rajasekaran N. A Nonlinear Constitutive Model for High Density Polyethylene at High Temperature. Master Thesis. University of Cincinnati. 2011.

69. Ritter A. Smart materials in Architecture, Interior Architecture and Design. Birkhauser. 2007.

70. Rollet A D. Microstructure-Properties: II The KJMA Equation. Carnegie Mellon University. Retrieved from <http://neon.mems.cmu.edu/rollett/27302/27302.html>

71. Ryhänen J. "Biocompatibility Evaluation Of Nickel-Titanium Shape Memory Metal Alloy". Academic Dissertation. University of Oulu. (1999).

72. Runesson K. Constitutive Modeling of Engineering Materials – Theory and Computation. Lecture notes. Chalmers University of Technology. 2006.

73. Sadeghipour, K., Salomon, R., Neogi, S., "Development of A Novel Electrochemically Active Membrane and 'Smart' Material Based Vibration Sensor/Damper", Smart Materials and Structures, Vol. 1, pp. 172-179, 1992.

74. Safransky D L, Gall K. Effect of Chemical Structure and Crosslinking Density on the thermomechanical properties and toughness of (meth) acrylate shape-memory polymer networks. Polymers 2008; 49-20: 4446-4455.

75. Shahinpoor, M. Conceptual Design, Kinematics and Dynamics of Swimming Robotic Structures Using Ionic Polymeric Muscles. Smart Materials and Structures, Vol 1 No 1 (1992) pp 91-94.

76. Shahinpoor, M.; Kwang, J. K. Ionic polymer–metal composites: I Fundamentals. Smart Materials and Structures Vol 10 (2001) pp 819-833.

77. Shahinpoor, M.; Kwang, J. K. Ionic polymer–metal composites: III Modeling and simulation as biomimetic sensors, actuators, transducers, and artificial muscles. Smart Materials and Structures, Vol 13 (2004) pp 1362-1388.

78. Simon T M, Reitich F, Jolly M R, Ito K, Banks H T. The Effective Magnetic Properties of Magnetorheological Fluids. Mathematical and Computer Modelling 33 (2001), pp 273-284

79. Simon T M. Modeling and computation of the effective magnetic properties of magnetorheological fluids. Doctoral Thesis (1999). North Carolina State University.

80. Srinivasan A V, Mc Farland D M. Smart Structures Analysis and Design. Cambridge University Press. 2001.

81. Susan-Resiga D, Vékás L, Susan-Resiga R. A Rheological Model for Magneto-Rheological Fluids. 3rd German Workshop on Turbomachinery Hydrodynamics, May 10-12, 2007, pp 141-158.

82. Ti K S, Huat B B K, Noorzaei J, Jaafar M. A Review of Basic Soil Constitutive Models for Geotechnical Application. The Electronic Journal of Geothecnical Engineering. Vol 14J. 2009.

83. UK Parliamentary Office of Science and Technology Smart materials and systems. Postnote. Number 299 January 2008.

84. Villarreal L, Cortes J, Martinez M. Characterization, Modeling and Simulation of Magnetorheological Damper Behavior under Triangular Excitation. Mechatronics for Safety, Security and dependability in a New Era. (2005), pp 353-358. Eiji Arai & Tatsuo Arai (eds.), Osaka University.

85. Wache H M, Tartakowka D J, Hentrich A, Wagner M H. Development of a polymer stent with shape memory effect as a drug delivery system. Journal of Materials Science: Materials in Medicine 14, pp 109-112, 2003.

86. Weiss K, Duclos T. Controllable fluids: the temperature dependence of post-yield properties. International Journal of Modern Physics B. Vol 8 No 20&21 (1994), pp 3015-3032.

87. Worden K, Bullough W A, Haywood J. Smart Technologies. World Scientific. 2003.

88. Xin M. Development of novel magneto-rheological polymer gels and magneto-rheological fluids. Doctoral Thesis (2003). University of Nevada Reno.

89. Yakacki C M, Lyons M B, Rech B, Gall K, Shandas R. Cytotoxicity and thermomechanical behavior of biomedical shape-memory polymer networks post-sterilization. Biomedical Materials 3, 2008.

90. Zang L. Kinetics of Phase Growth: *single-component or composition-invariant transformation* The University of Utah. 2010. Retrieved from <http://www.eng.utah.edu/~lzang/images/lecture-15.pdf>

91. Zhigilei L. Phase Transformations. University of Virginia. 2010. Retrieved from <http://people.virginia.edu/~lz2n/mse209/>

Appendix 1.

Additional Information about Smart Materials

With advancements in science and technology, new classes of multifunctional materials have emerged (Kumar, 2010) and progress in the field is predicted and expected, including among others, nanomaterials, biomaterials and SM, which issues decide development of materials engineering as one of the areas of development most important nowadays (Dobrzanski, 2011). Thus, bolstered by commercial applications, SM are experiencing a resurgence of growth and interest. In fact, many researchers in the field believe that the industry is on the threshold of achieving major technological breakthroughs that will enable additional applications in the aerospace, home construction, automotive, and machine tool industries (Ouellette, 1996).

The most widely used SM are piezoelectric ceramics, which expand and contract when voltage is applied. Although not as forceful as shape memory alloys (SMA), piezoelectric ceramics respond much more quickly, making them ideal for precise, high speed actuation and are used to generate electrically stimulated movement or to record movement by providing a movement related electric response. The most common piezoelectric ceramic used these days is Lead–Zirconate-Titanate. They tend to be brittle and somewhat heavy and the piezoelectric effect disappears above material dependent temperature thresholds. They are also difficult to scale to larger applications because of their limited stroke or displacement. SMA are metals that can be deformed and then returned to their original shape by heating. In the process, they generate an actuating force. The most popular one is a Nickel-Titanium alloy (NiTi) known as Nitinol, which has a corrosion resistance that makes it useful for biomechanical applications. However, SMA can respond only as quickly as the temperature can shift, which is slow for many advanced applications. Magnetorestrictive materials such as Terfenol-D are similar to piezoelectrics, but these respond to magnetic rather than electric fields. They are typically used in sonar transducers, motors, and hydraulic actuators. Along with NiTi, magnetorestrictive materials are considered promising candidates for achieving active damping of vibrations (Ouellette, 1996). Electroactive polymers (EAP) produce mechanical strain under the application of a mechanical stress (Leo, 2007). Thermochromic materials change color in response to changes in temperature and have been used in bath plugs that change color when the water is too hot. Photochromic materials change color in response to changes in light conditions

and have been used in reactive lenses that become darker in response to increased light (UK Parlament, 2008).

Materials scientists predict that intelligent materials will play a prominent role in the near future. They have significant potential applications in various fields. As a result, research on them is actively growing both in academic and industrial sectors (Hu, 2007) creating SM systems, defined as an engineering system that utilizes the coupling properties of SM to provide functionality (Leo, 2007), these also sense their environment and respond, but are not constructed from a single material and may incorporate smart materials, but can also be constructed using traditional technology (UK Parlament, 2008). However, it can also be considered that the 'smartness' comes from a systematic level, where sensor and actuator components are integrated into a structure capable of achieving enhanced functionality, hence the term 'smart structures' on which there is the addition of highly integrated control logic and signal conditioning and power amplification electronics (Ouellette, 1996).

SM open up new possibilities, such as clothes that can interact with a mobile phone or structures that can repair themselves. They also allow existing technology to be improved. Using a SM instead of conventional mechanisms to sense and respond, can simplify devices, reducing weight and the chance of failure (UK Parlament, 2008). Most industry insiders agree that the next generation of viable smart structure technology will be in applications for monitoring structural integrity, noise reduction, and vibration suppression (Ouellette, 1996).

Appendix 2.

Additional Information about Constitutive Models

The drive to increase understanding of nature and metallurgical processes has provided a substantial foundation for materials and process modeling. For the most part, the development of material behavior and process models has been spearheaded by metallurgical and mechanical engineers, respectively. Over the last two decades a great emphasis has been placed on the need for coupling material behavior and process models, leading to work that is truly interdisciplinary in nature. The linkage of component design, alloy design, and component manufacture through modeling and simulation methods will allow for advancement in the area of alloy research, advanced process and equipment development, and enhanced component capability. Modeling and simulation activities are increasing within the materials field as well as other science and engineering disciplines. The equations describing the physical phenomena in material behavior models and/or their coupling with process models are often too complex for solution by analytical means, except under restrictive conditions. This is usually the case for real world industrial processes. In such cases, numerical simulation methods must be used to describe material behavior, process mechanics, and processing-structure-mechanical behavior relationships (Furrer, 2009).

Process models describe manufacturing processes that require understanding of external independent parameters and boundary conditions and provide information about macroscopic component changes and/or information for metallurgical process models. The formulation and application of modeling and simulation methods for metallic materials and manufacturing process design and development is rapidly increasing. Classic models that predict the behavior of metals under processing conditions are used and enhanced with greater understanding of the mechanisms that control the evolution of microstructure, texture, and defects (Furrer, 2009), such as the presented by Han works on simulate precisely the temperature phase-deformation behavior of the steel strip on run out table taking into account that the phase transformation kinetics, temperature and deformation behavior of steel should be simultaneously analyzed, then using a model that he proposes the temperature-phase-deformation behavior of steels on the run out table was calculated (Han, 2002). Patil worked on a constitutive rheological equation for the paste extrusion of polytetrafluoroethylene (PTFE) that takes into account the continuous change of the microstructure during flow through fibril formation. Finite element simulations using the proposed

Manuel Ignacio Varela Jiménez

constitutive relation predict accurately the variations of the extrusion pressure with the apparent shear rate and die geometrical parameters (Patil, 2006).

Materials models describe how, for example, microstructure, crystallographic texture, and defects evolve as a function of local metallurgical process variables, including history and path dependences (Furrer, 2009). Examples of this are the works of Cortes who developed a constitutive model for strain-induced martensitic phase transformation and flow stress behaviors of austenitic stainless steels as an attempt to understand the main parameters that have influence on the phase transformation and on the flow stress under working conditions (Cortes, 1993). Da Costa on polymeric foams that are used in industry and domestic applications but whatever their use, their optimization needs the understanding of their microstructure/macroscopic mechanical property relationships, then work was done on modeling the relative density dependency effect on polymeric foams subjected to large deformations using a volumetric hardening law (da Costa Machado, 2007). Ti explains that there is a large variety of models which have been recommended in recent years to represent the stress-strain and failure behavior of soils but all of them inhibit certain advantages and limitations which largely depend on their application (Ti, 2009). Aravas mentions that development of realistic constitutive models for the mechanical behavior of the muscle tissue improves our basic understanding of the complex muscle function. Such models, combined with advanced imaging techniques computed tomography and magnetic resonance imaging, form the basis for realistic simulation of the human musculoskeletal system (Aravas, 2011). Nowadays the Center for Applied Biomechanics of University of Virginia is focusing on constitutive modeling of biological material in order to acquire a better knowledge of the response of biological materials under high strain rate loadings and to obtain material properties that can be integrated in finite element human body models (Crandall, 2011). Work has also been done about SM modeling, from 1980 up to now, constitutive modeling of SMA has been an active research subject (Auricchio, 2009), Villarreal worked on a constitutive model for MRF damping determined by simple power equation as a function of the electrical current that induces a magnetic field (Villarreal, 2006), while Guzman worked on a constitutive model for the bending deformation of a Nafion[®] Ionic Polymer-Metal Composite that works as an EAP (Guzman, 2009).

Appendix 3

MRF Datasheets

A3.1. MRF-122EG

LORD TECHNICAL DATA

MRF-122EG Magneto-Rheological Fluid

Description

LORD MRF-122EG fluid is a hydrocarbon-based magneto-rheological (MR) fluid formulated for general use in controllable, energy-dissipating applications such as shocks, dampers and brakes.

MRF-122EG fluid is a suspension of micron-sized, magnetizable particles in a carrier fluid. When exposed to a magnetic field, the rheology of MRF-122EG fluid reversibly and instantaneously changes from a free-flowing liquid to a semi-solid with controllable yield strength. Altering the strength of the applied magnetic field precisely and proportionally controls the consistency or yield strength of the fluid.

MRF-122EG fluid can be used in *valve mode* (fluid flowing through an orifice) or in *shear mode* (fluid shearing between two surfaces). In the absence of a magnetic field, MRF-122EG fluid flows freely or allows free movement. Upon application of a magnetic field, the fluid's particles align with the direction of the field in chain-like fashion, thereby restricting the fluid's movement within the gap in proportion to the strength of the magnetic field.

Features and Benefits

Fast Response Time – responds instantly and reversibly to changes in a magnetic field.

Dynamic Yield Strength – provides high yield strength in the presence of a magnetic field and very low yield strength in the absence of a magnetic field; allows for a wide range of controllability.

Temperature Resistant – performs consistently throughout a broad temperature range, meeting the requirements of demanding applications such as automotive shock absorbers.

Hard Settling Resistant – provides high resistance to hard settling; easily redispersed.

Non-Abrasive – formulated to not abrade the devices in which the MR fluid is used.

Application

For more information on MR technology, refer to the MR Design Guides located on www.lord.com/mr.

Mixing – Under common flow conditions, no separation is observed between particles and the carrier fluid. However, a degree of separation may eventually occur under static conditions. If needed, use a paint shaker to redisperse the particles into a homogeneous state prior to use.

Storage

Keep container tightly closed when not in use.

Typical Properties*

Appearance	Dark Gray Liquid
Viscosity, Pa-s @ 40°C (104°F) Calculated as slope 500-800 sec^{-1}	0.042 ± 0.020
Density	
g/cm^3	2.28-2.48
(lb/gal)	(19.0-20.7)
Solids Content by Weight, %	72
Flash Point, °C (°F)	>150 (>302)
Operating Temperature, °C (°F)	-40 to +130 (-40 to +266)

*Data is typical and not to be used for specification purposes.
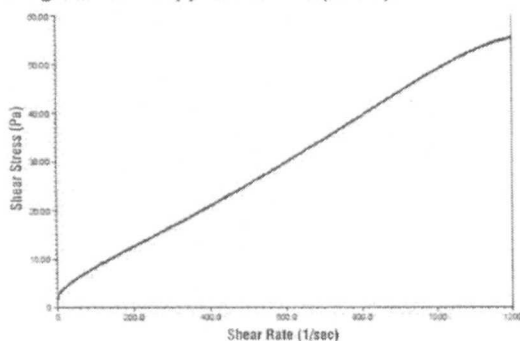
LORD
Ask Us How™

LORD TECHNICAL DATA
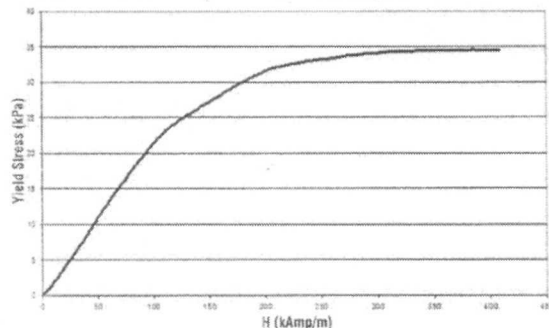
Cautionary Information

Before using this or any LORD product, refer to the Material Safety Data Sheet (MSDS) and label for safe use and handling instructions.

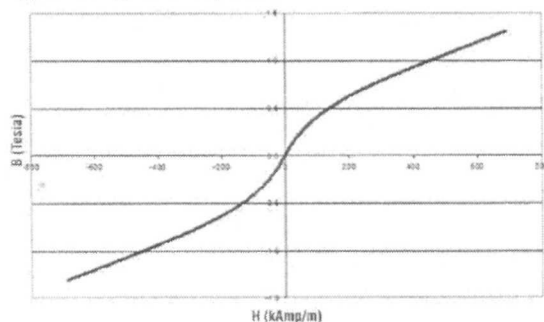*For industrial/commercial use only.* Not to be used in household applications. Not for consumer use.

Yield Stress vs. Magnetic Field Strength

Shear Stress as a function of Shear Rate with no Magnetic Field applied at 40°C (104°F)

Typical Magnetic Properties

Values stated in this technical data sheet represent typical values as not all tests are run on each lot of material produced. For formalized product specifications for specific product end uses, contact the Customer Support Center.

Information provided herein is based upon tests believed to be reliable. In as much as LORD Corporation has no control over the manner in which others may use this information, it does not guarantee the results to be obtained. In addition, LORD Corporation does not guarantee the performance of the product or the results obtained from the use of the product or this information where the product has been repackaged by any third party, including but not limited to any product end-user. Nor does the company make any express or implied warranty of merchantability or fitness for a particular purpose concerning the effects or results of such use.

"Ask Us How" is a trademark of LORD Corporation or one of its subsidiaries.

LORD provides valuable expertise in adhesives and coatings, vibration and motion control, and magnetically responsive technologies. Our people work in collaboration with our customers to help them increase the value of their products. Innovative and responsive in an ever-changing marketplace, we are focused on providing solutions for our customers worldwide . . . Ask Us How.

LORD Corporation
World Headquarters
111 Lord Drive
Cary, NC 27511-7923
USA
Customer Support Center (in United States & Canada)
+1 877 ASK LORD (275 5673)

www.lord.com

©2008 LORD Corporation OD:DS7027 (Rev 1 7/08)

LORD
AskUsHow™

Manuel Ignacio Varela Jiménez

A3.2. MRF-132DG

MRF-132DG Magneto-Rheological Fluid

Description

LORD MRF-132DG fluid is a hydrocarbon-based magneto-rheological (MR) fluid formulated for general use in controllable, energy-dissipating applications such as shocks, dampers and brakes.

MRF-132DG fluid is a suspension of micron-sized, magnetizable particles in a carrier fluid. When exposed to a magnetic field, the rheology of MRF-132DG fluid reversibly and instantaneously changes from a free-flowing liquid to a semi-solid with controllable yield strength. Altering the strength of the applied magnetic field precisely and proportionally controls the consistency or yield strength of the fluid.

MRF-132DG fluid can be used in *valve mode* (fluid flowing through an orifice) or in *shear mode* (fluid shearing between two surfaces). In the absence of a magnetic field, MRF-132DG fluid flows freely or allows free movement. Upon application of a magnetic field, the fluid's particles align with the direction of the field in chain-like fashion, thereby restricting the fluid's movement within the gap in proportion to the strength of the magnetic field.

Features and Benefits

Fast Response Time – responds instantly and reversibly to changes in a magnetic field.

Dynamic Yield Strength – provides high yield strength in the presence of a magnetic field and very low yield strength in the absence of a magnetic field; allows for a wide range of controllability.

Temperature Resistant – performs consistently throughout a broad temperature range, meeting the requirements of demanding applications such as automotive shock absorbers.

Hard Settling Resistant – provides high resistance to hard settling; easily redispersed.

Non-Abrasive – formulated to not abrade the devices in which the MR fluid is used..

Application

For more information on MR technology, refer to the MR Design Guides located on www.lord.com/mr.

Mixing – Under common flow conditions, no separation is observed between particles and the carrier fluid. However, a degree of separation may eventually occur under static conditions. If needed, use a paint shaker to redisperse the particles into a homogeneous state prior to use.

Storage

Keep container tightly closed when not in use.

Typical Properties*

Appearance	Dark Gray Liquid
Viscosity, Pa-s @ 40°C (104°F)	0.092 ± 0.015
Calculated as slope 800-1200 sec⁻¹	
Density	
g/cm³	2.98-3.18
(lb/gal)	(24.7-26.5)
Solids Content by Weight, %	80.98
Flash Point, °C (°F)	>150 (>302)
Operating Temperature, °C (°F)	-40 to +130 (-40 to +266)

*Data is typical and not to be used for specification purposes.
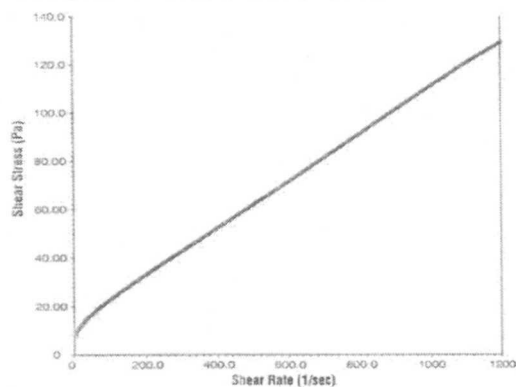
LORD
AskUsHow™

LORD TECHNICAL DATA
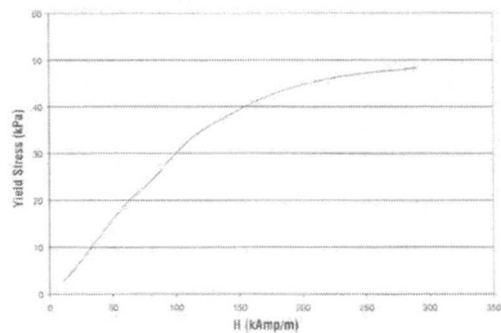
Cautionary Information

Before using this or any LORD product, refer to the Material Safety Data Sheet (MSDS) and label for safe use and handling instructions.

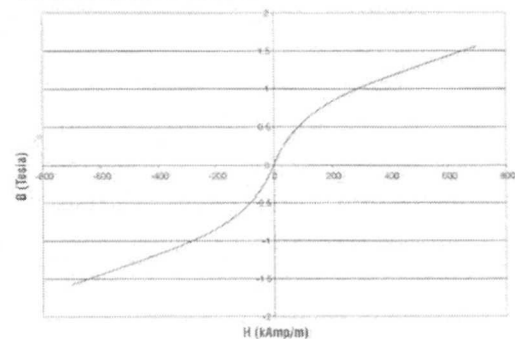*For industrial/commercial use only.* Not to be used in household applications. Not for consumer use.

Shear Stress as a function of Shear Rate with no Magentic Field applied at 40°C (104°F)

Yield Stress vs. Magnetic Field Strength

Typical Magnetic Properties

Values stated in this technical data sheet represent typical values as not all tests are run on each lot of material produced. For formalized product specifications for specific product end uses, contact the Customer Support Center.

Information provided herein is based upon tests believed to be reliable. In as much as LORD Corporation has no control over the manner in which others may use this information, it does not guarantee the results to be obtained. In addition, LORD Corporation does not guarantee the performance of the product or the results obtained from the use of the product or this information where the product has been repackaged by any third party, including but not limited to any product end-user. Nor does the company make any express or implied warranty of merchantability or fitness for a particular purpose concerning the effects or results of such use.

"Ask Us How" is a trademark of LORD Corporation or one of its subsidiaries.

LORD provides valuable expertise in adhesives and coatings, vibration and motion control, and magnetically responsive technologies. Our people work in collaboration with our customers to help them increase the value of their products. Innovative and responsive in an ever-changing marketplace, we are focused on providing solutions for our customers worldwide . . . Ask Us How.

LORD Corporation
World Headquarters
111 Lord Drive
Cary, NC 27511-7923
USA
Customer Support Center (in United States & Canada)
+1 877 ASK LORD (275 5673)

www.lord.com

©2008 LORD Corporation OD DS7015 (Rev 1 7/08)

LORD
AskUsHow™

A3.3. MRF-140CG

LORD TECHNICAL DATA

MRF-140CG Magneto-Rheological Fluid

Description

LORD MRF-140CG fluid is a hydrocarbon-based magneto-rheological (MR) fluid formulated for general use in controllable, energy-dissipating applications such as shocks, dampers and brakes.

MRF-140CG fluid is a suspension of micron-sized, magnetizable particles in a carrier fluid. When exposed to a magnetic field, the rheology of MRF-140CG fluid reversibly and instantaneously changes from a free-flowing liquid to a semi-solid with controllable yield strength. Altering the strength of the applied magnetic field precisely and proportionally controls the consistency or yield strength of the fluid.

MRF-140CG fluid can be used in *valve mode* (fluid flowing through an orifice) or in *shear mode* (fluid shearing between two surfaces). In the absence of a magnetic field, MRF-140CG fluid flows freely or allows free movement. Upon application of a magnetic field, the fluid's particles align with the direction of the field in chain-like fashion, thereby restricting the fluid's movement within the gap in proportion to the strength of the magnetic field.

Features and Benefits

Fast Response Time – responds instantly and reversibly to changes in a magnetic field.

Dynamic Yield Strength – provides high yield strength in the presence of a magnetic field and very low yield strength in the absence of a magnetic field; allows for a wide range of controllability.

Temperature Resistant – performs consistently throughout a broad temperature range, meeting the requirements of demanding applications such as automotive shock absorbers.

Hard Settling Resistant – provides high resistance to hard settling; easily redispersed.

Non-Abrasive – formulated to not abrade the devices in which the MR fluid is used.

Application

For more information on MR technology, refer to the MR Design Guides located on www.lord.com/mr.

Mixing – Under common flow conditions, no separation is observed between particles and the carrier fluid. However, a degree of separation may eventually occur under static conditions. If needed, use a paint shaker to redisperse the particles into a homogeneous state prior to use.

Storage

Keep container tightly closed when not in use.

Typical Properties*

Appearance	Dark Gray Liquid
Viscosity, Pa-s @ 40°C (104°F)	0.280 ± 0.070
Calculated as slope 800-1200 sec⁻¹	
Density	
g/cm³	3.54-3.74
(lb/gal)	(29.5-31.2)
Solids Content by Weight, %	85.44
Flash Point, °C (°F)	>150 (>302)
Operating Temperature, °C (°F)	-40 to +130 (-40 to +266)

*Data is typical and not to be used for specification purposes.

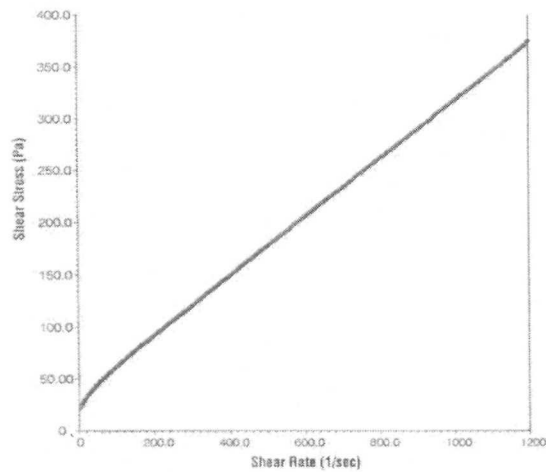**LORD**
AskUsHow™

Manuel Ignacio Varela Jiménez

LORD TECHNICAL DATA
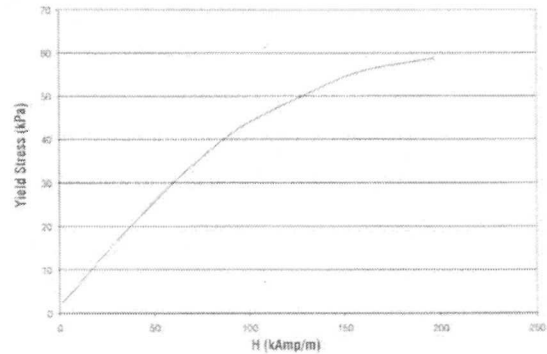
Cautionary Information

Before using this or any LORD product, refer to the Material Safety Data Sheet (MSDS) and label for safe use and handling instructions.

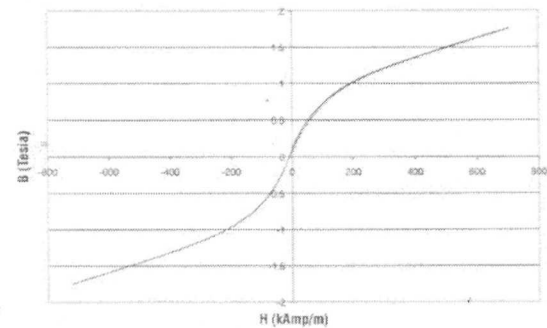*For industrial/commercial use only.* Not to be used in household applications. Not for consumer use.

Shear Stress as a function of Shear Rate with no Magentic Field applied at 40°C (104°F)

Yield Stress vs. Magnetic Field Strength

Typical Magnetic Properties

Values stated in this technical data sheet represent typical values as not all tests are run on each lot of material produced. For formalized product specifications for specific product end uses, contact the Customer Support Center.

Information provided herein is based upon tests believed to be reliable. In as much as LORD Corporation has no control over the manner in which others may use this information, it does not guarantee the results to be obtained. In addition, LORD Corporation does not guarantee the performance of the product or the results obtained from the use of the product or this information where the product has been repackaged by any third party, including but not limited to any product end-user. Nor does the company make any express or implied warranty of merchantability or fitness for a particular purpose concerning the effects or results of such use.

"Ask Us How" is a trademark of LORD Corporation or one of its subsidiaries.

LORD provides valuable expertise in adhesives and coatings, vibration and motion control, and magnetically responsive technologies. Our people work in collaboration with our customers to help them increase the value of their products. Innovative and responsive in an ever-changing marketplace, we are focused on providing solutions for our customers worldwide . . . Ask Us How.

LORD Corporation
World Headquarters
111 Lord Drive
Cary, NC 27511-7923
USA
Customer Support Center (in United States & Canada)
+1 877 ASK LORD (275 5673)

www.lord.com

©2008 LORD Corporation OD DS7012 (Rev.1 7/08)

LORD
AskUsHow™

Manuel Ignacio Varela Jiménez

List of Publications

Papers
- Varela I, Cortes J, Yi-Chao C. Constitutive Model for Glassy – Active Phase Transformation on Shape Memory Polymers considering Small Deformations. Journal of Materials Science and Engineering, May 2010.

Book Chapter
- Varela I, Bueno M, Cortes J. Reconfigurable Tooling by using a Reconfigurable Material. Manufacturing Sytem. Intech Open Acces Publisher. To be published in March 2012.

Conferences
- Varela I, Cortes J, Yi-Chao C. Constitutive Model for Glassy – Active Phase Transformation on Shape Memory Polymers considering Small Deformations. Annual Meeting of the Hokuriku Branch of the Japan Society of Polymer Science, Niigata Japan, August 2009.

- Varela I, Cortes J, Kobayashi T, Yi-Chao C. Constitutive Model for Flow Stress Prediction on Acrylate Shape Memory Polymer Membranes considering a Phase Transformation Approach. XIX International Materials Research Congress, Cancún México, August 2010.

- Varela I, Bueno M. Cortes J. Constitutive Model for Stress on Nickel – Titanium Shape Memory Alloy Considering an Austenite – Twinned Martensite – Detwinned Martensite Phase Transformation Approach. Society for Biomaterials Annual Meeting. Orlando FL USA, April 2011.

- Guzman J, Varela-Jimenez I, Cortes J. Modeling the Displacement in Three-layer Electroactive Polymers Using Different Counter-ions by a Phase Transformation Approach. To be presented at the International Conference on Modern Materials & Technologies. Montecatini Terme, Tuscany, Italy. June 2012.

- Varela-Jimenez I, Cortes J. Constitutive Model for Stress on Nickel - Titanium Shape Memory Alloy by Considering a Twinned Martensite-Detwinned Martensite-Austenite Phase Transformation Induced by Strain and/or Temperature. To be presented at the International Conference on Modern Materials & Technologies. Montecatini Terme, Tuscany, Italy. June 2012.